UNIVERSITY OF WARMIA AND MAZURY IN OLSZTYN

Technical Sciences

15(2)

PUBLISHER UWM

OLSZTYN 2012

The Technical Sciences is indexed in BazTech (http://baztech.icm.edu.pl) and Index Copernicus Journal Master List (http://publisherspanel.indexcopernicus.com/) and abstracted in BazTech

The Journal is also available in electronic form on the web sites:
http://www.uwm.edu.pl/techsci/
http://wydawnictwo.uwm.edu.pl (subpage *Czytelnia*)

The print edition is the primary version of the Journal

PL ISSN 1505-4675

Address
ul. Jana Heweliusza 14
10-718 Olsztyn-Kortowo, Poland
tel.: +48 89 523 36 61
fax: +48 89 523 34 38
e-mail: wydawca@uwm.edu.pl

Ark. wyd. 11,25, ark. druk. 9,25, nakład 120 egz.
Druk – Zakład Poligraficzny UWM w Olsztynie
zam. nr 58

Contents

Biosystems Engineering

Civil Engineering

Geodesy and Cartography

Information Technology

Mechanical Engineering

Production Engineering

TECHNICAL SCIENCES
Abbrev.: Techn. Sc., No 15(2), Y 2012

AN ANALYSIS OF DEMAND FOR THE SELECTED GROUP OF SPARE PARTS ILLUSTRATED WITH AN EXAMPLE OF FILTERS FOR AGRICULTURAL VEHICLES

Sławomir Juściński

Department of Power Industry and Vehicles
Faculty of Logistics and Enterprise Management
University of Life Sciences in Lublin

K e y w o r d s: spare parts, filters for agricultural vehicles.

A b s t r a c t

This paper contains presentation of problems of securing demand for spare parts for agricultural vehicles. Tasks carried out by a distribution and service company, which is the authorized dealer in the sector of agriculture service, have been characterized. The research was conducted for the group of parts including filters of: fuel, engine oil, oil for hydraulic system and gear box for JOHN DEERE agricultural vehicles. Selected parts were cyclically sold in connection with a change during the realization of technical inspections and post-technical inspections. The cycle of the conducted research encompassed the years 2003–2010. The research was carried out in the service department of the authorized dealer of agricultural vehicles of the DEERE & Company concern. The analysis of the number of sold filters in monthly, quarterly and annual arrangement was presented. The research results were statistically analyzed using the R program (v. 2.14.1.). The trend, random fluctuations and seasonal fluctuations for the series of monthly observations were determined. The analysis of the impact of works and agritechnical measures on demand for filters for agricultural vehicles was conducted.

Introduction

An increase in the competition on the market of farm vehicles and machines, reinforced by Poland's accession to the European Union, has caused intensive actions aimed at optimising the quality of customer service. Apart from the quality of offered products and their price, the ability to satisfy the clients' needs has become a dominant element of enterprise strategies. Recognising the expectations and preferences of future product users was carried out in order to develop procedures and satisfy the users' requirements through systemic solutions in the area of marketing logistics. Customer service, both in the pre-transaction and post-transaction mode, was modelled in such a way as

to meet the users' needs in the aspect of time, reliability, information exchange and convenience (CYPLIK et al. 2008, FRANKOWSKA, JEDLIŃSKI 2011, WOJCIECHOWSKI 2007).

Actions performed within distribution logistics include securing the demand of agricultural holdings in a wide range of fixed assets and their comprehensive servicing. According to market standards, the client requires the functional efficiency of products to be secured, and one of the conditions is the lack of time limits, quantitative and type restrictions in the implementation of spare parts purchase. The problem of financial encumbrances connected with the purchase of parts necessary for periodic servicing causes a considerable temporal variability of inspections, both within the warranty and post-warranty period. Authorised dealers conducting trade and services activity in the sector of services for agriculture implement strategies of long-term cooperation with vehicle users. Extending the distribution offer, they conduct comprehensive servicing involving check-ups and repairs of products made by particular producers according to the currently valid technical conditions (JUŚCIŃSKI, PIEKARSKI 2009e, RYBACKI 2011, SKROBACKI, EKIELSKI 2012).

The research problem

Securing the continuity of supplies of original spare parts, accessories and operation liquids was assumed as a standard on the distribution market of farm vehicles and machines. A specific feature of spare parts distribution is the possibility of establishing periodic contacts with the users of the products. In a long-term perspective, including the whole life cycle of a vehicle, the users need a wide range of elements for subsets and functional blocks. The sale of spare parts at present constitutes an important item in the income structure of distribution and services companies. Moreover, the sale of spare parts is an element stimulating the demand for servicing carried out by enterprises. Dealers, aware of the extensive market offer in the industry and mail order available to all users, make attempts to strengthen their market position among others by reducing costs within the outsourcing method (JUŚCIŃSKI 2011, JUŚCIŃSKI, PIEKARSKI 2009a, 2009b).

The issue of access to the group of spare parts with a significant and regular demand, which applies to filters for farm vehicles, is an important subject in the area of distribution logistics. The level and distribution of demand throughout the calendar year constitutes a significant problem in creating delivery schedules from plant warehouses.

The aim of the conducted research was to determine the quantitative structure of demand for the selected group of filters for JOHN DEERE

agricultural vehicles over a span of a calendar year and statistical analysis of demand by determining the trend, random fluctuations and seasonal fluctuations for the series of monthly observations.

The object of the survey was the authorised dealer of farm vehicles and machines dealing both with spare parts distribution and comprehensive servicing. The selected enterprise for over two decades conducts activities in the sector of services for agriculture in central-eastern area of Poland.

In the years 2003–2010 a selected group of spare parts was subject to the survey and analysis, including the following filters: fuel filter, engine oil filter, oil filter for hydraulic system and wheel case, used in vehicles produced by the DEERE & Company concern. The filters were selected for the survey because they constitute a specific group which, according to the producer's recommendation, are periodically replaced during warranty and post-warranty inspections of farm vehicles. It should be emphasised that trade and services enterprises are interested in connecting filter sale transactions with an inspection at a company service station.

The demand for inspections in the warranty and post-warranty period shows considerable variability in particular months of the year, which is determined by the method of using farm vehicles. A dominant group of vehicles are tractors used in field operations and work and for transporting agricultural produce. Such a model of operation in private holdings results in a relatively short period of intensive use of tractors, limited to agritechnical periods. Only tractors used in holdings as front-end loaders are characterised with longer and more evenly distributed periods of operation within a year.

The results of the survey of sales in the Sales Department in the years 2003–2010

The survey lasted eight years and includes the sales structure of 7393 filters for JOHN DEERE farm vehicles.

The distribution of demand between the following filters: fuel filter, engine oil filter, oil filter for hydraulic system and wheel case, used in the years 2003–2010 is presented in the histogram (Fig. 1). It should be emphasised that the first survey year was the second season of authorised sales of JOHN DEERE farm vehicles and spare parts by the given dealer.

In 2003 158 filters were sold. The demand in quarterly terms showed an upward tendency within the first three quarters. The demand at the beginning of the year was at a minimum level, and sales reached a maximum in the third quarter (Tab. 1). The lowest numbers of filters were purchased in January, February and March, and the largest numbers of purchases were recorded in August and September.

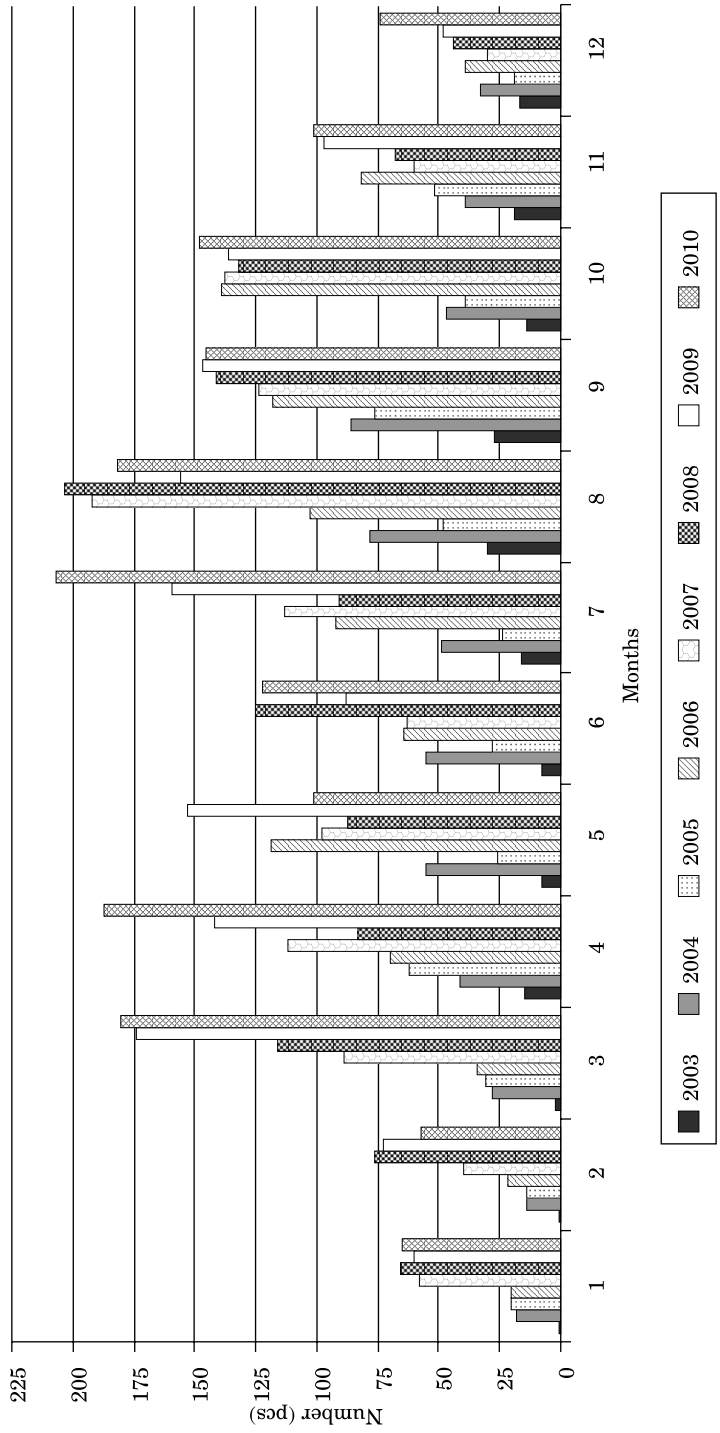

Fig. 1. The distribution of filters for farm vehicles from the surveyed group purchased in the years 2003–2010
Source: The author's own study

In 2004 users purchased 543 filters. The lowest demand was recorded in January and February. The sales of parts included in the survey were the lowest in August and September. The periodic analysis confirmed the upward tendency until the third quarter inclusive, when the maximum level of demand for the surveyed spare parts was recorded. In a year-on-year comparison an increase in sales amounted to as much as 243.6%.

In 2005 439 filters were purchased. In relation to the previous year, a decrease of 19.2% occurred. The lowest demand was recorded in January, February and December. The highest level of sales occurred in April and September. The maximum number of spare parts from the analysed group was purchased in the third quarter of the surveyed year.

Table 1

The sales structure of John Deere filters for far vehicles in the years 2003–2010

No.	The time of sales	Years [%]							
		2003	2004	2005	2006	2007	2008	2009	2010
1	I quarter	2.5	11.1	14.8	8.4	16.7	20.9	21.4	19.3
2	II quarter	19.6	27.8	26.4	28.1	24.5	24.0	26.7	26.1
3	III quarter	46.2	39.2	33.7	34.7	38.4	35.3	32.3	34.0
4	IV quarter	31.7	21.9	25.1	28.8	20.4	19.8	19.6	20.6
Total		100.0	100.0	100.0	100.0	100.0	100.0	100.0	100.0

In 2006 the Sales Department sold 902 filters. A minimum demand in quarterly terms was recorded at the beginning of the year, and the highest in the third quarter. In relation to the previous year, an increase in sales of 105.5% was recorded. The lowest demand for filters was in January and February, and the highest in May, September and October.

In 2007 the sales of 1117 filters was carried out. The quarterly demand was the lowest at the beginning of the year, and the highest in the third quarter. In comparison to the previous year, the sales increased by 23.8%. The lowest demand was identified in January and December, and the highest in August, September and October.

In 2008 vehicles users purchased 1232 filters. The lowest volume of purchases was recorded in January, November and December, and the highest in August and September. The analysis in quarterly terms showed a comparably low demand at the beginning and end of the year, and a maximum demand in the third quarter. In the year-on-year terms, an increase in transactions of 10.3% was recorded.

In 2009 1433 filters were sold. A low periodic demand was at the beginning and end of the year, and a maximum level of sales was reached by the Sales

Department in the third quarter. The lowest demand for parts subject to the survey was recorded in January, February and December, and the highest in March, May, August and September. In comparison to the previous year, the sales increased by 16.3%.

In 2010 clients purchased 1569 filters. The analysis in quarterly terms showed a comparably low demand at the beginning and end of the year, and a maximum demand in the third quarter. The demand for filters was the lowest in January, February and December, and the highest in March, April, July and August. In relation to the previous year, the sales increased by 9.5%.

The statistical analysis of filter sales in the years 2003–2010

The numbers of fuel filters, engine oil filters, oil filters for hydraulic system and wheel case were arranged in the form of monthly observations. They formed time series Y_t, subject to statistical analysis in order to assess the surveyed phenomenon in the distribution process. Changes in the structure of demand for filters were analysed in the aspect of work and operations applied in agriculture within a calendar year. The random variables obtained in the survey were subject to temporal sequencing in order to determine the trend, and random and seasonal fluctuations. The equalization of time series was done by using the method of aligned movable means. The lengths of moveable periods for the agricultural sector were $d = 12$. The analysis of sales filters was carried out with the use of the multiplicative model of time series components, which presents the correlation (ACZEL, SOUNDERPANDIAN 2008, PUŁASKA-TURYNA 2008):

$$Y_t = T_t \cdot S_t \cdot C_t \cdot I_t \tag{1}$$

where:
Y_t – the value of the series,
T_t – the trend of the series,
S_t – seasonal fluctuations,
C_t – cyclical fluctuations,
I_t – random fluctuations.

The times series consists of $t = 1, 2,..., 96$ observations in respective months $i = 1,..., 12$ for eight consecutive years of the conducted research.

The value of centred moving average $\bar{y}_{t_i}^{(d)}$ for the time series is described in the formula:

$$\bar{y}_{t_i}^{(d)} = \frac{1}{d}\left(\frac{1}{2}y_{t_i-\frac{d}{2}} + \sum_{t_i-t_0}^{t_i+t_0} y_{ti} + \frac{1}{2}y_{t_i+\frac{d}{2}}\right), \qquad t_0 = \frac{d}{2} - 1 \tag{2}$$

where:
y_{t_i} – empirical values of the series (the number of sold filters),
d – the length of the movable period, $d = 12$.

A matrix was created for the quotient of the empirical values of the series and aligned moveable means, in which the lines i are respective months and columns n are years of the conducted research. The index of average seasonalness of the particular i month is presented by the interrelation:

$$O_i = \frac{1}{c}\sum_{n=1}^{c}\frac{y_{t_m}}{\bar{y}_{t_m}^{(d)}} \cdot 100\ \mathrm{WK}^{(M)} \tag{3}$$

where:
n – the number of years of the conducted research $n = 1, ..., 8$;
c – the number of cycles of periodicity, $c = n - 1$
$\mathrm{WK}^{(M)}$ – the average multiplicative adjustment index to obtain $\sum_{i=1}^{12} O_i = 1200$.

The average multiplicative adjustment index was calculated on the basis of the formula:

$$\mathrm{WK}^{(M)} = \frac{1200}{\frac{1}{c}\sum_{n=1}^{c}\frac{y_{t_m}}{\bar{y}_{t_m}^{(d)}} \cdot 100} \tag{4}$$

The value of random fluctuations for the multiplicative is defined by the equation:

$$y_{t_i(\mathrm{skor})}^{(M)} = \frac{y_{t_i}}{O_i} \cdot 100 \tag{5}$$

For the surveyed series, the trend $\hat{y}_t^{(M)}$ was determined by using the weighted 5-period average according to the formula:

$$\hat{y}_{t_i}^{(M)} = \bar{y}_{t_i}^{(5)(M)} = \frac{1}{9}\sum_{t_i-2}^{t_i+2} y_{t_i(\mathrm{skor})}^{(M)} \cdot w_j \qquad \text{for } [w_j] = \begin{bmatrix}1\\2\\3\\2\\1\end{bmatrix} \tag{6}$$

Seasonal indices have an average value equal to 100%, which is a reference in the graphic analysis of the influence of seasonal fluctuations on the distribution of the set of variables. The statistical analysis of the sales of filters for farm vehicles was performed with the use of the R program, version 2.14.1 (CRAWLEY 2008, WALESIAK, GATNAR 2009).

Statistical analysis: the trend, random and seasonal fluctuations

The sales structure of filters subject to replacement during technical inspections of farm tractors in the years 2003–2010 had a variable structure (Fig. 1). The performed analysis of purchases provides grounds for formulating a thesis on the growing demand, with a simultaneous considerable differences in demand within each surveyed year. The level of demand from vehicle users had different values in the period of subsequent quarters of the year. The general rules was a lowered sales at the beginning and end of each year and a dynamic increase in demand in the third quarter. A comparison of the year-on-year sales results showed a rise in the number of filters purchased in most surveyed years.

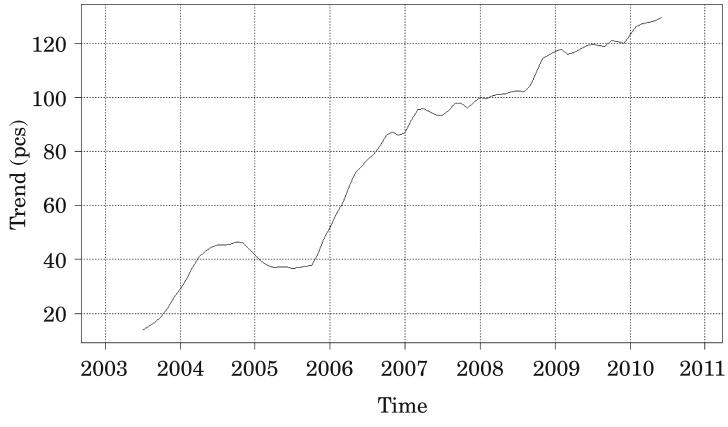

Fig. 2. The trend of the number of filters for farm vehicles sold from the group subject to the survey in the years 2003–2010

Source: The author's own study

Carrying out eight-year surveys of the distribution activities made it possible to define the trend which constitutes a graphic characterisation of long-term changes on the sales market relating to the selected group of filters for farm vehicles (Fig. 2). From 2003 to the third quarter of 2004, the trend was

increasing. At the turn of 2005 the trend decreased and the demand came to a standstill. From the fourth quarter of 2005 to the end of 2006, a trend with a high growth dynamics occurred. In the period from 2007 to 2010 a trend with a variable structure was recorded. The subsequent quarters saw a growing trend interchanging with periodic declines. Despite the trend adjustments, systematic growth was maintained and the maximum value was reached at the end of the surveyed period.

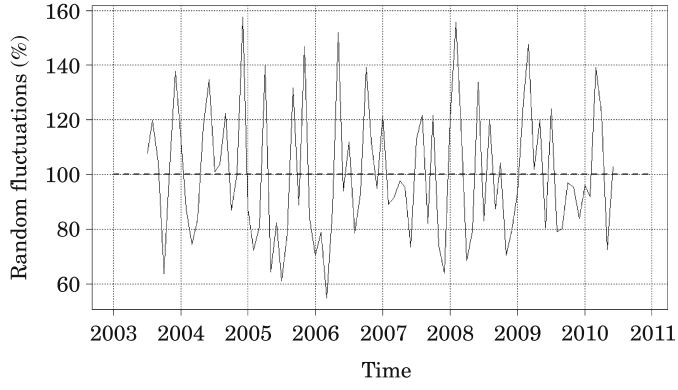

Fig. 3. The trend of the number of filters for farm vehicles sold from the group subject to the survey in the years 2003–2010

Source: The author's own study

The volume of demand changes for filters is presented in Fig. 3. The random fluctuations distinguished from the time series of filters sold make it possible to describe the variability of demand in the analysed market in particular months of subsequent years. The recorded changes reflect the dynamic increases of demand for the spare parts subject to the survey and the frequently occurring declines of demand. The course of changes in the years 2003–2010 is a proof of the unstable level of demand for filters from the surveyed group generated by farm vehicle owners. The highest value of random fluctuations occurred in 2005, 2006 and 2008.

The tasks carried out by distribution logistics require the preparation of a delivery schedule of spare parts. Random fluctuations occurring in filter purchases cause the changes in demand to reach minimum and maximum value in various months for particular years, which hinder the planning and carrying out of deliveries.

Eliminating the trend as well as cyclical and random fluctuations from the time series of the number of filters for farm vehicles sold made it possible to define the value of seasonal indices for several months in a year (Fig. 4).

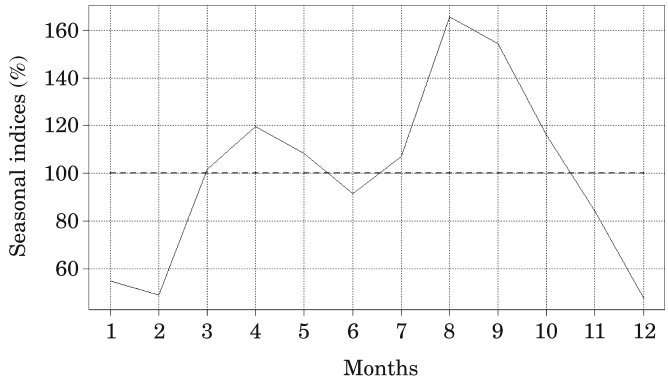

Fig. 4. The seasonal indices for the number of filters for farm vehicles sold from the group subject to the survey in the years 2003–2010
Source: The author's own study

Seasonal fluctuations influence the level of filter sales. In January and February, when field agrotechnical operations are not carried out, the number of filters sold was lower from the reference level by 45.1% and 50.9% respectively. The start of the season of farm vehicles use in March causes an increase of seasonal indices to the level by 1.6% higher than the reference level. As a result of seasonal fluctuation in April and May, the demand for the analysed spare parts grew above the average level by 19.7% i 8.3% respectively. The completion of spring field work coincided with a decline in the demand for filters by 8.4% below the reference level. The intensive operation of farm vehicles during harvest and collecting root crops generates demand for technical inspections. After a specific number of hours of operation it is necessary to replace the filters. Seasonal values cause that in July, August, September and October the indices reached a value below average, i.e. 7.1%, 65.5%, 54.2% and 16.0% respectively. In November and December, a high decrease in demand for parts was recorded, and seasonal indices were lower from the reference level by 15.8% and 52.3% respectively (JUŚCIŃSKI, PIEKARSKI 2008b, 2009c, KARCZMARCZYK 2005).

Conclusions

The sales of selected parts, for the group including filters of: fuel, engine oil, oil for hydraulic system and gear box for JOHN DEERE agricultural vehicles, displayed a growth dynamics at the level from several to several hundred percent in a year-on-year terms in as many as six surveyed periods. A comparison of the structure of demand for filters in annual terms for the years in

question from the beginning and end of the surveyed period showed an increase in demand by as many as ten times.

The sales structure of filters in quarterly terms indicated the lowest demand at the beginning and end of the year. An increase in the sales occurred in the second quarter, to reach a maximum in the third quarter of each surveyed year. This resulted in the implementation of warranty and post-warranty servicing inspections for the whole population of vehicles in the surveyed region. The servicing of tractors was carried out directly before using them for field work or right after intensive operation as a source of motive power for machines or traction energy.

The trend identified during the statistical analysis of the sales of filters for farm vehicles varied within the surveyed period. Years with an extensive increasing trend were dominant, and declines in demand did not last long. The value and dynamics of trend changes should be further analysed in order to develop systemic solutions for creating delivery schedules for distribution logistics. Getting to know the characteristics of demand for filters may constitute an additional source of information for planning the work in the company sales department providing technical servicing of farm vehicles.

The distribution of values of seasonal indices provides grounds for a hypothesis concerning the significant influence of the agritechnical work and operations on cyclical changes in demand for farm vehicles filters. The result of seasonal fluctuations is a high decline in demand for filters in the first and the last months of the year when field works are not carried out. A maximum increase of demand due to seasonal fluctuations occurs at the time of harvest and work in the field in autumn.

The statistical analysis of demand for filters was confirmed by the existence of considerable random fluctuations influencing the level of time series indices. The step increase of demand for filters selected to the survey requires the application of effective and efficient distribution systems or maintaining increased stocks. The phenomenon of unstable demand for selected spare part is a source of a number of organisational problems in managing the distribution chain.

The research on demand for filters of fuel, engine oil, hydraulic system oil and gear box oil and other groups of spare parts should be continued in a long period of time. Knowing the type structure and quantitative structure of the demand for spare parts for various brands of agricultural vehicles and machines will allow to optimizing processes in the logistics of the spare parts distribution.

Translated by AUTHOR

Accepted for print 19.09.2012

References

ACZEL A.D., SOUNDERPANDIAN J. 2008. *Complete Business Statistics*. 7th ed. Richard D. Irwin/McGraw-Hill, Boston.

Agrotechnika roślin uprawnych. 2005. Ed. S. Karczmarczyk. Wyd. Akademii Rolniczej w Szczecinie.

CRAWLEY M. J. 2008. *The R book*. John Wiley & Sons Ltd., Chichester.

CYPLIK P., GŁOWACKA D., FERTSCH M. 2008. *Logistyka przedsiębiorstw dystrybucyjnych*. Wyd. Wyższa Szkoła Logistyki, Poznań.

FRANKOWSKA M., JEDLIŃSKI M. 2011. *Efektywność systemu dystrybucji*. Wyd. Polskie Wydawnictwo Ekonomiczne, Warszawa.

JUŚCIŃSKI S. 2011. *Outsourcing in logistics management, Scientific Monograph*. Wyd. Polihymnia, Lublin.

JUŚCIŃSKI S., PIEKARSKI W. 2008a. *Systemy logistyczne w procesie zarządzania dystrybucją ciągników i maszyn rolniczych*. Acta Agrophisica, 12(1): 113–124.

JUŚCIŃSKI S., PIEKARSKI W. 2008b. *An analysis of farm tractors sales results in the aspect of the calendar of agrotechnical operations*. Technical Sciences, 11: 47–58.

JUŚCIŃSKI S., PIEKARSKI W. 2009a. *Outsourcing as a logistics function in distribution of spare parts for tractors and farm machines*. Maintenance and Reliability, 1(41): 54–62.

JUŚCIŃSKI S., PIEKARSKI W. 2009b. *An analysis of a supply process of spare parts for agricultural tractors and machines based on logistic services outsourcing*. Maintenance and Reliability, 2(42): 63–70.

JUŚCIŃSKI S., PIEKARSKI W. 2009c. *The analysis of sale results of selected group of tractors spare parts*. Journal of Research and Applications in Agricultural Engineering, 54(2): 57–62.

JUŚCIŃSKI S., PIEKARSKI W. 2009d. *Badanie statystyczne struktury popytu dla wybranej grupy części zamiennych do ciągników rolniczych*. Annales Universitatis Mariae Curie-Skłodowska, Sectio E, Agricultura, 64(4): 39–46.

JUŚCIŃSKI S., PIEKARSKI W. 2009e. *Systemy zarządzania logistycznego w przedsiębiorstwie prowadzącym autoryzowaną dystrybucję pojazdów i maszyn rolniczych*. Zarządzanie Przedsiębiorstwem, 2: 42–48.

PUŁASKA-TURYNA B. 2008. *Statystyka dla ekonomistów*. Wyd. Difin, Warszawa.

RYBACKI P., DURCZAK K., 2011. *Ocena jakości serwisu technicznego maszyn rolniczych*. Inżynieria Rolnicza, 9(134): 201–205.

SKROBACKI A., EKIELSKI A. 2012. *Pojazdy i ciągniki rolnicze*. Wyd. Wieś Jutra, Warszawa.

WALESIAK M., GATNAR E. 2009. *Statystyczna analiza danych z wykorzystaniem programu R*. Wyd. Naukowe PWN, Warszawa.

WOJCIECHOWSKI T. 2007. *Marketingowo-logistyczne zarządzanie przedsiębiorstwem* Wyd. Difin, Warszawa 2007.

TECHNICAL SCIENCES
Abbrev.: Techn. Sc., No 15(2), Y 2012

DETERMINATION OF SHAPE FACTORS AND VOLUME COEFFICIENTS OF SEEDS FROM SELECTED CONIFEROUS TREES

***Zdzisław Kaliniewicz*[1], *Paweł Tylek*[2], *Piotr Markowski*[1], *Andrzej Anders*[1], *Tadeusz Rawa*[1], *Michał Zadrożny*[1]**

[1] Department of Heavy Duty Machines and Research Metodology
University of Warmia and Mazury in Olsztyn
[2] Department of Mechanisation of Forest Works
University of Agriculture in Krakow

K e y w o r d s: seeds, shape factor, volume, geometric shape.

A b s t r a c t

The thickness, width and length of seeds from selected coniferous trees was measured. The obtained data was used to determine six shape factors (as proposed by Grochowicz, Mohsenin, Donev and Wróbel). The seeds were assigned nine simple geometric shapes, and the total volume of seeds from a given tree species was compared using a pycnometer. Based on the results, a geometric model of seed volume was selected for every analyzed species. It was concluded that the shape of seeds from coniferous trees can be described with the application of shape factors proposed by Mohsenin, Donev and Wróbel, used interchangeably or collectively. The volume of seeds from coniferous trees can be modeled with the use of an ellipsoid for Scots pine, European black pine, Norway spruce and English yew seeds, and a double right quadrangular pyramid for silver fir and Douglas-fir seeds.

Symbols:

d_w, d_z – equivalent diameter of basic seed dimensions, mm,
k – coefficient of seed volume,
k_{Mi} – volume coefficient of the i^{th} seed model,
K_m, K_w – Grochowicz's shape factors,
S – standard deviation of trait,
S_n – Mohsenin's shape factor,
T, W, L – seed thickness, width and length, mm,
V – seed volume, mm^3,
V_{Mi} – volume of the i^{th} geometric model, mm^3,
V_p – total volume of seed sample, mm^3,
x – average value of trait,
x_{max} – maximum value of trait,
x_{min} – minimum value of trait,
α, β – Donev's shape factors,
α_w – Wróbel's shape factor.

Introduction

The seeds of coniferous trees are characterized by considerable variation in dimensions. Their size is determined by the type of habitat and soil on which trees grow, atmospheric conditions during cone and seed development, genetic traits, geographic location of trees and the position of cones in the tree crown (MURAT 2002, *Nasiennictwo leśnych drzew*... 1995, SIVACIOGLU, AYAN 2010, TURNA, GÜNEY 2009). Shape is also a distinguishing feature of seeds. The above parameters are used in the process of cleaning and sorting seeds (GROCHOWICZ 1994).

The shape of seeds is described with the use of corresponding shape factors. In a simplified evaluation method, the geometric shape most closely resembling the analyzed seed is chosen (FRĄCZEK, WRÓBEL 2006). Detailed evaluations rely on virtual models which are developed with the use of parametric equations or by modeling real objects in virtual space (JAIN, BAL 1997, FRĄCZEK, WRÓBEL 2006, 2009, MABILLE, ABECASSIS 2003, MIESZKALSKI, SOŁODUCHA 2008). The above methods preserve shape features characteristic of a given species, nevertheless, they require specialist applications, and they are not popularly used.

The objective of this study was to determine the values of shape factors describing seeds of selected coniferous tree species, to analyze correlations between those values, and to select simple geometric shapes that best model seed volume.

Materials and Methods

The experimental materials consisted of seeds from the following coniferous tree species: Scots pine, European black pine, Norway spruce, European larch, silver fir, Douglas-fir and English yew (Fig. 1). The seeds of the Scots pine, European black pine, Norway spruce and European larch were harvested from the following stands entered into the National Register of Approved Basic Material:

a) MP/3/41008/05 (category of forest reproductive material – qualified, type – plantation, region of provenance – 253, municipality – Mały Płock (22.04°E, 53.18°N), forest habitat – fresh mixed coniferous forest, age – 15, 20 years),

b) MP/3/41225/05 (category of forest reproductive material – qualified, type – plantation, region of provenance – 157, municipality – Gardeja (18.54°E, 53.40°N), forest habitat – fresh mixed broadleaved forest, age – 19 years),

c) MP/1/46879/06 (category of forest reproductive material – source identified, type – tree stand, region of provenance – 205, municipality – Purda (20.41°E, 53.39°N), forest habitat – fresh mixed coniferous forest, age – 86 years),

d) MP/2/30944/05 (category of forest reproductive material – selected, type – tree stand, region of provenance – 202, municipality – Kowale Oleckie (22.15°E, 54.06°N), forest habitat – fresh mixed broadleaved forest, age – 129 years).

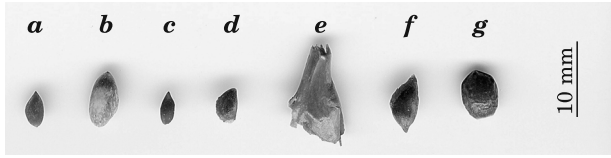

Fig. 1. Seeds of coniferous trees: *a* – Scots pine, *b* – European black pine, *c* – Norway spruce, *d* – European larch, *e* – silver fir, *f* – Douglas-fir, *g* – English yew

The seeds of the remaining species were supplied by Florpak Sp. z o.o., Branch in Młynki, Końskowola. The seeds were collected from the following areas:

a) silver fir – commune Mykanów (19.09°E, 50.59°N),

b) Douglas-fir – commune Ujsoły (19.11°E, 49.27°N),

c) English yew – commune Mogilno (17.96°E, 52.65°N).

To determine the dimensions of each seed species, the material was spread on a table and divided by halving (*Nasiennictwo leśnych drzew...* 1995) to obtain samples of more than 100 seeds each. The above method produced samples with the following size: Scots pine – 106 seeds, European black pine – 124, Norway spruce – 113, European larch – 109, silver fir – 122, Douglas-fir – 121, English yew – 125.

Seed dimensions were determined using the MWM 2325 workshop microscope and a dial indicator device, as described by Kaliniewicz (KALINIEWICZ et al. 2011).

The following shape factors were calculated:

a) Grochowicz's shape factors (1994):

$$K_m = \frac{W}{L} \tag{1}$$

$$K_w = \frac{T}{L} \tag{2}$$

b) Mohsenin's shape factor (1986):

$$S_n = \sqrt[3]{\frac{T \cdot W}{L^2}} = \frac{(T \cdot W \cdot L)^{\frac{1}{3}}}{L} \tag{3}$$

c) Donev's shape factors (DONEV et al. 2004):

$$\alpha = \frac{L}{T} \tag{4}$$

$$\beta = \frac{W}{T} \tag{5}$$

d) Wróbel's shape factor (2006):

$$\alpha_w = \frac{2 \cdot L}{T + W} \tag{6}$$

The correlations between Donev's and Wróbel's shape factors were determined on the assumption that the axis of rotation and seed length overlap, and the remaining two dimensions correspond to seed width and thickness.

The volume of all seeds in the sample (V_p) was calculated using a 25 cm^3 pycnometer equipped with a thermometer and a capillary tube. Based on seed volume and dimensions, the value of the seed volume coefficient was calculated using the below formula:

$$k = \frac{V_p}{\Sigma T \cdot W \cdot L} \tag{7}$$

We assumed that the shape of seeds could be modeled by geometric shapes whose volume is equivalent to the volume of the analyzed seeds. The following geometric models were considered (Fig. 2): sphere ($M1$), cylinder ($M2$), spheroid ($M3$), ellipsoid ($M4$), cuboid ($M5$), right triangular prism ($M6$), double cone ($M7$), double quadrangular pyramid ($M8$) and double triangular pyramid ($M9$). The volume of the above geometric shapes was determined based on the following general formulas:

$$V_{M1} = \frac{\pi \cdot d_w^3}{6} \tag{8}$$

$$V_{M2} = \frac{\pi \cdot d_z^2 \cdot L}{4} \tag{9}$$

$$V_{M3} = \frac{\pi \cdot d_z^2 \cdot L}{6} \tag{10}$$

$$V_{M4} = \frac{\pi \cdot T \cdot W \cdot L}{6} \tag{11}$$

$$\mathrm{V_{M5}} = T \cdot W \cdot L \tag{12}$$

$$V_{M6} = \frac{T \cdot W \cdot L}{2} \tag{13}$$

$$V_{M7} = \frac{\pi \cdot d_z^2 \cdot L}{12} \tag{14}$$

$$V_{M8} = \frac{T \cdot W \cdot L}{3} \tag{15}$$

$$V_{M9} = \frac{T \cdot W \cdot L}{6} \tag{16}$$

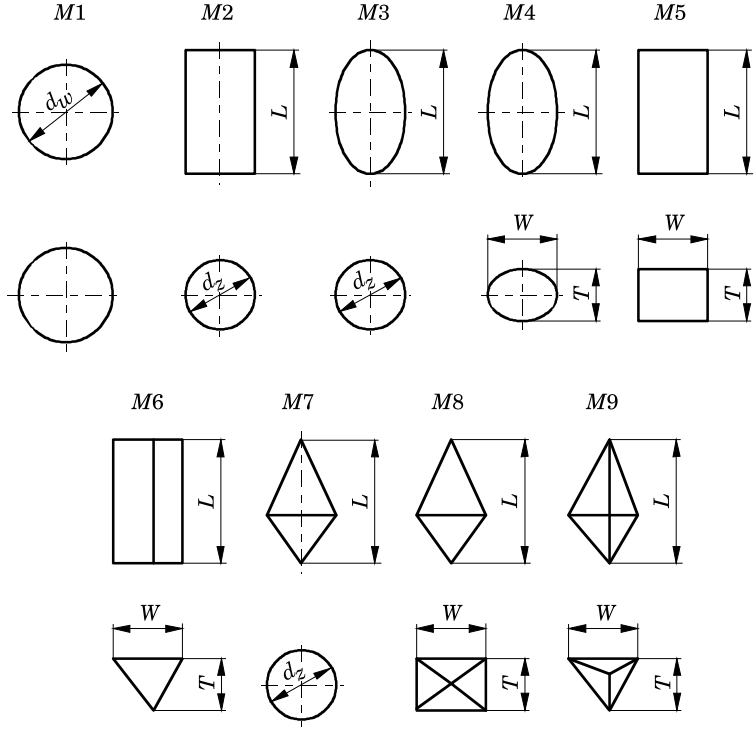

Fig. 2. Geometric shape models: *M*1 – sphere, *M*2 – cylinder, *M*3 – spheroid, *M*4 – ellipsoid, *M*5 – cuboid, *M*6 – right triangular prism, *M*7 – double cone, *M*8 – double quadrangular pyramid, *M*9 – double triangular pyramid

Geometric shapes were selected depending on whether their volume could be calculated with the use of three basic geometric dimensions: the thickness, width and length of modeled particles. Equivalent diameters in models $M1$, $M2$, $M3$ and $M7$ were determined based on the below formulas (GROCHOWICZ 1994):

$$d_w = \frac{T + W + L}{3} \tag{17}$$

$$d_z = \frac{T + W}{2} \tag{18}$$

In models $M7$, $M8$ and $M9$, the location of the largest cross-section was not significant because it did not affect seed volume. In extreme cases, the above models can take on the form of an individual shape, such as a cone, a quadrangular pyramid or a triangular pyramid.

The volume coefficients of the geometric models of different seed species were determined using the following formula:

$$k_{Mi} = \frac{V_{Mi}}{T \cdot W \cdot L} \tag{19}$$

The results were processed statistically by analysis of variance and correlation analysis, using Winstat and Statistica software.

Results and Discussion

The statistical parameters describing the distribution of seed dimensions are presented in Table 1. The seeds of the English yew were characterized by the lowest dimensional variation (coefficient of variation did not exceed 7.3). The highest coefficient of variation was observed with regard to the width of silver fir seeds (15.5). The range of variations corresponds to the dimensional characteristics of seeds harvested in Poland (CZERNIK 1983, *Nasiennictwo leśnych drzew*... 1995, TYLEK 1998, 2004, 2005). The thickness of seeds from various tree species varied between 0.95 mm (European larch) to 4.78 mm (English yew), seed width – from 1.76 mm (European larch) to 8.01 mm (silver fir), and length – between 3.10 mm (European larch) to 14.18 (silver fir). Based on their average dimensions, seeds were classified in ascending order:

a) seed thickness – European larch, Scots pine, Norway spruce, Douglas-fir, European black pine, silver fir, European yew,

b) seed width – Norway spruce, Scots pine, European larch, European black pine, Douglas-fir, English yew, silver fir,

c) seed length – Norway spruce, Scots pine, European larch, European black pine, English yew, Douglas-fir, silver fir.

Table 1

Statistical parameters describing the distribution of seed dimensions

Seed species	Dimension	x_{min}	x_{max}	x	S	V_s
Scots pine	T	1.09	1.80	1.45^{f}	0.142	9.78
	W	1.88	3.00	2.50^{e}	0.241	9.63
	L	3.22	5.31	4.19^{e}	0.416	9.92
European black pine	T	1.92	3.19	2.46^{c}	0.214	8.69
	W	2.37	4.47	3.43^{c}	0.385	11.22
	L	4.83	8.36	6.46^{c}	0.582	9.00
Norway spruce	T	1.13	1.92	1.53^{e}	0.149	9.70
	W	1.77	3.01	2.25^{f}	0.260	11.57
	L	3.21	5.39	4.15^{e}	0.439	10.59
European larch	T	0.95	1.82	1.37^{g}	0.156	11.37
	W	1.76	3.34	2.62^{d}	0.325	12.38
	L	3.10	5.38	4.36^{d}	0.528	12.10
Silver fir	T	2.17	4.24	3.22^{b}	0.393	12.23
	W	3.53	8.01	5.53^{a}	0.857	15.50
	L	5.89	14.18	10.82^{a}	1.123	10.38
Douglas-fir	T	1.44	2.52	1.83^{d}	0.170	9.29
	W	2.80	4.63	3.49^{c}	0.346	9.91
	L	5.24	8.60	6.93^{b}	0.624	9.00
English yew	T	3.45	4.78	4.05^{a}	0.295	7.29
	W	3.64	5.49	4.67^{b}	0.315	6.74
	L	5.55	7.62	6.62^{c}	0.416	6.28

$^{a, b, c, d, e, f, g}$ – different lowercase letters in the superscript indicate significant differences at a level of 0.05
Source: own calculations

The average values of seed dimensions reported in this study are similar to those cited in literature (BURACZYK 2010, CZERNIK 1983, *Nasiennictwo leśnych drzew...* 1995, SIVACIOGLU, AYAN 2010, TYLEK 1998). An analysis of variance revealed significant differences between the dimensions of the analyzed seed species. Significant differences were not observed only with regard to the width of European black pine and Douglas-fir seeds, the length of Scots pine and Norway spruce seeds, and the length of European black pine and English yew seeds.

The statistical parameters describing the distribution of seed shape factors are shown in Table 2. The lowest spread of shape factor values was noted for S_n in all cases, and the highest spread was reported in respect of:

a) shape factor K_m – Norway spruce and English yew seeds,

b) shape factor K_w – Scots pine and European larch seeds,

c) shape factor β – European black pine, silver fir and Douglas-fir seeds.

Table 2

Statistical parameters describing the distribution of seed shape factors

Seed species	Shape factor	x_{min}	x_{max}	x	S	V_s
Scots pine	K_m	0.385	0.860	0.600^b	0.063	10.47
	K_w	0.250	0.512	0.349^d	0.042	11.97
	S_n	0.458	0.761	0.593^b	0.041	6.97
	α	1.952	4.008	2.910^d	0.346	11.89
	β	1.413	2.304	1.730^b	0.145	8.40
	α_w	1.457	3.151	2.131^d	0.222	10.42
European black pine	K_m	0.315	0.686	0.533^c	0.059	10.97
	K_w	0.281	0.507	0.383^b	0.043	11.18
	S_n	0.453	0.690	0.588^b	0.037	6.35
	α	1.971	3.557	2.646^e	0.300	11.32
	β	1.019	2.117	1.404^d	0.167	11.87
	α_w	1.732	3.273	2.204^c	0.222	10.07
Norway spruce	K_m	0.379	0.790	0.547^c	0.075	13.75
	K_w	0.296	0.454	0.371^c	0.037	9.95
	S_n	0.490	0.690	0.587^b	0.041	7.01
	α	2.201	3.383	2.719^e	0.265	9.75
	β	1.142	1.983	1.475^c	0.165	11.16
	α_w	1.677	2.890	2.204^c	0.239	10.85
European larch	K_m	0.478	0.929	0.604^b	0.066	10.93
	K_w	0.229	0.423	0.316^e	0.038	12.04
	S_n	0.493	0.732	0.575^c	0.038	6.54
	α	2.365	4.368	3.205^c	0.375	11.71
	β	1.450	2.432	1.926^a	0.223	11.58
	α_w	1.480	2.742	2.192^c	0.201	9.19
Silver fir	K_m	0.288	0.956	0.515^d	0.089	17.25
	K_w	0.181	0.535	0.299^f	0.041	13.61
	S_n	0.414	0.800	0.534^d	0.044	8.30
	α	1.870	5.539	3.398^b	0.447	13.17
	β	1.017	2.964	1.741^b	0.323	18.56
	α_w	1.342	3.541	2.495^b	0.313	12.53
Douglas-fir	K_m	0.373	0.734	0.506^d	0.053	10.44
	K_w	0.199	0.377	0.266^g	0.032	12.02
	S_n	0.430	0.627	0.512^e	0.032	6.21
	α	2.655	5.036	3.805^a	0.445	11.68
	β	1.512	2.660	1.918^a	0.237	12.37
	α_w	1.869	3.413	2.610^a	0.234	8.97
English yew	K_m	0.549	0.886	0.708^a	0.065	9.14
	K_w	0.502	0.776	0.614^a	0.051	8.39
	S_n	0.659	0.872	0.757^a	0.041	5.37
	α	1.306	1.992	1.640^f	0.135	8.22
	β	1.000	1.319	1.155^e	0.078	6.76
	α_w	1.226	1.870	1.523^e	0.123	8.08

$^{a, b, c, d, e, f, g}$ – different lowercase letters in the superscript indicate significant differences at a level of 0.05

Source: own calculations

The investigated seed species were classified in ascending order based on the average values of seed shape factors:

a) shape factor K_m – Douglas-fir, silver fir, European black pine, Norway spruce, Scots pine, European larch, English yew,

b) shape factor K_w – Douglas-fir, silver fir, European larch, Scots pine, Norway spruce, European black pine, English yew,

c) shape factor S_n – Douglas-fir, silver fir, European larch, European black pine, Norway spruce, Scots pine, English yew,

d) shape factor α – English yew, European black pine, Norway spruce, Scots pine, European larch, silver fir, Douglas-fir,

e) shape factor β – English yew, European black pine, Norway spruce, Scots pine, silver fir, Douglas-fir, European larch,

f) shape factor α_w – English yew, Scots pine, European larch, Norway spruce, European black pine, silver fir, Douglas-fir.

The average values of shape factors K_m and K_w for the seeds of Scots pine, Norway spruce, European larch and silver fir are comparable with those reported by CZERNIK (1983) and TYLEK (1998). Homogeneous groups (showing no significant differences between the average values of the analyzed factors) were obtained for the following seed species:

a) shape factor K_m – Scots pine and European larch, European black pine and Norway spruce, silver fir and Douglas-fir,

b) shape factor K_w – deficiency,

c) shape factor S_n – Scots pine, European black pine and Norway spruce,

d) shape factor α – European black pine and Norway spruce,

e) shape factor β – European larch and Douglas-fir, Scots pine and silver fir,

f) shape factor α_w – European black pine, Norway spruce and European larch.

In this experiment, we also set out to determine the shape factor or a group of shape factors that best described the seeds of coniferous trees. Based on Fig. 1 and the results of seed examinations, shape factors should account for:

a) considerable differences between the shape of silver fir seeds and seeds of the remaining tree species,

b) considerable differences between the shape of English yew seeds and seeds of the remaining tree species,

c) minor similarities in the shape of European larch and Douglas-fir seeds,

d) minor similarities in the shape of Scots pine and Norway spruce seeds.

The results of an analysis of variance indicate that the above requirements were not fully met by any of the examined shape factors. Although they satisfied the first two conditions, the shape factors proposed by Grochowicz (K_m and K_w) seemed to be least suited for describing the shape of seeds from

coniferous trees. Grochowicz's shape factors should be primarily used to describe seeds that are polyhedral (FRĄCZEK, WRÓBEL 2006), such as silver fir seeds. In remaining seeds, in particular English yew and European black pine seeds, the axis of rotation and seed length overlap, therefore they could be described with the application of Donev's shape factors (DONEV et al. 2004, FRĄCZEK, WRÓBEL 2006). The above conditions were also partially met by Mohsenin's and Wróbel's shape factors which could be used interchangeably to describe the shape of seeds from coniferous tree species native to Poland.

The results of a correlation analysis of the discussed shape factors are presented in Table 3. The values of Pearson's correlation coefficients are determined by seed species, which implies that the values of different shape factors are not mutually convertible. The most significant correlation was observed between shape factors K_w and α. Relatively significant correlations were noted between Mohsenin's shape factor (S_n) and the factors proposed by Grochowicz (K_m and K_w), Donev (α) and Wróbel (α_w), as well as between the shape factors described by Grochowicz (K_m) and Wróbel (α_w). No significant correlations (except for Norway spruce and silver fir seeds) were found between Donev's shape factor β and the shape factors proposed by Mohsenin (S_n) and Wróbel (α_w).

Table 3

Pearson's coefficients of correlation between seed shape factors

Correlation	Seed species						
	Scots pine[1]	European black pine[2]	Norway spruce[3]	European larch[4]	Silver fir[5]	Douglas-fir[6]	English yew[7]
$K_m \leftrightarrow K_w$	0.743	0.444	0.585	0.496	0.343	0.408	0.698
$K_m \leftrightarrow S_n$	0.925	0.850	0.921	0.847	0.865	0.805	0.928
$K_m \leftrightarrow \alpha$	-0.724	-0.451	-0.588	-0.457	-0.257	-0.389	-0.702
$K_m \leftrightarrow \beta$	0.202	0.523	0.703	0.410	0.675	0.456	0.492
$K_m \leftrightarrow \alpha_w$	0.943	-0.894	-0.940	-0.916	-0.915	-0.896	-0.935
$K_w \leftrightarrow S_n$	0.941	0.848	0.853	0.881	0.763	0.868	0.914
$K_w \leftrightarrow \alpha$	-0.981	-0.986	-0.994	-0.986	-0.953	-0.986	-0.994
$K_w \leftrightarrow \beta$	-0.498	-0.520	-0.160	-0.580	-0.447	-0.616	-0.278
$K_w \leftrightarrow \alpha_w$	-0.874	-0.767	-0.799	-0.771	-0.577	0.741	-0.892
$S_n \leftrightarrow \alpha$	-0.927	-0.849	-0.854	-0.856	-0.695	-0.854	-0.915
$S_n \leftrightarrow \beta$	-0.182	0.001	0.376	-0.133	0.221	-0.155	0.135
$S_n \leftrightarrow \alpha_w$	-0.977	-0.982	-0.990	-0.974	-0.949	-0.970	-0.995
$\alpha \leftrightarrow \beta$	0.507	0.516	0.155	0.615	0.511	0.634	0.267
$\alpha \leftrightarrow \alpha_w$	0.889	0.782	0.806	0.754	0.556	0.737	0.903
$\beta \leftrightarrow \alpha_w$	0.057	-0.126	-0.454	-0.051	-0.422	-0.051	-0.173

Critical values of correlation coefficients: [1] – 0.191; [2] – 0.177; [3] – 0.185; [4] – 0.188; [5] – 0.178; [6] – 0.179; [7] – 0.176

The average value of the coefficient of seed volume k, determined based on pycnometer measurements, ranged from 0.335 (silver fir seeds) to 0.522 (Norway spruce seeds) (Tab. 4). The sphere ($M1$), cylinder ($M2$), cuboid ($M5$), double cone ($M7$) and double triangular pyramid ($M9$) did not adequately model the equivalent diameter of coniferous tree seeds because their volume coefficients differed significantly from those measured with a pycnometer. The performed measurements produced the smallest relative error for Norway spruce seeds on the assumption that they had an ellipsoid shape (0.4%). The above model quite accurately described the seeds of the Scots pine (relative error of 7.6%), European black pine (10.1%) and English yew (3.4%). The volume of the above seeds was most accurately modeled by a right triangular prism ($M6$) which produced relative errors of 2.7%, 5.0% and 1.4%, respectively. The above model can also be used to describe the volume of European larch seeds, although the relative error was quite high at 19.0%. The volume coefficient of silver fir and Douglas-fir seeds was similar to that produced by a double quadrangular pyramid ($M8$) where the relative error was determined at 0.6% and 11.4%, respectively. The proposed models can be used for the purpose of designing seed transport, separation, drying and storage processes.

Table 4

Coefficients of seed volume and geometric shape models

Seed species	Volume coefficient									
	k	k_{M1}	k_{M2}	k_{M3}	k_{M4}	k_{M5}	k_{M6}	k_{M7}	k_{M8}	k_{M9}
Scots pine	0.487	0.693	0.847	0.564				0.282		
European black pine	0.476	0.676	0.810	0.540				0.270		
Norway spruce	0.522	0.682	0.817	0.545				0.272		
European larch	0.420	0.727	0.874	0.583	0.524	1	0.5	0.291	0.333	0.167
Silver fir	0.335	0.767	0.851	0.567				0.284		
Douglas-fir	0.376	0.811	0.873	0.582				0.291		
English yew	0.507	0.561	0.790	0.527				0.263		

Conclusions

1. The shape of coniferous tree seeds native to Poland can be described using one of the three groups of shape factors proposed by Mohsenin, Donev and Wróbel. The values of shape factors can be converted between groups only if the three principal seed dimensions, namely length, width and thickness, are known.

2. The shape and volume of coniferous tree seeds can be modeled with an ellipsoid for Scots pine, European black pine, Norway spruce and English yew

seeds, and a double right quadrangular pyramid for silver fir and Douglas-fir seeds. The volume of European larch seeds can be modeled with a right triangular prism.

Translated by Aleksandra Poprawska

Accepted for print 22.04.2012

References

Buraczyk W. 2010. *Właściwości nasion a cechy morfologiczne siewek sosny zwyczajnej (Pinus Sylvestris L.)*. Leśne Prace Badawcze, 71(1): 13–20.

Czernik Z. 1983. *Badania właściwości geometrycznych nasion sosny zwyczajnej, świerka pospolitego i modrzewia europejskiego*. Sylwan, 7: 31–40.

Donev A., Cisse I., Sachs D., Variano E.A., Stillinger F.H., Connelly R., Torquato S., Chaikin P.M. 2004. *Improving the density of Jammed Disordered Packings using Elipsoids*. Science, 303: 990–993.

Frączek J., Wróbel M. 2006. *Metodyczne aspekty oceny kształtu nasion*. Inżynieria Rolnicza, 12: 155–163.

Frączek J., Wróbel M. 2009. *Zastosowanie grafiki komputerowej w rekonstrukcji 3D nasion*. Inżynieria Rolnicza, 6(115): 87–94.

Grochowicz J. 1994. *Maszyny do czyszczenia i sortowania nasion*. Wydawnictwo Akademii Rolniczej, Lublin.

Jain R.K., Bal S. 1997. *Properties of Pearl Millet*. Journal of Agricultural Engineering Research, 66: 85–91.

Kaliniewicz Z., Grabowski A., Liszewski A., Fura S. 2011. *Analysis of correlations between selected physical attributes of Scots pine seeds*. Technical Sciences, 14(1): 13–22.

Mabille F., Abecassis J. 2006. *Parametric Modelling of Wheat Grain Morphology: a New Perspective*. Journal of Cereal Science, 37: 43–53.

Mieszkalski L., Sołoducha H.K. 2008. *Metody modelowania zbioru brył nasion*. Postępy Techniki Przetwórstwa Spożywczego, 1: 39–44.

Mohsenin N.N. 1986. *Physical properties of plant and animal materials*. Gordon and Breach Science Public, New York.

Murat E. 2002. *Szczegółowa hodowla lasu*. Oficyna Edytorska „Wydawnictwo Świat", Warszawa.

Sivacioğlu A., Ayan S. 2010. *Variation in cone and seed characteristic in a clonal seed orchard of Anatolian black pine [Pinus nigra Arnold subsp. paliasiana (Lamb.) Holmboe]*. Journal of Environmental Biology, 31: 119–123.

Turna I., Güney D. 2009. *Altitudinal variation of some morphological characters of Scots pine (Pinus sylvestris L.) in Turkey*. African Journal of Biotechnology, 8(2): 202–208.

Tylek P. 1998. *Cechy planimetryczne nasion drzew liściastych*. Przegląd Techniki Rolniczej i Leśnej, 1: 22–24.

Tylek P. 2004. *Wybrane cechy rozdzielcze i kryteria separacji nasion modrzewia europejskiego*. Sylwan, 4: 27–33.

Tylek P. 2005. *Charakterystyka agrofizyczna nasion jodły pospolitej po separacji pneumatycznej*. Acta Scientiarum Polonorum, Sivarum Colendarum Ratio et Industria Lignaria, 4(1): 99–105.

Wróbel M. 2006. *Pomiar liczby punktów styku oraz pola powierzchni kontaktu między nasionami*. Praca doktorska zrealizowana na Wydziale Agroinżynierii AR Kraków, maszynopis.

Nasiennictwo leśnych drzew i krzewów iglastych. 1995. Red. A. Załęski. Oficyna Edytorska „Wydawnictwo Świat", Warszawa.

TECHNICAL SCIENCES
Abbrev.: Techn. Sc., No 15(2), Y 2012

CORRELATIONS BETWEEN THE GERMINATION CAPACITY AND SELECTED ATTRIBUTES OF EUROPEAN LARCH SEEDS (*LARIX DECIDUA* MILL.)

***Zdzisław Kaliniewicz*[1], *Piotr Markowski*[1], *Andrzej Anders*[1], *Tadeusz Rawa*[1], *Arkadiusz Liszewski*[1], *Sławomir Fura*[2]**

[1] Department of Heavy Duty Machines and Research Methodology
University of Warmia and Mazury in Olsztyn
[2]Zdzisław Boroński Seed Extraction Plant in Ruciane-Nida, Maskulińskie Forest Inspectorate

K e y w o r d s: European larch seeds, separation properties, germination.

A b s t r a c t

The critical transport velocity, basic dimensions (thickness, width and length), the angle of sliding friction and weight of European larch seeds from three batches were determined. The values of shape factors, cross-sectional area, volume and density were calculated for all seeds. The seeds were germinated, and germination time was determined. The investigated attributes were compared by single classification analysis of variance and correlation analysis. The germination capacity of seeds from the same stand varied between harvest years, and germination time was most highly correlated with critical transport velocity and density. The lightest seeds should be separated from the batch to improve germination capacity, and seeds of the heaviest fractions should be used to promote even germination.

Symbols:

F – seed cross-sectional area, mm^2,
m – seed weight, mg,
S – standard deviation of trait,
T, W, L – seeds thickness, width and length, mm,
T_n – time required to produce a healthy germ, day,
T_o – time of germination test, day
W_k – germination time,
v – critical transport velocity of seeds, $m \cdot s^{-1}$,
V – seed volume, mm^3,
V_s – coefficient of trait variability, %,
x, x_{max}, x_{min} – average, maximum and minimum value of trait,
α, β – Donev's shape factors,
γ – angle of sliding friction, °,
ε_k – germination capacity, %,
ε_w – separation efficiency of non-germinating seeds, %,
ρ – seed density, $g \cdot cm^{-3}$.

Introduction

The European larch (*Larix decidua* Mill.) is a tree that reaches 50 m in height and 200 cm in diameter at breast height (BHD). The species, which thrives in sunny and wind-shielded habitats, is tolerant of cold and vast temperature fluctuations and shows a preference for open spaces. The European larch avoids dry habitats, and it grows best on deep and medium-compact soils (JAWORSKI 2011, JOHNSON, MORE 2011, MURAT 2002, PIRC 2006). In Poland, larch trees do not form dense stands that cover extensive areas, and they are mostly encountered in the form of clusters (FONDER et al. 2007).

European larch seeds can be harvested when trees growing in open spaces reach 15 years of age. Dense stands begin to produce seeds when they are 30 years old. Large quantities of seeds are produced every 2–3 years. Cones are harvested between November and February before they open and release seeds (*Nasiennictwo...* 1995, MURAT 2002). In the natural habitat, seeds fall out of the cone due to the continuous bending and flexing of the scales. In extraction plants, seeds are removed from cones by a combination of mechanical and thermal extraction methods (*Nasiennictwo...* 1995, TYLEK 2004). Mechanical extraction devices dewing seeds, but they also grind and crush cone scales. As the result, the separation of seeds from impurities is more problematic than in thermal extraction systems. The processed material often contains many empty seeds which cannot be separated with the involvement of conventional cleaning machines (pneumatic separators, mesh sieves) (*Nasiennictwo...* 1995, MURAT 2002). Liquid-based cleaning methods, such as PRE-VAC (LESSTANDER, BERGSTEN 1985) and IDS (DEMELASH et al. 2002, 2003, PASQUINI et al. 2008, POULSEN 1995), are more effective in removing impurities from seed lots.

Only seeds of the highest quality should be used for the generative reproduction of trees (JANSON, ZAŁĘSKI 1998). Their germination capacity is determined by a variety of factors, including habitat type, soil class, geographic location, weather conditions during cone and seed development, incidence of diseases and pests that affect cones and seeds, the genetic traits of tree stands and the position of cones within the tree crown (BODYŁ et al. 2007, KLUCZYŃSKI 1992, *Nasiennictwo...* 1995, SKRZYPCZYŃSKA, KOZIOŁ 2001). Seed quality can deteriorate due to improper methods of harvesting, storage and sowing pre-treatment (ANIŚKO et al. 2006, BODYŁ et al. 2007, JANSON, ZAŁĘSKI 1995, *Nasiennictwo...* 1995, TYLEK 2010). The minimum germination capacity of certified reproductive material varies between species. Due to a high number of empty seeds, the reproductive material of the European larch should be characterized by minimum 10% germination capacity (*Nasiennictwo...* 1995, PN-R-65700:1998). According to the above standard, prime quality seeds have germination capacity higher than 41% and minimum germination energy of 31%.

There is a general scarcity of information about correlations between the physical attributes and germination capacity of European larch seeds. The relevant data could be of key significance for designing seed cleaning and sorting processes. At present, the parameters of seed cleaning and separating machines are selected intuitively based on the results of several cleaning trials (SARNOWSKA, WIĘSIK 1998).

The objective of this study was to determine correlations between the basic physical attributes (critical transport velocity, dimensions, the angle of sliding friction, weight, shape factors, cross-sectional area, volume and density) and germination capacity of European larch seeds to eliminate poor-quality seeds from the material and promote even germination.

Materials and Methods

The experimental material comprised three batches of European larch from a seed extraction plant in Ruciane-Nida. The analyzed batches were harvested from the following tree stands:

a) registration number – MP/2/30945/05, municipality – Kowale Oleckie, region of provenance – 202, forest habitat – fresh forest, age – 130 years, year of cone harvest – 2007 (symbol – M1-07),

b) registration number – MP/2/30988/05, municipality – Ruciane Nida, region of provenance – 206, forest habitat – fresh mixed forest, age – unknown, year of cone harvest – 2007 (symbol – M2-07),

c) registration number – MP/2/30988/05, municipality – Ruciane Nida, region of provenance – 206, forest habitat – fresh mixed forest, age – unknown, year of cone harvest – 2008 (symbol – M2-08).

The analyzed material was divided by halving (*Nasiennictwo...* 1995), to obtain samples of slightly above 100 seeds each. The selected method produced samples of size: M1-07 – 119, M2-07 – 124, M2-08 – 122.

The critical transport velocity, basic dimensions (thickness, width and length), the angle of sliding friction and weight of the studied seeds were determined in accordance with the methodology described by KALINIEWICZ et al. (2011, 2012a). The following laboratory devices were used: Petkus K-293 pneumatic classifier, MWM 2325 workshop microscope, an apparatus for measuring seed thickness, an inclined plate with angle control and WAA 100/C/2 laboratory scales.

Donev's shape factors (DONEV et al. 2004) were applied to determine the shape of the studied seeds. The axis of rotation and seed length overlapped, therefore, Donev's shape factors took on the following form:

$$\alpha = \frac{L}{T} \tag{1}$$

$$\beta = \frac{W}{T} \tag{2}$$

It was assumed that the cross-sectional shape of European larch seeds resembled an ellipsoid. Thus, the cross-sectional area of individual seeds was calculated using the below formula:

$$F = \frac{\pi \cdot W \cdot T}{4} \tag{3}$$

Seed volume was calculated from an experimentally derived correlation with the use of a pycnometer (KALINIEWICZ et al. 2012b):

$$V = 0.420 \cdot L \cdot W \cdot T \tag{4}$$

Seed density ρ was calculated from the formula:

$$\rho = \frac{m}{V} \tag{5}$$

To determine germination capacity, the seeds were placed on moistened filter paper in a glass tank covered with a glass pane. The experiment was carried out at the recommended temperature of 20 to 30°C under exposure to natural light. Evaporated water was supplemented daily with a sprinkler, and filter paper was kept moist. Germination progress was evaluated daily between 8 to 9 a.m. Germinated seeds were classified as seeds that produced a sprout with a minimum length of 3/4 of seed length (*Nasiennictwo...* 1995). Observations were continued for 26 days until all seeds had germinated. The germination process was completed when the analyzed seeds ceased to produce new, correctly formed sprouts over a period of five successive days.

Germination time W_k was determined with the use of the below equation:

$$W_k = \frac{T_o - T_n}{T_o} \tag{6}$$

Germination time was the time required by the last germinated seed to produce a healthy sprout plus one day. In this experiment, germination time was 21 days.

Non-germinated seeds were eliminated from the analyzed seed lots to improve germination efficiency on the assumption that live seed loss would not exceed 5%. Germination capacity ε_k was calculated as the number of germinated seeds in a given analytical period in the total number of seeds in the sample.

Separation efficiency of non-germinating seeds ε_w was determined as the number of non-viable seeds separated according to a selected physical attribute in the total number of non-germinating seeds in the sample.

The obtained results were processed statistically using Winstat and Statistica Pl ver. 10 software. The level of significance was $\alpha = 0.05$. The following methods were used:

– analysis of variance with Snedecor's F distribution (single classification), to compare the mean values of the analyzed traits for different batches of European larch seeds. In case of statistically significant differences, homogeneous subsets were determined by Duncan's test (GAWĘCKI, WAGNER 1984, GREŃ 1984);

– correlation analysis, to determine correlations between germination time and the physical attributes of European larch seeds, based on the coefficients of Pearson's linear correlation.

Results and Discussion

The measured traits and the coefficients calculated for the analyzed material are presented in Table 1. The highest values of the coefficient of variation in physical traits were noted for seed weight (from 26.4% to 30.3%). The value of the coefficient of variation for the remaining attributes was reported in the range of around 9.3% to 20.2%, which is consistent with the observations made by other authors (CZERNIK 1983a, TYLEK 1998, 1999, 2004). Critical transport velocity ranged from 4.7 to 8.0 $m \cdot s^{-1}$, with an average of 6.0 $m \cdot s^{-1}$. The above results are somewhat higher than the data reported by TYLEK (1999, 2004) and CZERNIK (1983b), and this discrepancy could be attributed to differences in seed origin. The seeds harvested in the Regions of Mazury and Podlasie are larger and, consequently, heavier, than those from southern parts of Poland. The analyzed seeds had the following dimensions: thickness – 1.41÷1.56 mm, width – 2.60÷2.69 mm and length – 4.39÷4.53 mm, and they were plumper than the material investigated by other authors CZERNIK 1983a, *Nasiennictwo leśnych drzew...* 1995, TYLEK 1998, 2004). The weight of the studied seeds ranged from 2.2 to 12.3 mg.

Table 1

Statistical distribution of the physical attributes of European larch seeds

Batch of seeds	Attribute/indicator	x_{min}	x_{max}	x	S	V_s
M1-07	ν	4.675	7.425	5.96^b	0.614	10.29
	T	1.10	1.84	1.45^b	0.135	9.35
	W	1.82	3.27	2.63^a	0.330	12.55
	L	2.86	5.75	4.51^a	0.601	13.35
	γ	21	63	39.6^a	7.988	20.15
	m	2.4	12.3	6.2^b	1.627	26.42
	α	2.228	4.315	3.119^a	0.399	12.78
	β	1.255	2.346	1.817^a	0.206	11.34
	F	1.766	4.465	3.006^b	0.570	18.95
	V	2.702	12.776	7.362^b	2.145	29.14
	ρ	0.510	1.119	0.854^a	0.131	15.32
	W_k	0	0.714	0.279^a	0.239	85.88
M2-07	ν	4.675	6.875	5.92^b	0.610	10.30
	T	0.98	1.83	1.41^c	0.163	11.55
	W	1.83	3.38	2.60^a	0.340	13.09
	L	2.81	5.85	4.39^a	0.584	13.31
	γ	28	64	39.1^a	6.351	16.23
	m	2.2	9.8	5.8^b	1.773	30.32
	α	2.153	3.953	3.118^a	0.333	10.68
	β	1.254	2.467	1.855^a	0.211	11.35
	F	1.553	4.513	2.912^b	0.615	21.11
	V	2.389	11.990	$6.963b$	2.139	30.71
	ρ	0.584	1.129	0.849^a	0.127	14.96
	W_k	0	0.667	0.247^a	0.231	93.42
M2-08	ν	4.675	7.975	6.24^a	0.594	9.52
	T	1.20	1.98	1.56^a	0.145	9.29
	W	1.75	3.48	2.69^a	0.356	13.21
	L	3.32	6.17	4.53^a	0.538	11.88
	γ	29	55	38.3^a	5.288	13.81
	m	3.0	11.5	6.8^a	1.832	27.08
	α	2.344	3.757	2.911^b	0.322	11.08
	β	1.151	2.245	1.733^b	0.230	13.27
	F	2.016	5.023	3.315^a	0.616	18.57
	V	3.579	14.632	8.138^a	2.243	27.56
	ρ	0.514	1.142	0.843^a	0.135	15.98
	W_k	0	0.714	0.203^b	0.256	126.08

$^{a, b, c}$ – different letters in the superscript indicate significant differences at a level of 0.05
Source: own calculations

Shape factors α and β were characterized by the smallest variation, and germination time W_k – by the highest variation. Owing to their large size, the cross-sectional area and volume of the analyzed seeds were also somewhat higher than the values reported by CZERNIK (1983a) and TYLEK (1998, 2004).

The results of a single classification analysis of variance revealed an absence of significant differences in the width, length, angle of sliding friction and density of European larch seeds. Seed lots harvested in the same year

(M1-07 and M2-07) differed significantly only with regard to seed thickness. Seeds collected from the same tree stand in successive years (M2-07 and M2-08) showed significant variations in critical transport velocity, thickness, weight, shape factors, cross-sectional area, volume and germination time. In general, seeds harvested in 2008 were thicker and heavier than the material obtained in 2007, and the above contributed to an increase in their critical transport velocity.

A comparison of the physical traits of germinated and non-germinated European larch seeds is presented in Figure 1. The analyzed groups significantly differed with regard to critical transport velocity, weight and density. Seeds harvested from the same stand varied in length, and those collected in 2008 had different shape factors. Some of the non-germinated seeds were empty, and their basic parameters, cross-sectional area, volume and springiness values differed from full seeds (TYLEK 2004). No significant differences were observed between the lots of germinated seeds harvested in 2007, but those batches differed from the material collected in 2008 with regard to critical transport velocity, thickness, weight, shape coefficients, cross-sectional area and volume. A comparison of non-germinated seeds did not reveal significant differences in their average width, length, volume or density.

During the experimental period, the following number of seeds produced healthy sprouts: M1-07 – 75, M2-07 – 75 and M2-08 – 51. The germination capacity of the analyzed batches reached 63.0%, 60.5% and 41.8%, respectively, indicating that the studied material falls into the premium quality category. The germination efficiency of seeds harvested from a given stand varied between years. Meteorological conditions during the formation and development of cones significantly affect the quality of harvested seeds (*Nasiennictwo...* 1995). Seeds harvested in various parts of the Regions of Warmia and Podlasie during the same year had similar germination capacity. Although they had been stored for one year less than the remaining batches, the seeds harvested in 2008 were characterized by significantly lower germination capacity.

Due to the noted differences in selected attributes of germinating and non-germinating seeds, non-viable seeds were separated to improve the germinating capacity of the batch. The effects of separating non-germinating seeds according to the lower limit of classification are shown in Table 2. The highest separation efficiency was obtained when critical transport velocity and density were used as the separation traits. Our observations are consistent with the results reported by TYLEK (2004). The use of a vertical air stream and the selection of cleaning parameters which promoted the separation of lightest seeds produced the best results. Germination capacity increased to 72.4% in M1-07, 74% in M2-07 and 56.5% in M2-08 when 17.6%, 22.6% and 30.3% of the

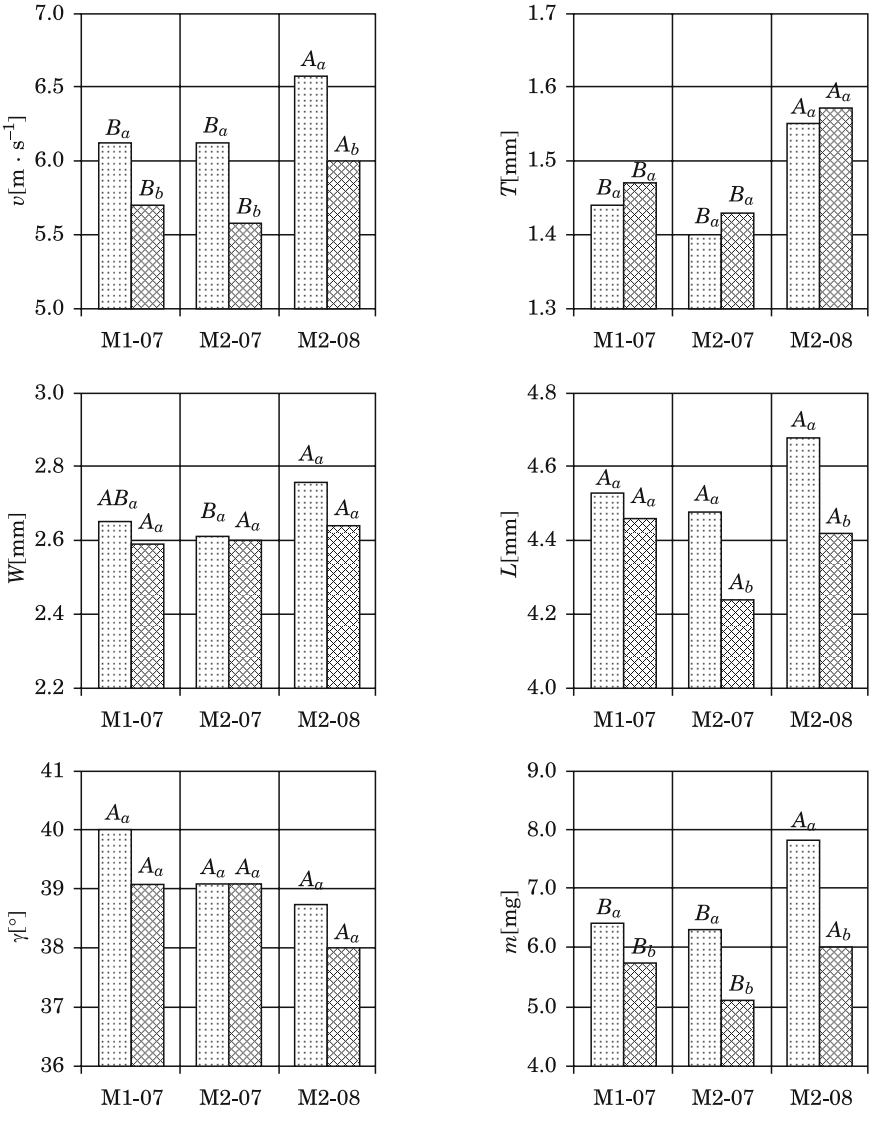
v[m · s⁻¹]
7.0
6.5
6.0
5.5
5.0
Ba
Bb
Ba
Bb
Aa
Ab
M1-07
M2-07
M2-08
T[mm]
1.7
1.6
1.5
1.4
1.3
Ba
Ba
Ba
Ba
Aa
Aa
M1-07
M2-07
M2-08
W[mm]
3.0
2.8
2.6
2.4
2.2
ABa
Aa
Ba
Aa
Aa
Aa
M1-07
M2-07
M2-08
L[mm]
4.8
4.6
4.4
4.2
4.0
Aa
Aa
Aa
Ab
Aa
Ab
M1-07
M2-07
M2-08
γ[°]
41
40
39
38
37
36
Aa
Aa
Aa
Aa
Aa
Aa
M1-07
M2-07
M2-08
m[mg]
9.0
8.0
7.0
6.0
5.0
4.0
Ba
Bb
Ba
Bb
Aa
Ab
M1-07
M2-07
M2-08

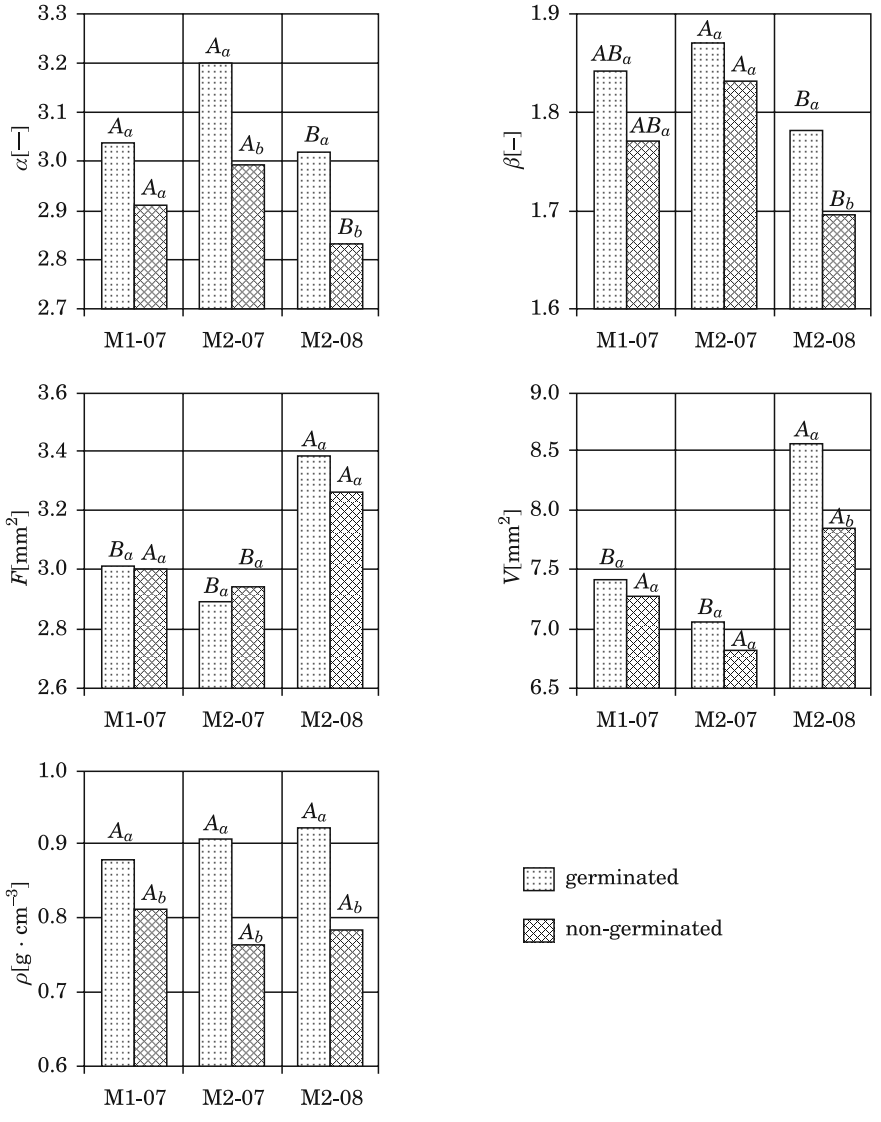

Fig. 1. Significance of differences (at a level of 0.05) between the attributes of European larch seeds: *A, B* – different letters indicate significant differences between different seed batches; *a, b* – different letters in the superscript indicate significant differences between germinated and non-germinated seeds

Source: own study

Table 2
Separation efficiency ε_w of non-germinating seeds and germination capacity ε_k of European larch seeds according to the adopted limit of classification in the separation process

Batch of seeds	Limit of classification	ε_w [%]	ε_k [%]
M1-07 (ε_k = 63.0%)	v = 5.1 m · s^{-1}	38.6	72.4
	T = 1.65 mm	11.4	64.6
	W = 2.18 mm	18.2	66.4
	L = 3.60 mm	9.1	64.0
	γ = 30°	18.2	66.4
	m = 3.9 mg	11.4	64.5
	ρ = 0.68	22.7	67.6
M2-07 (ε_k = 60.5%)	v = 5.1 m · s^{-1}	49.0	74.0
	T = 1.62 mm	16.3	63.4
	W = 2.12 mm	8.2	61.2
	L = 3.60 mm	8.2	61.2
	γ = 30°	6.1	60.7
	m = 3.8 mg	24.5	65.7
	ρ = 0.73	46.9	73.2
M2-08 (ε_k = 41.8%)	v = 5.6 m · s^{-1}	47.9	56.5
	T = 1.76 mm	11.3	43.2
	W = 2.25 mm	16.9	44.9
	L = 4.03 mm	25.4	47.5
	γ = 31°	8.5	42.5
	M = 5.5 mg	40.8	53.3
	ρ = 0.77	52.1	58.5

Source: own calculations

Table 3
Coefficients of Pearson's linear correlation between germination time and other attributes of European larch seeds from three batches

Variables		Coefficients of correlation calculated for:		
X	Y	M1-07[1]	M2-07[2]	M2-08[3]
W_k	v	0.349	0.427	0.505
	T	-0.106	-0.113	-0.045
	W	0.033	0.002	0.171
	L	0.004	0.153	0.221
	γ	0.102	0.033	0.041
	m	0.167	0.274	0.476
	α	0.050	0.284	0.268
	β	0.107	0.101	0.187
	F	-0.038	-0.067	0.100
	V	-0.020	0.022	0.151
	ρ	0.281	0.507	0.502

Critical value of the correlation coefficient: [1] – 0.180; [2] – 0.176; [3] – 0.178
Source: own calculations

seeds were discarded, respectively. The above process efficiently separates around 40% of non-viable seeds. Density can also be used as a separation trait, but due to the complexity of the process (solution density has to be adjusted precisely to the batch of floated seeds) and the need to dry the seeds, it is not recommended.

An analysis of the linear correlation between germination time and the remaining attributes of European larch seeds (Table 3) indicates that the critical value of the correlation coefficient for all three seed batches was exceeded only for critical transport velocity and density. The above results suggests that in order to produce a more evenly distributed germination pattern, a pneumatic separator, a liquid separator or a pneumatic vibratory table should be used to split the material into fractions.

Table 4 shows the germinating capacity of three potential seed fractions separated by a vertical stream of air to eliminate non-germinating seeds according to the lower limit of classification. According to the presented data, the sorting of seeds based on their critical transport velocity can narrow down sprouting times. The above particularly applies to seeds characterized by the

Table 4

Effect of germination time on the percentage of three fractions of European larch seeds (sorted by critical transport velocity)

Batch of seeds	Range W_k	Percentage of seeds [%]			
		total	division into fractions		
			$v < 6.0$ m · s^{-1}	$v = 6.0 \div 6.5$ m · s^{-1}	$v > 6.5$ m · s^{-1}
M1-07	0.001÷0.100	1.0	1.0	0	0
	0.101÷0.200	3.0	1.0	1.0	1.0
	0.201÷0.300	2.0	1.0	1.0	0
	0.301÷0.400	15.3	5.1	9.2	1.0
	0.401÷0.500	30.8	9.2 (25.8)	14.3 (28.0)	7.3 (54.9)
	0.501÷0.600	8.2	2.1	5.1	1.0
	0.601÷0.700	11.2	4.1	6.1	1.0
	0.701÷0.800	1.0	0	1.0	0
	0*	27.5	12.2 (34.2)	13.3 (26.1)	2.0 (15.0)
M2-07	0.001÷0.100	2.0	1.0	1.0	0
	0.101÷0.200	8.3	2.1	3.1	3.1
	0.201÷0.300	3.1	0	3.1	0
	0.301÷0.400	16.8	6.3	8.3 (18.1)	2.2
	0.401÷0.500	27.2	12.5 (33.3)	5.3	9.4 (56.3)
	0.501÷0.600	8.3	0	7.3	1.0
	0.601÷0.700	8.3	3.1	5.2	0
	0.701÷0.800	0	0	0	0
	0*	26.0	12.5 (33.3)	12.5 (27.3)	1.0 (6.0)
M2-08	0.001÷0.100	1.2	0	0	1.2
	0.101÷0.200	1.2	0	1.2	0
	0.201÷0.300	0	0	0	0
	0.301÷0.400	7.1	3.5 (29.7)	2.4	1.2
	0.401÷0.500	22.4	2.4	8.2 (16.6)	11.8 (30.4)
	0.501÷0.600	13.0	0	2.4	10.6 (27.3)
	0.601÷0.700	7.0	1.2	3.4	2.4
	0.701÷0.800	4.6	0	1.2	3.4
	0*	43.5	4.7 (39.8)	30.6 (61.9)	8.2 (21.1)

* Seeds that did not germinate over the experimental period

Source: own calculations

highest critical transport velocity (at $v > 6.5$ m · s^{-1}). The share of seeds from the most populous germination time interval reached 54.9%, 56.3% and 30.4% in each fraction. Non-viable seeds had a significantly smaller share (15.0%, 6.0% and 21.1%, respectively), implying that this material could be used in container nurseries where only prime quality seeds are sown. Similar results were reported in a study of Norway spruce seeds (KALINIEWICZ et al. 2012a).

The germination capacity of three potential seed fractions separated based on density values is presented in Table 5. As before, non-germinating seeds were eliminated according to density classification limits indicated in Table 2. In this case, the germination interval was also narrowed down for the last fraction ($\rho > 0.95$ g · cm^{-3}). The share of seeds from the most abundant

Table 5

Effect of germination time on the percentage of three fractions of European larch seeds (sorted by density)

Batch of seeds	Range W_k	Percentage of seeds [%]			
		total	after division into fractions		
			ρ<0.85 g · cm^{-3}	ρ=0.85÷0.95 g · cm^{-3}	ρ>0.95 g · cm^{-3}
M1-07	0.001÷0.100	1.0	1.0	0	0
	0.101÷0.200	2.9	2.9	0	0
	0.201÷0.300	2.0	1.0	0	1.0
	0.301÷0.400	14.1	4.7	3.7	5.7
	0.401÷0.500	28.6	10.5 (23.4)	7.6 (31.9)	10.5 (33.4)
	0.501÷0.600	7.7	2.9	2.9	1.9
	0.601÷0.700	10.4	4.7	2.9	2.8
	0.701÷0.800	1.0	0	0	1.0
	0*	32.3	17.1 (38.2)	6.7 (28.2)	8.5 (27.1)
M2-07	0.001÷0.100	3.1	2.1	1.0	0
	0.101÷0.200	8.3	1.0	2.1	5.2
	0.201÷0.300	3.0	1.0	1.0	1.0
	0.301÷0.400	16.5	3.1	8.2	5.2
	0.401÷0.500	25.7	4.1 (12.1)	10.3 (30.3)	11.3 (35.3)
	0.501÷0.600	8.3	2.1	5.2	1.0
	0.601÷0.700	8.3	3.1	3.1	2.1
	0.701÷0.800	0	0	0	0
	0*	26.8	17.5 (51.5)	3.1 (9.1)	6.2 (19.4)
M2-08	0.001÷0.100	1.2	0	0	1.2
	0.101÷0.200	2.4	1.2	1.2	0
	0.201÷0.300	0	0	0	0
	0.301÷0.400	7.4	2.5	3.7	1.2
	0.401÷0.500	23.2	4.9 (16.7)	7.3 (17.6)	11.0 (37.7)
	0.501÷0.600	12.1	1.2	4.8	6.1
	0.601÷0.700	7.3	1.2	3.7	2.4
	0.701÷0.800	4.9	1.2	3.7	0
	0*	41.5	17.1 (58.4)	17.1 (41.2)	7.3 (25.0)

* Seeds that did not germinate over the experimental period
Source: own calculations

germination time interval was around 35% in a given fraction. The material characterized by the highest density had a smaller share of non-viable seeds than the entire batch, therefore it could be successfully used in container nurseries.

The combination of pre-treatment cleaning based on a selected separation trait (e.g. critical transport velocity) and seed sorting based on another attribute (e.g. density) did not significantly improve the quality of the resulting material, which is why the results of the above analyses are not presented in this paper.

Conclusions

1. The germinating capacity of European larch seeds ranged from 42% to 63% which qualifies the studied material for the prime quality group. Germinating capacity is largely affected by the year of cone harvesting and the prevalent weather conditions during the formation and development of seeds.

2. Germinating seeds and non-viable seeds differed most significantly with regard to their critical transport velocity, weight and density. In order to improve seed quality, pneumatic and hydraulic separators or pneumatic vibratory tables should be used to eliminate the lightest fraction from seed material. Separation efficiency reaches around 40%, and it increases germination capacity to 56-74%.

3. The germination capacity of European larch seeds can be improved and more evenly distributed germination patterns can be obtained by fractioning seeds. This can be achieved with the use of the above cleaning machines. The heaviest seeds (with the highest critical transport velocity and density) should be used for sowing.

Translated by Aleksandra Poprawska

Accepted for print 30.10.2012

References

Aniśko E., Witowska O., Załęski A. 2006. *Wpływ warunków suszenia nasion brzozy brodawkowatej, olszy czarnej, sosny zwyczajnej i świerka pospolitego na ich żywotność*. Leśne Prace Badawcze, 2: 91–13.

Bodył M., Witowska O., Załęski A. 2007. *Przyczyny obniżonej żywotności niektórych partii nasion sosny zwyczajnej (Pinus sylvestris L.), pozyskanych w Polsce zimą 2005/2006*. Leśne Prace Badawcze, 4: 47–65.

Czernik Z. 1983a. *Badania właściwości geometrycznych nasion sosny zwyczajnej, świerka pospolitego i modrzewia europejskiego*. Sylwan, 7: 31–40.

Czernik Z. 1983b. *Badania właściwości aerodynamicznych nasion sosny zwyczajnej, świerka pospolitego i modrzewia europejskiego*. Sylwan, 9/10: 31–40.

Demelash L., Tigabu M., Oden P.C. 2002. *Separation of empty and dead-filled seeds from a seed lot on Pinus patula with IDS technique*. Seed Science and Technology, 30: 677–681.

DEMELASH L., TIGABU M., ODEN P.C. 2003. *Enhancing germinability of Schinus molle L. seed lot from Ethiopia with specific gravity and IDS techniques*. New Forests, 26: 33–41.

DONEV A., CISSE I., SACHS D., VARIANO E.A., STILLINGER F.H., CONNELLY R., TORQUATO S., CHAIKIN P.M. 2004. *Improving the Density of Jammed Disordered Packings using Ellipsoids*. Science, 303: 990–993.

FONDER W., MATRAS J., ZAŁĘSKI A. 2007. *Leśna baza nasienna w Polsce*. Centrum Informacyjne Lasów Państwowych, Warszawa.

GAWĘCKI J., WAGNER W. 1984. *Podstawy metodologii badań doświadczalnych w nauce o żywieniu i żywności*. PWN, Warszawa.

GREŃ J. 1984. *Statystyka matematyczna. Modele i zadania*. PWN, Warszawa.

JANSON L., ZAŁĘSKI A. 1998. *Wykorzystanie biologicznych właściwości nasion w produkcji szkółkarskiej*. Sylwan, 2: 59–70.

JAWORSKI A. 2011. *Hodowla lasu*. Tom III. *Charakterystyka hodowlana drzew i krzewów leśnych*. PWRiL, Warszawa.

JOHNSON O., MORE D. 2011. *Przewodnik Collinsa. Drzewa*. Multico Oficyna Wydawnicza, Warszawa.

KALINIEWICZ Z., GRABOWSKI A., LISZEWSKI A., FURA S. 2011. *Analysis of correlations between selected physical attributes of Scots pine seeds*. Technical Sciences, 14 (1): 13–22.

KALINIEWICZ Z., MARKOWSKI P., RAWA T., GRABOWSKI A., FURA S. 2012a. *Współzależność między zdolnością kiełkowania a wybranymi cechami nasion świerka pospolitego (Picea abies)*. Inżynieria Przetwórstwa Spożywczego, 1/4: 13–17.

KALINIEWICZ Z., TYLEK P., MARKOWSKI P., ANDERS A., RAWA T., ZADROŻNY M. 2012b. *Determination of shape factors and volume coefficients of seeds from selected coniferous trees*. Technical Sciences, 15(2): 217–228.

KLUCZYŃSKI B. 1992. *Plonowanie i jakość świerka pospolitego (Picea bies (L.) Karst) w zależności od strefy w koronie oraz wybranych biologicznych i siedliskowych cech drzew*. Sylwan, 5: 25–35.

LESTANDER T., BERGSTEN U. 1985. *PREVAC-en metod for att avlagsna mekaniskt skadat fro*. Sverige Skogsv4rdsforbunds, Tidskrift, 1: 35–42.

LMURAT E. 2002. *Szczegółowa hodowla lasu*. Oficyna Edytorska „Wydawnictwo Świat", Warszawa.

Nasiennictwo leśnych drzew i krzewów iglastych. 1995. Ed. A. Załęski. Oficyna Edytorska „Wydawnictwo Świat", Warszawa.

PASQUINI N.M., DEFOSSE G.E., LONGO DEL O. 2008. *Upgrading germinability of ponderosa pine seeds from Patagonia, Argentina, by adjusting prechilling periods and applying the IDS technique*. New Forests, 36: 93–102.

POULSEN K.M. 1995. *Application of IDS-method to Pinus caribaea seed*. Seed Science and Technology, 23: 269–275.

PIRC H. 2006. *Drzewa od A do Z*. Klub dla Ciebie, Warszawa.

PN-R-65700:1998. *Materiał siewny – Nasiona drzew i krzewów leśnych i zadrzewieniowych*. Polish Committee for Standardization.

SARNOWSKA G., WIĘSIK J. 1998. *Wyłuszczarnia w Czarnej Białostockiej*. Część III. *Czyszczenie i separacja nasion*. Przegląd Techniki Rolniczej i Leśnej, 1: 19–21.

SKRZYPCZYŃSKA M., KOZIOŁ M. 2001. *Ocena jakościowa nasion modrzewia europejskiego Larix Decidua Mill. pochodzących z wybranych stanowisk południowej Polski*. Sylwan, 5: 39–44.

TYLEK P. 1998. *Cechy planimetryczne nasion drzew liściastych*. Przegląd Techniki Rolniczej i Leśnej, 1: 22–98.

TYLEK P. 1999. *Problemy selekcji pneumatycznej nasion drzew leśnych*. Sylwan, 12: 65–72.

TYLEK P. 2004. *Wybrane cechy rozdzielcze i kryteria separacji nasion modrzewia europejskiego*. Sylwan, 4: 27–33.

TYLEK P. 2010. *Fizyczne i biologiczne aspekty mechanicznej separacji nasion buka zwyczajnego (Fagus sylvatica L.)*. Zeszyty Naukowe Uniwersytetu Rolniczego im. Hugona Kołłątaja w Krakowie. Rozprawy, 344.

TECHNICAL SCIENCES
Abbrev.: Techn. Sc., No 15(2), Y 2012

METHOD OF DETERMINING THE MINIMUM BREAKING STRENGTH OF THE MUSTARD SEED COAT

***Piotr Szczyglak*[1], *Zbigniew Żuk*[2]**

[1] Department of Vehicle and Machine Design and Operation
[2] Department of Heavy Duty Machines and Research Methodology
University of Warmia and Mazury in Olsztyn

K e y w o r d s: mustard seeds, modeling, susceptibility.

A b s t r a c t

This paper proposes a method for determining the breaking strength and the resulting deformations of the mustard seed coat. A compression test stand for determining breaking strength and seed coat deformations was described. The results of the experiment were processed and analyzed.

Introduction

Mustard is an annual oily plant of the family *Brassicaceae* which produces yellow flowers. Mustard is a well-established crop with numerous applications, and white mustard (*Sinapis Alba*) is the most popular species (WAŁKOWSKI 1997). White mustard grows wild in the Mediterranean region where it is regarded as a weed. Today, it is cultivated in moderate climate zones around the world. White mustard is an annual oily plant which is less susceptible to freezing temperatures than winter rape. The annual yield of white mustard seeds reaches two tons per hectare. It is the basic ingredient in the production of mustard and spices, and it is also grown as a forage plant. In comparison with black mustard, white mustard seeds are characterized by higher fat and protein concentrations and a lower fiber content of the seed coat. White mustard seeds are husked to remove harmful substances, including large quantities of fiber and crude fiber (OCHODZKI, RAKOWSKA 1996).

Stringent requirements set for food products spur a search for raw materials of the highest quality. The microstructure, morphological and anatomical structure of seeds determine the choice of the most effective seed coat removal method in the husking process (MIESZKALSKI 2009).

The size of mustard seeds varies from 1.5 to 3.2 mm, subject to species and variety as well as weather conditions in the year of harvest (PYKAŁO 2002). At the micro and macro level, geometric and mechanical attributes of seeds condition the parameters of a husking device.

The minimal force that causes the seed coat to rupture is one of the key parameters affecting the husking process. A method of determining impact energy has been described by several authors (MIESZKALSKI, SARNIAK 1997). Impact energy values can be used to calculate the breaking strength of the seed coat, but they do not support determinations of minimum breaking strength. The proposed method involves a 5 kg drop-weight which generates impact energy. The determined impact force is a sum of the minimum force required to rupture the seed coat, the seed's deformation strength after coat rupture, the force required to overcome aerodynamic resistance and friction of the drop-weight guide. The force breaking the seed coat causes the seed to become deformed. This is also an important parameter which should be taken into account when setting the parameters of a husking device which removes the seed coat through deformation (SCHNEIDER 1982).

The application of excessive breaking force or deforming force in the husking process lowers the quality of the processed material and increases husking costs. The study set out to investigate the minimum force required to break the seed coat and deform the seed.

Materials and Methods

The objective of this study was to determine the deformation strength of mustard seeds subjected to a load applied perpendicularly to the parting plane of cotyledons.

The adopted model is presented in Figure 1 (NIZIŃSKI 2002, MICHALSKI, SZCZYGLAK 2005).

In the adopted model, the set of constant values C contains the following elements:

– c_1 – seed moisture content (7%);
– c_2 – mustard seed variety (Nakielska).

In the adopted model, the set of interfering factors Z contains the following elements:

– z_1 – ridged seed surface;
– z_2 – uneven seed diameter;
– z_3 – non-linear measurement path.

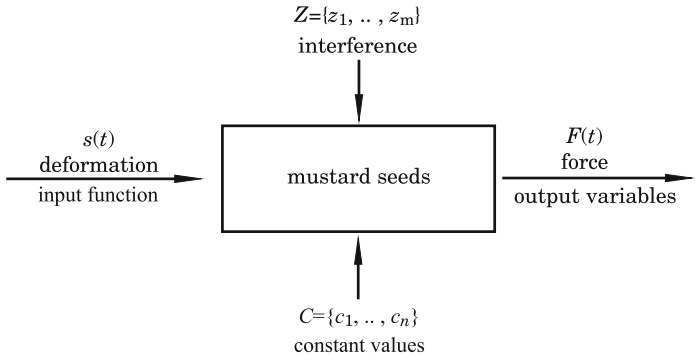

Fig. 1. Analyzed mustard seeds: $s(t)$ – time waveform of mustard seed deformation, $F(t)$ – time waveform of load application, C – set of constant values, Z – set of interfering factors

A seed compression test stand was built for the needs of the experiment (Fig. 2). Seeds were placed on a test platform. The movement of the loading yoke relative to the specimen platform was controlled by a mechanical actuator. The yoke was connected to a power transducer. The position of the yoke relative to the platform was determined with the use of a potentiometric position sensor.

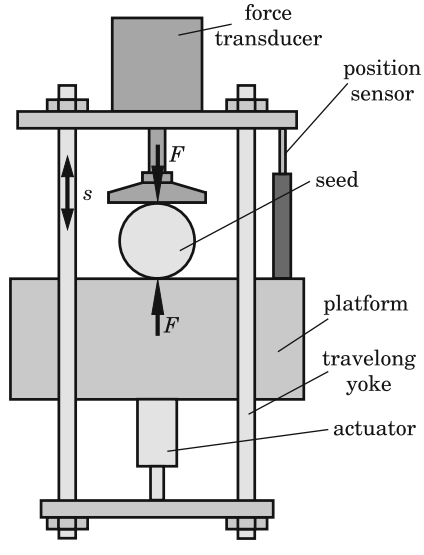

Fig. 2. Seed compression test stand: F – force, s – displacement

The list of measured values and the corresponding measuring transducers are shown in Table 1.

Table 1

List of measured values and the corresponding measuring transducers

Measured value	Symbol	Transducer	Measurement range
Deformation	$s\ (t)$	potentiometric position sensor MM10 10 kΩ	0–11 [mm] (resolution <0.00275 mm)
Load	$F(t)$	tensometric power transducer AR 201 50 N	0-50 [N] (resolution 0.0005 N)

A shared sampling time base was used to synchronize the measurements (T_p = 0.01 s). The measured values were registered by a computer connected to an MG-TAE1 logger (Fig. 3).

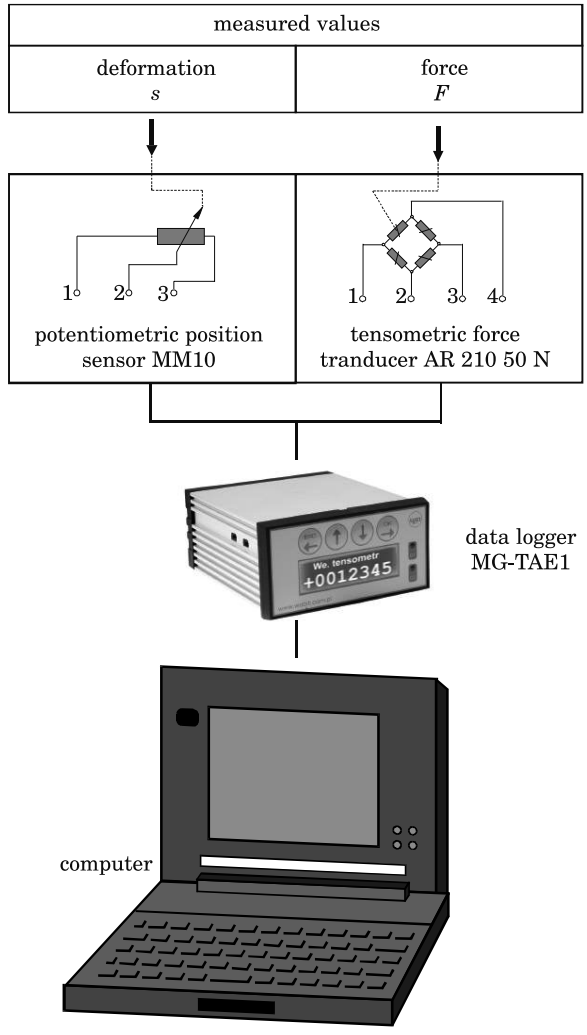

Fig. 3. Measurement path for registering time waveforms of input function and output variables

The resulting time waveforms of deformations and the accompanying loads were subjected to frequency filtration in the MatLab application using the Chebyshev filter (MOLER 2004).

Results

Filtered time waveforms of deformation and load noted in the experiment are exemplified in Figure 4. When breaking strength was exceeded during seed compression, a cracking sound could be heard with an unarmed ear. The above

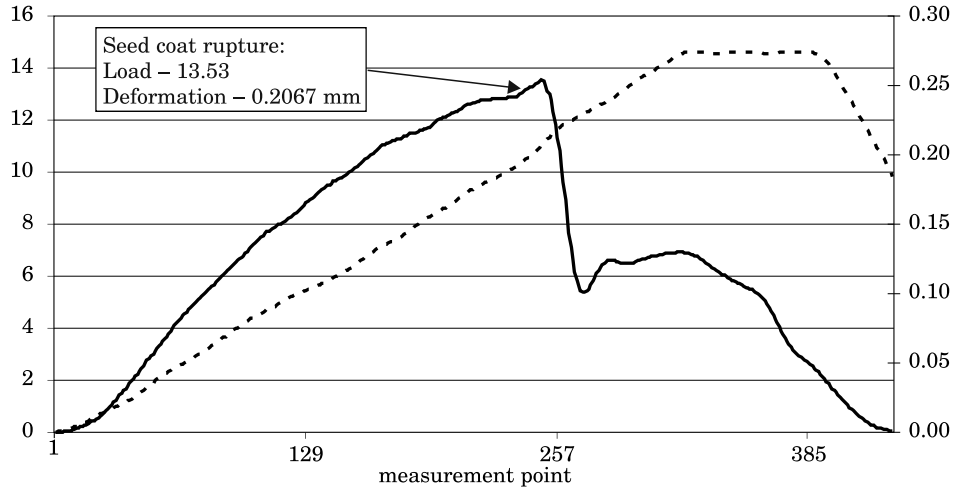

Fig. 4. Time waveforms of mustard seed deformation and the accompanying load

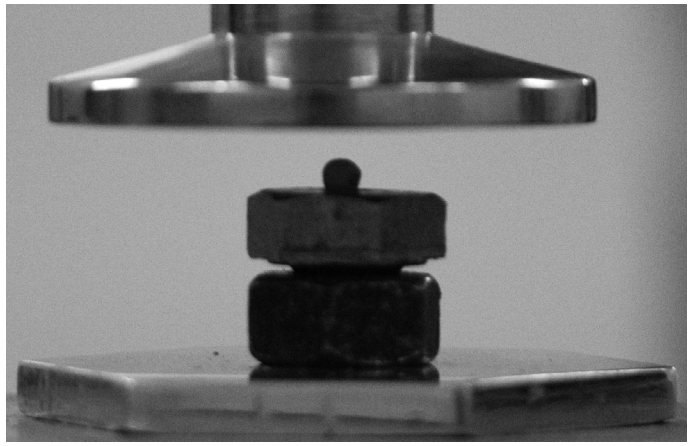

Fig. 5. A compressed seed

was accompanied by a rapid decrease in radial rigidity of the tested seed (Fig. 4). An image of a compressed seed is presented in Figure 5, and the corresponding time waveforms are shown in Figure 4.

The results of the experiment are presented in Table 2.

Table 2

Experimental results

Parameter	Value
Number of samples	30
Average force required to break the seed coat	17.54046 N
Minimum force required to break the seed coat	11.381554 N
Maximum force required to break the seed coat	23.680499 N
Standard deviation (force)	4.941420 N
Median (force)	19.165556 N
Average deformation of the seed coat caused by breaking force	0.213468 mm
Minimum deformation of the seed coat caused by breaking force	0.179499 mm
Maximum deformation of the seed coat caused by breaking force	0.263214 mm
Standard deviation (deformation)	0.026104 mm
Median (deformation)	0.214235 mm

Conclusions

The proposed method supports precise determinations of the minimum force required to break the seed coat. At breaking point, a cracking sound can be heard with an unarmed ear. The above is accompanied by a rapid decrease in the seed's radial rigidity. In the tested samples, the average breaking force was 17.54046 N, and the average deformation was 0.213468 mm. The results were reported for mustard seeds var. Nakielska with a 7% moisture content. We believe that our findings can expand the knowledge base of husking machine designers. Owing to a broad range of mustard seed species, further work is needed to investigate other varieties with different moisture content levels.

Translated by Aleksandra Poprawska

Accepted for print 31.10.2012

References

Moler C.B. 2004. *Numerical Computing With MATLAB*. Published by the Society for Industriel and Applied Mathematics. 2004.

Michalski R., Szczyglak P. 2005. *Radial flexibility of pneumatic wheels*. PROCEEDINGS OF THE 10 th INTERNATIONAL CONFERENCE MECHANIKA. April 7–8. Lithuania, p. 363–369.

MIESZKALSKI L., SARNIAK M. 1997. *Badanie energii uderzenia nasion rzepaku na użytek matematycznego modelowania procesu obłuskiwania*. Zeszyty Problemowe Podstępów Nauk Rolniczych, 1997, str. 61–66.

MIESZKALSKI L., ŻUK Z. 2009. *Analiza mikrostruktury nasion gorczycy w kontekście ich obłuskiwania*. Postępy Techniki Przetwórstwa Spożywczego, 19(2): 16–19.

NIZIŃSKI S. 2002. *Modelowanie procesów eksploatacji maszyn*. Wydawnictwo MARKAR-BZ. Bydgoszcz-Sulejówek.

OCHODZKI P., RAKOWSKI M. 1996. *Porównanie składu chemicznego i wartości żywieniowej odtłuszczonych nasion rzepaków brązowo- i żółto nasiennych*. Rośliny Oleiste, XVII: 477–482.

PYKAŁO I. 2002. *Wpływ herbicydów na plonowanie i skład chemiczny nasion gorczycy białej* (*Sinapis alba L.*). Rozprawa doktorska.

SCHNEIDER F.H. 1982. *Sposób zdejmowania łusek z nasion zawierających olej i proteiny*. Opis patentowy nr 112720, Essen.

WAŁKOWSKI T. 1997. *Gorczyce*. IHAR, Poznań.

TECHNICAL SCIENCES
Abbrev.: Techn. Sc., No 15(2), Y 2012

EFFECT OF REFURBISHED THERMAL INSULATION OF EXTERIOR PARTITIONS IN A BUILDING ON THE PRIMARY ENERGY AND THE AIR POLLUTANT EMISSION FACTORS

Piotr Bogacz, Jacek Zabielski

Department of Materials Engineering and Building Processes
University of Warmia and Mazury in Olsztyn

K e y w o r d s: thermal insulation renovation, an energy performance certificate, airborne pollutant emission, renewable energy sources.

A b s t r a c t

The paper contains an analysis of a multi-flat building located in Lębork. The calculations made for the existing building as required to issue an energy performance certificate demonstrated its high energy consumption. Renovation of the thermal insulation of the building was simulated, including all partitions enclosing rooms with regulated temperature, independent from the outdoor environment, and other unheated rooms. The effect of the thermal insulation renovation on the Primary Energy Factor and the Air Pollutant Emission Factor was tested. It was proven that the analyzed refurbishment of thermal insulation was insufficient to fulfill the reference value of primary non-renewable energy input, which would ensure considerable savings on costs (amounts of fuels) of heating.

Introduction

In 2009, according to the Directive of the European Union 2002/91/EC (Official Journal of the European Communities L 1/65 of 2002) of 16 December 2002 on the energy performance of buildings, the Polish law imposed in certain cases an obligation to obtain an energy performance certificate of a building, also known as an energy certificate. A model certificate as well as a methodology for making relevant calculations are included in the Regulation of the Minister for Infrastructure of 6 November 2008 on the methodology of calculating energy performance of a building, a residential flat or a self-contained, technical and functional part of a building, and on methods of preparing energy performance certificates, including model certificates (Journal of Law of 2008, No 201, item 1240). The objective was to promote low energy consumption buildings, both new and renovated ones.

Role of an energy performance certificate

The role of an energy performance certificate is to provide an objective and independent opinion about the primary, final and usable energy demand of a given building. These types of energy comprise the energy demand for heating (in all buildings), hot water (in all buildings), ventilation and air conditioning (if a building is equipped with a cooling installation) and lighting (in public buildings).

The usable energy for heating is calculated in monthly balances during a heating season. The usable energy for cooling is calculated in monthly balances during a cooling season. The usable energy spent on hot water heating is calculated in an annual balance, as a product of the factors that significantly influence its value. A similar calculation method is deployed for calculating the energy expended on built-in lighting installation.

The final energy is balanced out at a building's exterior boundaries, and its value expresses the demand for energy to be delivered to the building, taking into account all losses due to the efficiency of all installation systems. The demand for non-renewable primary energy determines the total efficiency of a whole building. Apart from final energy, it includes an additional, non-renewable primary energy expenditure on delivering each of the used energy carriers (e.g. coal, heating oil, gas, electricity, renewable energies, etc.) to the building's boundaries as well as auxiliary energy necessary to power auxiliary devices.

The value of primary energy is most significantly shaped by the technical condition of exterior partitions in a building. According to the laws of physics, thermal energy flows from a medium of higher temperature to a medium of lower temperature. The higher the difference in temperatures, the faster the energy flow. Approximate heat losses through partitions and a ventilation system are presented in table 1.

Table 1

Per cent heat losses thorough ventilation and exterior partitions of a building

Type of loss	Percentage [%]
Ventilation	25–35
Exterior walls in contact with atmospheric air	20–30
Exterior partitions in contact with the ground	5
Roof	20–30
Exterior windows and doors	10–20

Source: the authors.

Of the total heat losses in a building, about 70–80% are the losses through exterior partitions, which separate the interior of the building, where the temperature is regulated independently from the external environment.

According to the methodology for issuing energy performance certificates of buildings, the coefficient of heat transmission through partitions is the sum of the product of the correction coefficient of a calculated difference in exterior and interior temperatures and heat losses through particular partitions, including linear thermal bridges – complaint with the norms PN-EN 12831 and PN-EN ISO 6946.

$$H_{\mathrm{tr}} = \Sigma_i \left[b_{\mathrm{tr},i} \cdot (A_i \cdot U_i + \Sigma_i \, l_i \cdot \Psi_i) \right] \quad [\mathrm{W/K}] \tag{1}$$

where:

$b_{\mathrm{tr},i}$ – correction coefficient of the calculated exterior-interior temperature difference for the i^{th} partition,

A_i – surface area of the i^{th} partition enveloping regulated temperature space, calculated from exterior dimensions, of the partition (dimensions of windows and doors are taken as dimensions of apertures in walls) [m^2],

U_i – coefficient of heat transmission through the i^{th} partition between the heated space and the exterior [$\mathrm{W/(m^2\ K)}$],

l_i length of the i^{th} linear thermal bridge [m],

Ψ_i – linear coefficient of heat transmission through a thermal bridge according to PN-EN ISO 14683 or calculated according to PN-EN ISO 10211 [W/(m K)].

The coefficient of heat transmission by ventilation is calculated as the product of the interior heat capacity of air per volume and the sum of the product of correction coefficients of the ventilation airflow and occurring ventilation flows:

$$H_{\mathrm{ve}} = \rho_a \cdot c_a \cdot \Sigma_k \, (b_{\mathrm{ve},k} \cdot V_{\mathrm{ve},k,\mathrm{mn}}) \ [\mathrm{W/K}] \tag{2}$$

The achieved values of heat loss coefficients H_{tr} and H_{ve} enable calculation of total heat flows.

The total heat transmission through partitions and ventilation is calculated in monthly balances – due to different external monthly temperatures.

$$Q_{\mathrm{tr}} = H_{\mathrm{tr}} \cdot (\theta_{\mathrm{int},H} - \theta_e) \cdot t_M \cdot 10^{-3} \ [\mathrm{kWh/month}] \tag{3}$$

$$Q_{\mathrm{ve}} = H_{\mathrm{ve}} \cdot (\theta_{\mathrm{int},H} - \theta_e) \cdot t_M \cdot 10^{-3} \ [\mathrm{kWh/month}] \tag{4}$$

where:

Q_{tr} – total heat flow by transmission through walls over a month [kWh/month],

Q_{ve} – total heat flow by ventilation over a month [kWh/month],

H_{tr} – coefficient of heat loss by transmission through all exterior partitions [W/K],

H_{ve} – coefficient of heat loss through ventilation [W/K],

$\theta_{int,H}$ – exterior temperature for the heating season in a building or a flat according to the requirements defined in civil engineering and technical regulations [°C],

θ_e – average air temperature during the analyzed monthly interval according to the data supplied by the nearest meteorological station [°C],

t_M – number of hours in a month (during the heating season) [h].

The sum of total heat flow through transmission and ventilation is defined as heat losses.

$$Q_{H,ht} = Q_{tr} + Q_{ve} \text{ [kWh/month]} \tag{5}$$

The demand for usable energy for heating and ventilation, in monthly balances, is calculated by taking into account the gains from solar radiation through glass panes (windows, skylights, glazed partitions) and internal gains (heat gains from occupants, household devices, etc.).

$$Q_{H,nd,n} = Q_{H,ht} - \eta_{H,gn} \cdot Q_{H,gn} \text{ [kWh/month]} \tag{6}$$

where:

$Q_{H,nd}$ – amount of heat necessary to meet the heating demand of a building (a flat, part of a building) in a month or a year [kWh/month],

$Q_{H,ht}$ – heat losses through transmission and ventilation in a month [kWh/month],

$Q_{H,gn}$ – internal and solar heat gains in a month [kWh/month],

$\eta_{H,gn}$ – heat gain utilization factor under the heating regime.

Values of monthly heat gains from solar radiation through windows in vertical partitions of a building should be computed from the formula:

$$Q_{s1,s2} = \Sigma_i \, C_i \cdot A^{3i} \cdot I_i \cdot g \cdot k_\alpha \cdot Z \text{ [kWh/month]} \tag{7}$$

where:

C_i – ratio of the glazed surface area to the total area of a window, which depends on the size and construction type of a window; the average value is 0.7,

A_i – surface area of a window or a French window within the inside diameter of the aperture in the partition [m^2],

I_i – value of solar energy within the analyzed month relative to the vertical plane in which a window of the surface area Ai is fitted, according to the data from the nearest solar radiation measuring station [kWh/(m^2 month)],

g – coefficient of the solar energy transmission through the glazed surface,

k_α – correction coefficient of the value Ii due to the inclination of the roof to the vertical wall, $k\alpha = 1.0$,

Z – coefficient of the shading of a building due to its orientation and shading components on the building facade.

Value of internal heat gains is calculated from the equation:

$$Q_{\text{int}} = q_{\text{int}} \cdot A_f \cdot t_M \cdot 10^{-3} \text{ [kWh/month]} \tag{8}$$

where:

q_{int} – heat load of internal gains in a given room [W/m^2],

A_f – is the total floor area of rooms in a building or a flat where temperature is regulatedą [m^2],

t_M – number of hours in a month (during the heating season)]h].

As seen from dependence (1), when the value of coefficient U for construction partitions (walls, roof, windows, doors) declines, so does the value of the heat loss coefficient and, consequently, the value to the total heat flow through transmission and the value of the heat amount necessary to fulfill the heating demand of the building – dependence (6). This is reflected in the values of the final and primary usable energy needed for heating and ventilating the buildings, and in the values of the PE and FE factors.

Description of the building

The analyzed building (Fig. 1) is a multi-family, four-storey building, with two aboveground floors, a partly habitable attic and a basement. The building was constructed in 1961. The basement is not heated. In the basement, there are cellars and 11 car garages used by the building's residents. There are 16 flats in the building, situated on three floors. Three heated staircases lead to the flats. The roof is a timber, hipped construction covered with ceramic roof tiles. The building is of traditional masonry brick construction. It is fitted with the following installations:

– electric installation – repaired in 1999;
– gas installation – refurbished in 1997;
– central heating;
– sewage installation.

In 2000, the building's thermal insulation was improved by replacing old windows with new PVC ones.
Specification of the building's characteristics:
The net floor area of the building – 1169.80 m^2;
The usable floor area of the flats – 727.90 m^2;
The cubage of the building – 4 840 m^3;
The length of the building 34.73 m;
The width of the building – 11.15 m.

Fig. 1. The analyzed building
Source: the authors.

The exterior partitions, which separate the building's interior with regulated temperature and other unheated rooms from the exterior environment, consist of:
The exterior walls – 42 cm thick:
– cement and lime plaster 1.5 cm,
– a wall of face hollow blocks 25 cm,
– an air cavity 2 cm,
– a wall of solid clay bricks 12 cm,
– cement and lime plaster 1.5 cm.

The interior staircase wall – 30 cm thick:
- cement and lime plaster 1.5 cm,
- a wall of ceramic solid brick 25 cm,
- cement plaster 1 cm,
- structural cement 2.5 cm.

The ceiling above the basement – 35 cm thick:
- pinewood floor parquet on asphalt pitch 2.5 cm,
- cement screed 4 cm,
- DSM floor system 27 cm,
- cement and lime plaster 1.5 cm.

The floor above the second floor – 47.5 cm thick:
- rockwool 15 cm,
- cement screed 4 cm,
- DSM floor system 27 cm,
- cement and lime plaster 1.5 cm.

Walls between rooms in the attic – walls adjacent to the attic – 35 cm thick:
- cement and lime plaster 1.5 cm,
- a wall of face brick 18 cm,
- Styrofoam 15 cm,
- dry set wall plaster mesh 0.5 cm.

The exterior walls of the dormer windows – 42 cm thick:
- cement and lime plaster 1.5 cm,
- a wall of face hollow blocks 25 cm,
- an air cavity – 2 cm,
- a wall of solid clay brick 12 cm,
- cement and lime plaster 1.5 cm,

The exterior oblique walls (at the roof) – 28 cm thick:
- cement and lime plaster 1.5 cm,
- a wall of solid clay brick 25 cm,
- cement and lime plaster 1.5 cm.

The roof above the dormer windows:
- cement and lime plaster 1.5 cm,
- chipboard and cement board 6 cm,
- rafters 14 cm,
- a well-ventilated air cavity,
- battens 3 cm,
- ceramic roof tiles.

The central heating and hot water supply system

The building is connected to the municipal heat distribution network (hard coal). Inside the building, there is a c/h heat exchanger. Hot water is boiled in

Junkers boilers located in each flat. The general technical state of the boilers is average.
Windows
The old windows were replaced in all the building with three-chamber PVC windows of $U_f = 1.5$ W/m^2 K for the window frame; double glazed with $U_g = 1.1$ W/m^2 K for the glazing.
Location of the building: Lębork (climatic zone I).

Analysis of the actual energy performance situation

The data collected during our on-site visit were entered into a computer programme called ArCadia Thermo Pro 4.1.76 Edu. Having run the computations, values of the U factor [W/m^2 K] for particular exterior partitions, separating the regulated-temperature cubage from the external environment, were achieved, such as $U = 1.01$ W/m^2 K for the 42-cm-thick exterior walls, $U = 1.57$ W/m^2 K for the 30-cm-thick exterior walls of the staircases, $U = 1.52$ W/m^2 K for the 35-cm-thick floor above the basement, $U = 0.28$ W/m^2 K for the 47.5-cm-thick floor above the second floor (separating residential flats from the unheated attic), $U = 0.25$ W/m^2 K for the 35-cm-thick walls of residential flats in the attic adjacent to the unheated attic, $U = 1.01$ W/m^2 K for the 42-cm-thick exterior walls in the dormer windows, $U = 1.88$ W/m^2 K for the 28-cm-thick exterior oblique walls(sides of the dormer windows), and $U = 0.93$ W/m^2 K for the ceiling (floor) above the dormer windows.

The calculations yielded the value of the consumed non-renewable primary energy PE = 372.9 kWh/(m^2 year) against the reference PE = 139.48 kWh/(m^2 year).

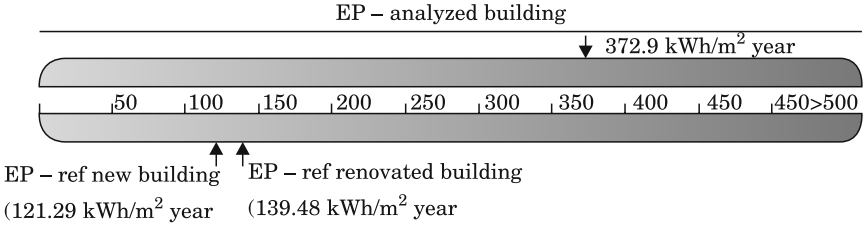

Fig. 2. Value of the consumed, non-renewable primary energy for the analyzed building
Source: ArCadia Thermo PRO, educational version, Intersoft.

Below, the final energy value for the existing condition of the building is specified alongside the quantities of fuels needed to supply the households with heating and hot water, according to the reference norms.

Table 2

Values of the final energy for the actual energy performance situation

Type of fuel – c/h	Share %	$\eta_{H.tot}$	H_u	Unit	$Q_{K.H}$ [kWh/year]	Fuel consumption B	Unit
Fuel – coal	100.0	0.63	7.70	kWh/kg	178 829.47	23 224.61	kg/year
Type of fuel – hot water	Share %	$\eta_{W.tot}$	H_u	Unit	$Q_{K.W}$ [kWh/year]	Fuel consumption B	Unit
Fuel – natural gas	100.0	0.36	9.97	kWh/m^3	69 371.32	6 958.01	m^3/year

H_u – heating value
Source: the authors, using ArCadia Thermo PRO, educational version, Intersoft.

In order to simulate the amounts of pollutants emitted to the environment depending on the type of fuel used in the central heating and hot water systems, an application of the programme ArCadia Thermo PRO, educational version, called The Eco Effect, was used. From the input data, it helps to calculate amounts of emitted airborne SO_2, NOX, CO, CO_2, ash, soot and B-a-P. This kind of analysis is necessary when an investment project is audited in order to apply for EU funds or for support from the Polish Environmental Protection Fund. Calculations of the emission of pollutants rely on the information and instructions published by the Ministry of the Environmental Protection, Natural Resources and Forestry 1/96, titled Emission factors of pollutants introduced to air from fuel combustion for energy generation. The above indices also include auxiliary electric devices necessary to keep central heating and hot water systems working.

Table 3

Parameters of the emission of pollutants in the existing state of the building – c/h and h/w

Parameters of the emission of pollutants – the c/h and h/w systems	Unit	SO_2	NO_x	CO	CO_2	ASH	SOOT	B-a-P
	kg/year	445.9	32.1	1 047.6	60 114.7	244.0	8.1	0.3

Source: the authors, using ArCadia Thermo PRO, educational version, Intersoft.

Analysis of the energy performance after the thermal insulation renovation

In order to improve the building's energy performance, we tested simulated refurbishment of thermal insulation of all partitions enveloping heated parts of the building which at present do not fulfill the maximum value U_{max} according to the 2008 Technical Conditions.

In our model, the exterior walls and the floor above the basement were insulated with EPS70 Styrofoam boards, of the coefficient λ = 0.042 W/m K.

The roof above the habitable part of the attic was insulated with a single layer of rockwool, of the coefficient λ = 0,035 W/m K.
Exterior walls – 42 cm thick:
- cement and lime plaster 1.5 cm,
- a wall of face hollow block 25 cm,
- an air cavity 2 cm,
- a wall of ceramic solid brick 12 cm,
- cement and lime plaster 1,5 cm,
- EPS70 Styrofoam- 15cm.

The floor above the basement – 35 cm thick:
- Pinewood floor parquet on asphalt pitch 2.5 cm,
- Cement screed 4 cm,
- DSM floor system 27 cm,
- Cement and lime plaster 1.5 cm,
- EPS70 Styrofoam – 10 cm.

Exterior walls in the dormer windows – 42 cm thick:
- Cement and lime plaster 1.5 cm,
- A wall of face hollow blocks 25 cm,
- An air cavity – 2 cm,
- A wall of solid clay brick 12 cm,
- Cement and lime plaster 1.5 cm,
- EPS70 Styrofoam – 15 cm.

Exterior oblique walls (at the roof) – 28 cm thick:
- Cement and lime plaster 1.5 cm,
- A wall of solid clay brick 25 cm,
- Cement and lime plaster 1.5 cm,
- A wall of ceramic solid brick 25 cm,
- Cement and lime plaster 1.5 cm,
- EPS70 Styrofoam – 15 cm.

The roof above the dormer windows:
- Cement and lime plaster 1.5 cm,
- Chipboard and cement board 6 cm,
- Rafters 14 cm / roockwool 14 cm,
- Battens 3 cm,
- Ceramic roof tiles.

The modelled improvement of the partitions lowered the PE to 249.4 kWh/(m^2 year), which means 33.12% savings relative to the analyzed initial value. Unfortunately, it does not modify the PE value so as to meet the requirements set in the 2008 Technical Conditions.

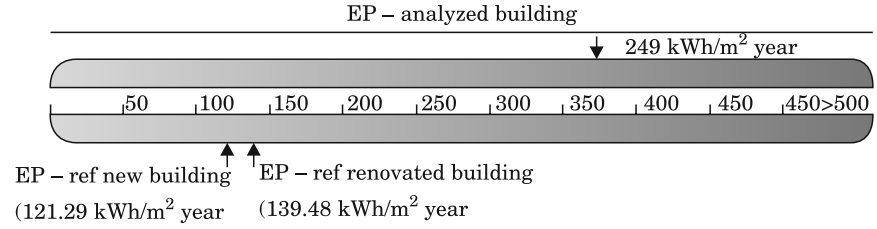

Fig. 3. Value of non-renewable energy input for the analyzed building after the proposed renovation of the thermal insulation of partitions
Source: ArCadia Thermo PRO, educational version, Intersoft.

Below, we present the final energy value of the building after the thermal insulation renovation and the amounts of fuel needed to supply the building with heat and hot water, according to the norms.

Table 4

Values of final energy for the building after thermal insulation renovation

Type of fuel – c/h	Share %	$\eta_{H.tot}$	H_u	Unit	$Q_{K.H}$ [kWh/year]	Fuel consumption B	Unit
Fuel – coal	100.0	0.63	7.70	kWh/kg	95 285.67	12 374.76	kg/year
Type of fuel – hot water	Share %	$\eta_{W.tot}$	H_u	Unit	$Q_{K.W}$ [kWh/year]	Fuel consumption B	Unit
Fuel – natural gas	100.0	0.36	9.97	kWh/m^3	69 371.32	6 958.01	m^3/year

H_u – heating value
Source: the authors, using ArCadia Thermo PRO, educational version, Intersoft.

Parameters of the emission of pollutants:

Table 5

Parameters of the emission of pollutants for the building after thermal insulation renovation – c/h and h/w

Parameters of the emission of pollutants – the c/h and h/w systems	Unit	SO_2	NO_x	CO	CO_2	ASH	SOOT	B-a-P
	kg/year	237.6	21.3	559.4	38 415.0	130.0	4.3	0.2

Source: the authors, using ArCadia Thermo PRO, educational version, Intersoft.

For comparison, the value of the final energy for the central heating system (thermal insulation renovation modifies only this value) will decrease by nearly 46.72% after the tested renovation. Fuel consumption will decrease by 46.72% relative to the initial value.

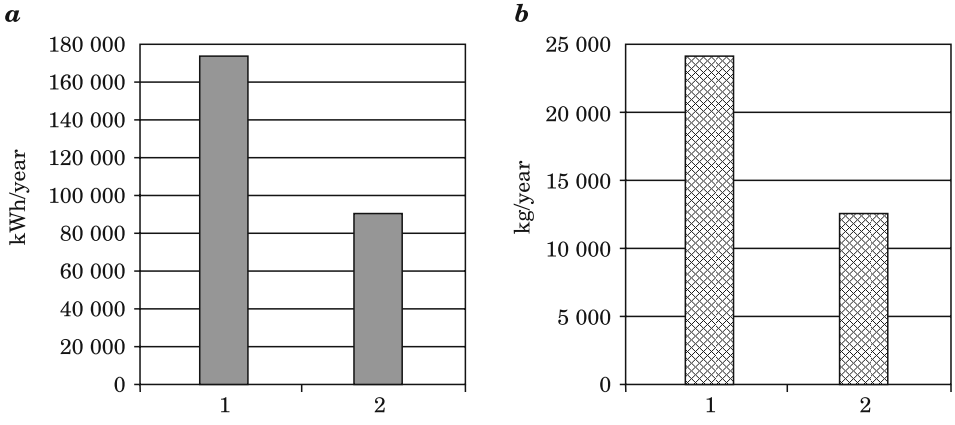

Fig. 5. Values of *a* – final energy, *b* – fuel consumption: 1. before and 2. after thermal insulation renovation

Source: the authors.

The modelled renovation of the building's thermal insulation also reduced the parameters of the emission of contamination. The change in presented in Table 6.

Table 6

Per cent change in parameters of the emission of pollutants after the renovation of thermal insulation – c/h and h/w

Change in parameters of the emission of contamination – c/h and h/w systems	Unit	SO_2	NO_x	CO	CO_2	ASH	SOOT	B-a-P
	[%]	46.71	33.64	46.60	36.10	130.0	46.72	33.33

Source: the authors, using ArCadia Thermo PRO, educational version, Intersoft.

Summary

The value of primary energy is an important source of information about the energy performance of a building. If the factor of non-renewable energy input is high, the user will know that the maintenance costs of the building are high as well. A low value of the PEF tells us that a given building will be inexpensive to maintain. Our analysis clearly demonstrates that improved thermal insulation has a significant impact on the PEF. The analyzed building, after renovation of its thermal insulation consisting in added insulation of the exterior partitions, which separate the building's space with the regulated temperature and other unheated interior space from the outdoor climate, considerably lowered the value of the PEF. As this factor corresponding to the

non-renewable primary energy input decreases, so does the emission of airborne pollutants.

However, the results of our analysis prove that renovation of thermal insulation such as refurbished insulation of exterior partitions, which envelope heated and unheated rooms inside a building from the external environment, does not improve the building's energy performance well enough to fulfill the rigorous reference values given in the Regulation of the Minister for Infrastructure on technical conditions to be fulfilled by buildings and their orientation (Journal of Law2002 no 75 item 690 with further amendments). Thus, in order to meet these requirements, a major refurbishment of the central heating and hot water supply systems, which at present also generate high losses, is needed.

Translated by JOLANTA IDŹKOWSKA

Accepted for print 15.10.2012

References

Directive 2002/91/EC of European Parliament and the Council of 16 December 2002 on the Energy Performance of the Buildings.

The Act of 7 July 1994 – Construction Law (Journal of Laws of 1994 No 89, item. 414 as. Amended.).

Information and instructional materials MOŚZNiL 1/96 "The emission of pollutants into the air from fuel combustion processes".

Council Directive 96/62/EC of 27 September 1996 on ambient air quality assessment and management

Act of 27.04.2001 year – Environmental Protection Law (Journal of Laws No. 61, item. 627 of 2001., As amended. Amended.).

Regulation of the Minister of Infrastructure dated 12 April 2002 on the technical conditions to be met by buildings and their location (Journal of Laws 2002 No. 75, item. 690, as amended. Amended.).

Regulation of the Minister of Infrastructure of 6 November 2008 on the methodology for calculating the energy performance of the building which is the whole technical-independent utility and the preparation and presentation of certificates of energy performance (OJ 2008 No 201, item. 1240).

TECHNICAL SCIENCES
Abbrev.: Techn. Sc., No 15(2), Y 2012

THE IMPACT OF OPTIMIZING THE NUMBER OF POINTS OF ALS DATA SET ON THE ACCURACY OF THE GENERATED DTM

Wioleta Błaszczak-Bąk

Institute of Geodesy
University of Warmia and Mazury in Olsztyn

K e y w o r d s: optimization, ALS point cloud, filtration, DTM.

A b s t r a c t

Airborne laser scanning technology delivers the result of the survey in the form of a point cloud. In order to construct a digital terrain model, it is necessary to perform filtration, which consists in separating data reflecting the relief features from the data reflecting situational details. In view of the very large amount of data in the survey data set, as well as the time consumption and difficulty in automatic filtration of the point cloud, it is possible to apply an optimization algorithm reducing the size of the point cloud while deriving a digital terrain model. This study presents the stages of compiling an airborne laser scanning point cloud using filtration and optimization. The filtration was carried out using the adaptive TIN model and the method of robust moving surfaces, while optimization was carried out with the application of an already existing algorithm to reduce the size of the survey data set. The effect of reducing the size of the data set on the accuracy of the generated DTM was tested and empirical and numerical tests have been performed.

Introduction

Airborne Laser Scanning (ALS) is a survey technology used for quickly gathering a set of coordinates concerning spatial field points of the surveyed area. The most important parameters describing the data obtained from the airborne laser scanning include: scan angle, flying height, scan rate and point density (BRIESE, PFEIFER 2001). Very frequently, the point density obtained is not adjusted for the needs of the planned compilations. We usually deal with a very high (too high) number of points, therefore it is necessary to reduce it to ensure effective, less labour-consuming and less time-consuming generation of a digital terrain model (DTM) (BŁASZCZAK, KAMIŃSKI 2007, BŁASZCZAK-BĄK et al. 2010b).

The method of deriving a DTM from the ALS point cloud consists of a preliminary processing stage and a main processing stage. The preliminary

processing stage consists of filtration (F), i.e. separating the data reflecting the relief features from the data representing situational details, while the main processing stage consists of DTM construction. In view of the fact that the point cloud makes the so-called large set of data an optimization algorithm is added to the methodology of DTM generation at the stage of preliminary processing (BŁASZCZAK, KAMIŃSKI 2007, BŁASZCZAK-BĄK et al. 2010a). The purpose of the optimization algorithm (O) is to reduce the size of the survey data set before (O – F) or after (F – O) filtration.

A modified methodology of ALS point cloud compilation can be therefore presented in the following diagram (Fig. 1).

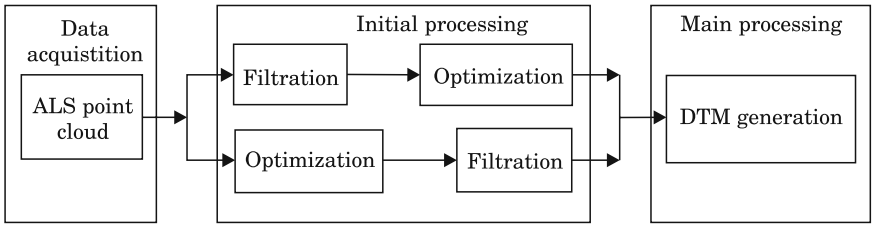

Fig. 1. A general scheme of the modified methodology for processing the ALS point cloud

The application of the O – F variant facilitates operation of the data filtration algorithm, shortens filtration time and influences the effective i.e. faster preparation of data for DTM construction without losing information required for proper implementation of the task. On the other hand, the application of the F – O variant makes it possible to reduce the data set obtained after filtration, i.e. directly used for construction of a DTM (BŁASZCZAK-BĄK et al. 2010a, BŁASZCZAK-BĄK et al. 2011).

The study presents the stages of DTM compilation with the application of the O – F variant, F – O variant and F variant for comparison. The optimization was carried out with the use of an optimization algorithm. The algorithm uses the Visvalingam – Whyatt (V – W) cartographic generalization method (VISVALINGAM, WHYATT 1992). The filtration was carried out with the use of the adaptive TIN (Triangular Irregular Network) model (AXELSSON 2000) and the method of robust moving surfaces (ELMQVIST 2002, SHUT 1976, HUBER 1981). The effect of reducing the size of the data set on the accuracy of the generated DTM was tested.

Optimization algorithm

The density of the ALS point cloud obtained is usually between a few and a few dozen points per 1 m^2 of the surveyed area. Such a data set makes the stage of main processing more difficult. Construction of a DTM requires a set

of data containing significant information about the area, while the points which do not contribute any significant information for DTM generation are unnecessary. Therefore, the point cloud can be reduced at the stage of preliminary processing by applying an algorithm optimizing the size of the survey result data set (BŁASZCZAK, KAMIŃSKI 2007, BŁASZCZAK-BĄK et al. 2010).

The optimization algorithm consists of the following stages:

– Defining survey strips in the XY plane, parallel to the Y axis.

– Selecting the method of cartographic generalization to reduce the size of the survey data set.

– Application of the chosen generalization method in each strip (in the YZ plane).

An important phase is the choice of the method in the survey strip, as well as selection of appropriate tolerance ranges in the method. The choice of tolerance ranges determines the degree of the ALS set reduction (number of removed points).

The V – W generalization algorithm was selected in the study which creates a generalized line of triangles from the nearest points. The surface of the calculated areas of triangles is compared to the area of the tolerance triangle, the size of which determines how many points are to be removed. The size of the tolerance triangle area is established by the user on the basis of statistical characteristics of the survey result data set. It is possible, for example, to assume that its value equals the area of the equilateral triangle with a side corresponding to a minimum distance between the points of the data set. If the area of the triangle defined on the basis of the survey results exceeds the area of the tolerance triangle, then the second point of the analysed triangle is maintained, otherwise it is removed.

ALS point cloud filtration

The literature contains many reports of filtration methods. The filtration methods presented in the literature are based, among others, on morphological filters (ZHANG 2003, VOSSELMAN 2001), gradient methods (HYYPPÄ et al. 2002, WACK, WIMMER 2002), modelling of active surfaces (ELMQVIST 2002), spline interpolation (BROVELLI et al. 2002) or the adaptive TIN model method (AXELSSON 2000).

The study applied two methods: an adaptive TIN model method and the robust moving surfaces method.

Adaptive TIN model method (ATIN)

The algorithm of the adaptive TIN model method is run iteratively and can be presented in the following way (AXELSSON 2000, BŁASZCZAK-BAK et al. 2010a):

– creating a GRID (Regular Raster Grid) net on the basis of the ALS point cloud, and selecting, in each mesh of the net, a point of the lowest altitude;

– carrying out triangulation of selected points (usually by Delauney's method);

– calculating, in each of the triangles obtained, the distances and angles between points situated within its vertical projection, and on their basis, the medians of the distances and medians of the angles;

– establishing new points belonging to the topographic area based on the criteria assumed (i.e. values of calculated angles and distances lower than the respective median);

– iterative return to the triangulation stage from selected points, until all points have been checked or the established threshold value of the analysed parameters is exceeded.

Robust moving surface (MS)

While carrying out filtration using the moving surface method, we can use a polynomial of the first degree in the following form:

$$z(x, y) = a + bx + cy \tag{1}$$

where:
x, y, z are coordinates of points obtained from ALS survey, a, b, c are polynomial coefficients. The present study applies a polynomial of the first degree for analysis purposes, therefore, the equation of adjustments can be written in the following form:

$$V_i = a + bx_i + cy_i - z_i \tag{2}$$

where:
$i = 1, 2,..., k$ (k is the number of observations in analyzing data set).

Equation (2) can also be written as:

$$\mathbf{V} = \mathbf{A}\hat{\mathbf{X}} - \mathbf{z} \tag{3}$$

where:
$\mathbf{V} = [V_1, V_2,..., V_k]^T$ residuals vector, $\hat{\mathbf{X}} = [\hat{a}, \hat{b}, \hat{c}]^T$ is estimated polynomial coefficients vector, $\mathbf{z} = [z_1, z_2,..., z_k]^T$ is a vector of heights of points obtained from ALS, $\mathbf{A}$ is a matrix of coefficients.

Solving equation (3) with the least squares method, yields the estimated parameters vector:

$$\hat{\mathbf{X}}^{\mathbf{LS}} = (\mathbf{A}^{\mathbf{T}}\mathbf{P}\mathbf{A})^{-1}\mathbf{A}^{\mathbf{T}}\mathbf{P}\mathbf{z} \tag{4}$$

where:

$\mathbf{P} = \mathrm{Diag}(p_1,..., p_k)$ diagonal weight matrix, in which, $p_i = \frac{1}{D_{P_iP_0}}$, $D_{P_iP_0}$ is a distance between P_i and the point with interpolated height P_0, $i=1,...,k$, k is the number of points being processed. Estimated parameters can be derived by means of robust estimation (HUBER 1981, KRAUS, PFEIFER 1998). In robust estimation the weights of observations p_i, which standardized residuals $\bar{V}_i = \frac{V_i}{m_{V_i}}$ (where $m_{V_i} = \sqrt{\mathbf{P}^{-1} - \mathbf{A}(\mathbf{A}^{\mathbf{T}}\mathbf{P}\mathbf{A})^{-1}\mathbf{A}^{\mathbf{T}}}$ is mean error of residuum) are outside of a certain range <–g; g> are damped by dampening function. In presented research, the one sided form of weight function according to Huber's method is used (HUBER 1981). The function is written as:

$$w_i(V_i) = \begin{cases} 1 & \text{when } |\bar{V}_i| \le g \\ \frac{g}{\bar{V}_i}\, sng(V_i) & \text{when } |\bar{V}_i| > g \end{cases} \tag{5}$$

Calculations in robust estimation are carried out in an iterative process, in which equivalent weights $\bar{p}_i$ are determined from the following relation:

$$\bar{p}_i = p_i\, w_i\, (\bar{V}_i) \tag{6}$$

Polynomial parameters resistant to outliers (objects belonging to the area coverage) are obtained by performing the following iterative procedure:

$$\hat{\mathbf{X}} = (\mathbf{A}^{\mathbf{T}}\bar{\mathbf{P}}^{\mathbf{l-1}}\mathbf{A})^{-1}\mathbf{A}^{\mathbf{T}}\bar{\mathbf{P}}^{\mathbf{l-1}}\mathbf{z} \tag{7}$$

where:
$\bar{\mathbf{P}} = \mathrm{Diag}(\bar{p}_1, \bar{p}_2,..., \bar{p}_l)$ is an equivalent weight matrix, (l = 1, 2,..., is the number of iterations). Results obtained by the least squares method: $\hat{\mathbf{X}}^{\mathbf{0}} = \hat{\mathbf{X}}^{\mathbf{LS}}$ usually provide a starting point for an iterative process.

Practical tests

The modified methodology of ALS point cloud processing was applied to reduce the number of observations in a point cloud from surveying a section of Olsztyn. The tested large dataset comes from Visimind surveying system, which comprises of Riegl LMS-Q240 laser, GPS Topcon, IMU, and digital cameras. The laser scanning angle equaled 60 degrees, with a resolution of 10 000 Hz. The scan was made during a helicopter flight with the speed of around 50 km/h at the height of around 70 m. The subset of ALS data used for digital tests contains 80589 points. Point density is about 25 points per 1 m^2. The subset is presented in Fig. 2.

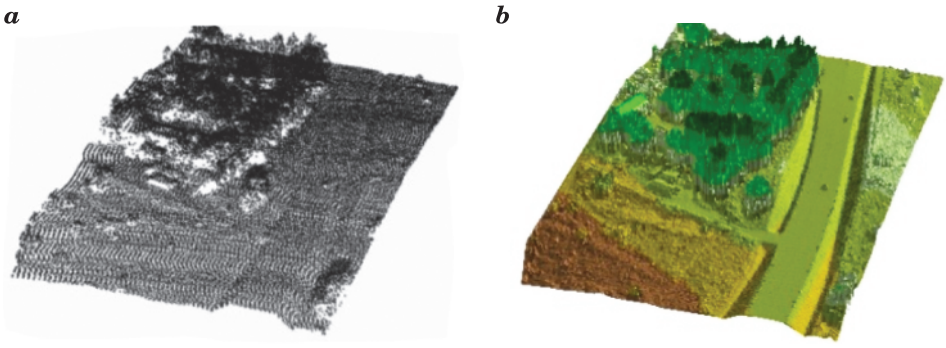

Fig. 2. Perspective presentation the original ALS point cloud: a) points, b) TIN model

Variant O – F

The size of the presented data set was reduced by applying an optimization algorithm. The optimization algorithm used the V – W method. During the reduction, the assumed width of search belt was 2 m and the tolerance triangle surface was 0.05 m^2. The width of search belt has been establish on results of earlier studies conducted with similar datasets. Area of tolerance triangle is an area of equilateral triangle with side equals mean distance between points from dataset (0,12 m). Point density after optimization is about 12 points per 1 m^2. The optimized ALS data set is presented in Fig. 3.

The optimized ALS point cloud was then filtrated using the ATIN method and the MS method. The ATIN method assumed that the size of the grid in which the height of the lower value was searched was 10 m $\times$ 10 m. Triangulation of selected points was made by Delauney's method in 84 iterations. In the MS method, a 10 m $\times$ 10 m square was used for calculation purposes, while the acceptable value of estimated adjustment was 3 m.

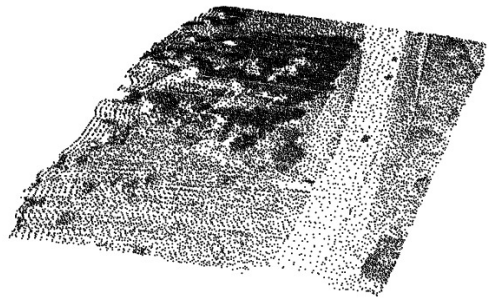

Fig. 3. Perspective presentation the ALS data set after optimization

Results of processing with the use of variant O – F are presented in Fig. 4 and Fig. 5.

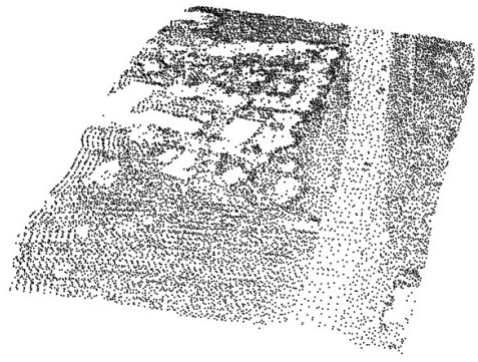

Fig. 4. The optimized data set after ATIN model method filtration

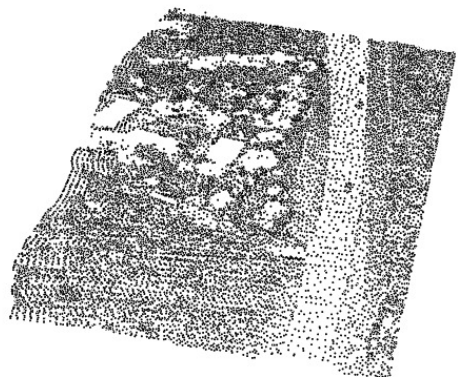

Fig. 5. The optimized data subset after MS method filtration

Variant F – O

The original point cloud has been subjected to filtration by ATIN method and MS method. For filtration the same parameters as in variant O – F were applied.

In ATIN method triangulation of selected points was made in 172 iterations. Filtered data sets are shown in Fig. 6 and Fig. 7.

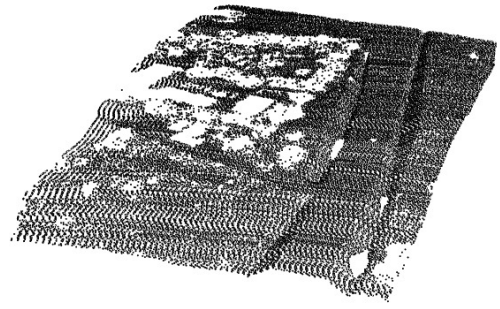

Fig. 6. The original data set after ATIN model method filtration

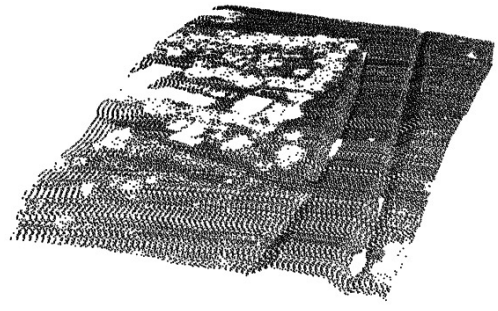

Fig. 7. The original data set after MS method filtration

Filtered data sets were optimized using V – W method. During the reduction, the assumed width of search belt was 2 m and the tolerance triangle surface was 0.05 m^2 (as in O – F variant). Results are presented in Fig. 8 and Fig. 9.

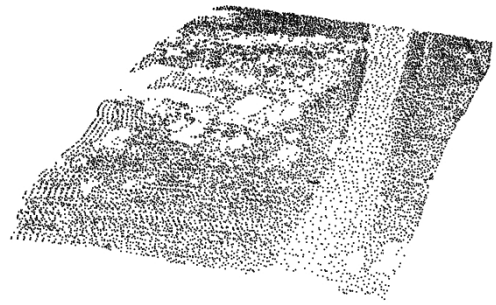

Fig. 8. The data set after ATIN method filtration and after optimization

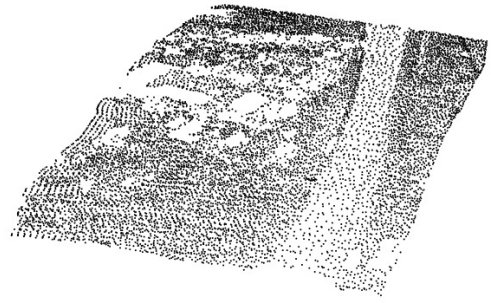

Fig. 9. The original data set after MS method filtration and after optimization

Analysis of results

The table below presents the number of points obtained after O – F variant and F – O variant.

In the case of F – O variant the application of the optimization algorithm has reduced the size of the data set after filtering by ATIN and MS to about 24%. The optimization was performed on the terrain points, which were directly used for DTM generation. In the case of O – F variant optimization was performed on the original (whole) data set (points showing the terrain and points showing situational details) and the point cloud is reduced to about 46%. Then the optimized sets were filtered by ATIN and MS method to obtain sets of points showing the area with the number of 15 515 points and 17 447 points, respectively.

Four data sets were obtained for such optimization and filtration parameters. For variant F – O there are very similar numbers of points (12 075 and 12 436 for ATIN and MS), while for variant O – F the number of points in the collection varies by about two thousand points.

Table 1

The number of points in data subsets

Variant F – O			Variant O – F		
Total number of points in original ALS data set 80587					
Filtration	number of terrain points in ALS data subset after ATIN method filtration	48550	total number of points in ALS data subset after optimization	37080	Optimization
	number of terrain points in ALS data subset after MS method filtration	49765			
Optimization	number of terrain points in ALS data subset filtered by means of ATIN method after optimization	12075	number of terrain points in optimized ALS data subset after ATIN method filtration	15515	Filtration
	number of terrain points in ALS data subset filtered by means of MS method after optimization	12436	number of terrain points in optimized ALS data subset after MS method filtration	17447	

DTM generation

Calculation results of two variants were used to generate DTMs.

The O – F variant generated $DTM^{ATIN\ O\text{-}F}$ and $DTM^{MS\ O\text{-}F}$ and the F – O variant $DTM^{ATIN\ F\text{-}O}$ and $DTM^{MS\ F\text{-}O}$. To compare the DTMs generated from the two datasets: O – F and F – O, there were also two DTMs generated from dataset obtained by using standard methodology for ALS point cloud processing (called as F variant): $DTM^{ATIN\ F}$ and $DTM^{MS\ F}$. The DTM was generated by the Kriging method (SLUITER 2008), assuming a grid mesh of 1 m. DTMs generated are presented in Fig. 10, Fig. 11, Fig. 12, Fig. 13, Fig. 14 and Fig. 15.

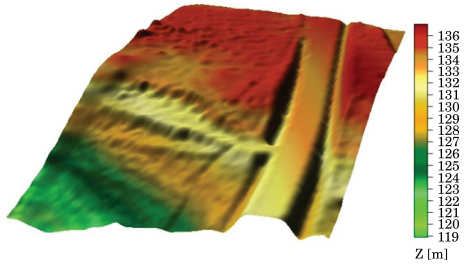

Fig. 10. $DTM^{ATIN\ O\text{-}F}$

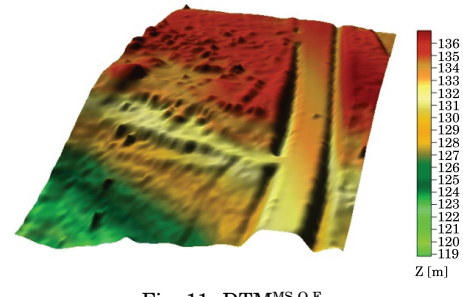

Fig. 11. $DTM^{MS\ O\text{-}F}$

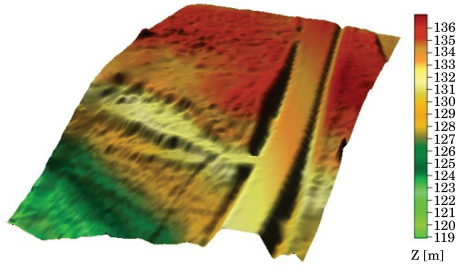

Fig. 12. $DTM^{ATIN\ F\text{-}O}$

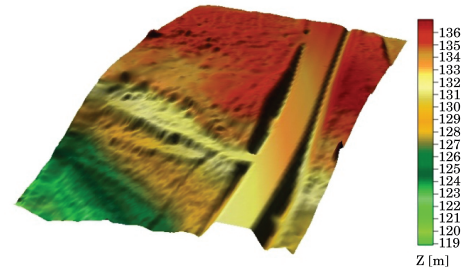

Fig. 13. $DTM^{MS\ F\text{-}O}$

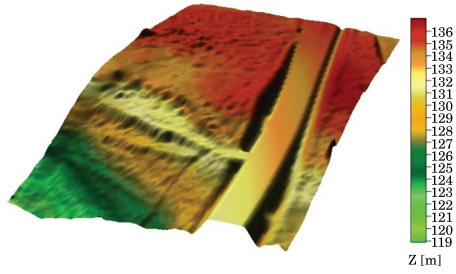

Fig. 14. $DTM^{ATIN\ F}$

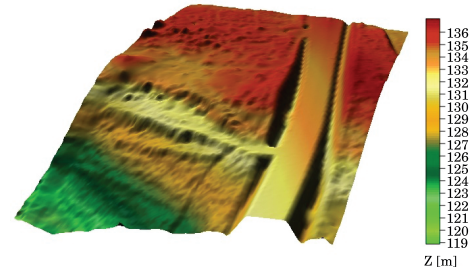

Fig. 15. $DTM^{MS\ F}$

The generated DTMs represent the same area preserving the general character of the terrain. However, they differ in the level of detail. DTM^{ATIN} has a more smoothed form when compared to DTM^{MS}, which was affected by the number of points in the filtrated data sets.

Assessment of DTM accuracy

Generated DTMs were subject to statistical comparison. The following parameters were used for DTM comparison (OKSANEN, SARJAKOSKI 2005, HEJMANOWSKA et al. 2008):

a) mean error:

$$m_0 = \sqrt{\frac{\Sigma(z_{\text{mean}} - z_i)^2}{k - 1}} \tag{8}$$

where:

z_{mean} is a mean height calculated from heights of both DTMs, z_i (i=1,2,..., k) are heights of the point assumed for creating DTM, k is the size of the subset used for DTM construction,

b) range $R = z_{\max} - z_{\min}$, where $z_{\max}$ is the maximum height and $z_{\min}$ is the minimum height,

c) mean value of height difference:

$$\Delta h_{\text{mean}} = \frac{\Sigma_{i=1}^{k}(\tau)}{k} \tag{9}$$

where:

$\tau = \tau_1,\ \tau_2,\ \tau_3$ or τ_4

$\tau_1 = Z_{\text{DTM}_{\text{ATIN O-F}}} - Z_{\text{DTM}_{\text{ATIN F}}},\ \tau_2 = Z_{\text{DTM}_{\text{ATIN F-O}}} - Z_{\text{DTM}_{\text{ATIN F}}},$

$\tau_3 = Z_{\text{DTM}_{\text{MS O-F}}} - Z_{\text{DTM}_{\text{MS F}}},\ \tau_4 = Z_{\text{DTM}_{\text{MS F-O}}} - Z_{\text{DTM}_{\text{MS F}}}$

d) root-mean-square error (RMSE), which describes the absolute altitude accuracy of DTM:

$$\text{RMSE} = \sqrt{\frac{\Sigma_{i=1}^{k}(\rho)^2}{k}} \tag{10}$$

where:

$\rho = \rho_1,\ \rho_2,\ \rho_3$ or ρ_4

$\rho_1 = \tau_1 - \Delta h_{\text{mean}},\ \rho_2 = \tau_2 - \Delta h_{\text{mean}},\ \rho_3 = \tau_3 - \Delta h_{\text{mean}},\ \rho_4 = \tau_4 - \Delta h_{\text{mean}}$

e) coefficient of determination, which is the measure of model adjustment (the closer to 1, the better the match of the model to another model):

$$D_1^2 = \frac{\Sigma_{i=1}^{k}(Z_{\text{DTM}_{\text{ATIN O-F}}} - Z_{\text{mean}})^2}{\Sigma_{i=1}^{k}(Z_{\text{DTM}_{\text{ATIN F}}} - Z_{\text{mean}})^2} \text{ and } D_2^2 = \frac{\Sigma_{i=1}^{k}(Z_{\text{DTM}_{\text{ATIN F-O}}} - Z_{\text{mean}})^2}{\Sigma_{i=1}^{k}(Z_{\text{DTM}_{\text{ATIN F}}} - Z_{\text{mean}})^2}$$
$$D_3^2 = \frac{\Sigma_{i=1}^{k}(Z_{\text{DTM}_{\text{MS O-F}}} - Z_{\text{mean}})^2}{\Sigma_{i=1}^{k}(Z_{\text{DTM}_{\text{MS F}}} - Z_{\text{mean}})^2} \text{ and } D_4^2 = \frac{\Sigma_{i=1}^{k}(Z_{\text{DTM}_{\text{MS F-O}}} - Z_{\text{mean}})^2}{\Sigma_{i=1}^{k}(Z_{\text{DTM}_{\text{MS F}}} - Z_{\text{mean}})^2} \tag{11}$$

The results of received parameters for all variants are presented in Table 2:

Table 2

The parameters values for all variants

Parameters	$\text{DTM}^{\text{ATIN O-F}}$	$\text{DTM}^{\text{ATIN F-O}}$	$\text{DTM}^{\text{ATIN F}}$	$\text{DTM}^{\text{MS O-F}}$	$\text{DTM}^{\text{MS F-O}}$	$\text{DTM}^{\text{MS F}}$
m_0	3.64 m	3.65 m	3.63 m	3.71 m	3.75 m	3.70 m
R	18.09 m	18.10 m	18.02 m	18.18 m	18.20 m	18.15 m
Δh_{mean}	0.05 m	0.05 m	–	0.05 m	0.05 m	–
RMSE	0.04 m	0.03 m	–	0.05 m	0.04 m	–
D^2	1.01	0.99	–	0.97	0.98	–

Parameters calculated for the purpose of assessing the accuracy of the DTM obtained reveal a similar character. The mean error is higher for DTM^{MS}, which is influenced by a range which is also higher in case of this surface. The

RMSE error has a very similar value in the case of all surfaces. On the other hand, the determination coefficient calculated indicates that the surfaces are well matched.

Conclusion

In this paper the effect of reducing the size of the data set on the accuracy of the generated DTM was tested. The presented research proposes a modified methodology of analysing the ALS point cloud in variant O – F and variant F – O. Filtration in both variants was executed with the application of the ATIN method and MS method. Optimization was made by using the V – W method. From the data sets after optimization and filtration four DTMs were generated: $DTM^{ATIN\ O\text{-}F}$, $DTM^{ATIN\ F\text{-}O}$ and $DTM^{MS\ O\text{-}F}$, $DTM^{MS\ F\text{-}O}$. To compare the DTMs generated from the variants: O – F and F – O, there were also two DTMs generated from dataset obtained by using standard methodology for ALS point cloud processing: $DTM^{ATIN\ F}$ and $DTM^{MS\ F}$. On the basis of the analyses presented above, the following conclusions are:

a) parameters for assessing the accuracy of the generated DTM are similar,

b) optimization does not adversely affect the accuracy of the generated DTM,

c) optimization reduces the number of points of an ALS point cloud and streamlines the methodology of processing a set of measurement for generating DTM,

d) generated DTMs exhibit a similar nature terrain.

Detailed findings can be summarized as follows:

a) mean error for DTMs generated from data sets filtrated with MS method is larger than mean error for DTMs generated from data set filtrated with ATIN method,

b) mean error for DTMs generated from data sets which were subjects only to filtration (ATIN and MS method) is smallest because the range was smallest,

c) mean value of the height difference is the same for all generated DTMs,

d) RMSE is the smallest for $DTM^{ATIN\ F\text{-}O}$, in comparison to other DTMs' errors the difference is not larger than 1 cm,

e) coefficient of determination is the best for $DTM^{ATIN\ F\text{-}O}$ and $DTM^{ATIN\ O\text{-}F}$ and the worst for $DTM^{MS\ F\text{-}O}$.

Studies conducted for two variants F – O and O – F show that optimization can be applied during ALS point cloud processing. It does not disturb DTM generation, has an impact on the time of data processing, because smaller dataset means shorter time of processing.

Translated by ANNA SOBIERAJ

Accepted for print 24.09.2012

References

AXELSSON P. 2000. *DEM generation from laser scanner data using adaptive TIN models*. International Archives of Photogrammetry and Remote Sensing, Vol. XXXIII/4B, Amsterdam.

BŁASZCZAK W., KAMIŃSKI W. 2007. *Data number reduction in measurement results set using optimization algorithm.* Proceedings of FIG Working Week, CD.

BŁASZCZAK-BĄK W., JANOWSKI A., KAMIŃSKI W., RAPIŃSKI J. 2010a. *Proposition of modification of aerial laser survey point cloud processing methodology*. Archives of Geomatics "New technology and instruments In survey".

BŁASZCZAK-BĄK W., JANOWSKI A., KAMIŃSKI W., RAPIŃSKI J. 2010b. *Modification of Lidar Point Cloud Processing Methodology*. Sydney The XXX FIG General Assembly and Working Week, Sydney 13.05 – 17.05 2010. CD.

BŁASZCZAK-BĄK W., JANOWSKI A., KAMIŃSKI W., RAPIŃSKI J. 2011. *ALS Data Filtration with Fuzzy Logic*. Journal of the Indian Society of Remote Sensing, 39(4): pp 591–597.

BRIESE C., PFEIFER N. 2001. *Airborne laser scanning and derivation of digital terrain models*. In Fifth Conference on Optical 3-D Measurement Techniques, Vienna, Austria.

BROVELLI M.A., BANNATA M., LONGONI U.M. 2002. *Managing and processing LIDAR data within GRASS*. Proceedings of the Open source GIS – GRASS user conference, Trento.

ELMQVIST M. 2002. *Ground surface estimation from airborne laser scanner data using active shape models*. ISPRS, Commission III, Symposium Photogrammetric Computer Vision, September 9–13, Graz, pp. 114–118.

HEJMANOWSKA B., DRZEWIECKI W., KULESZA Ł. 2008. *The quality of Digital Terrain Models*. Archives of Photogrammetry and Remote Sensing, 18: 163–175.

HUBER P.J. 1881. *Robust Statistics*. John Wiley and Sons.

HYYPPÄ J., PYSSALO U., HYYPPÄ H., SAMBERG A. 2002. *Elevation accuracy of laser scanning – derived digital terrain and target models in forest environment*. International Archives of Photogrammetry and Remote Sensing, XXXIV/ 3A, Graz.

KRAUS K., PFEIFER N. 1998. *Determination of terrain models in wooded areas with airborne laser scanner data*. ISPRS Journal of Photogrammetry and Remote Sensing, 53: 193–203.

OKSANEN J., SARJAKOSKI T. 2005. *Error propagation of DEM-basd surface derivatives*. Computers and Geosciences, 31: 1015–1027.

SCHUT G.H. 1976. *Review of interpolation methods for digital terrain models*. XII th Congress of the International Society for Photogrammetry. Helsinki .

SLUITER R. 2008. *Interpolation methods for climate data: literature review*. De Bilt, Royal Netherlands Meteorological Institute (KNMI).

VISVALINGAM M., WHYATT J.D. 1992. *Line generalization by repeated elimination of point*. Cartographic Information Systems Research Group, University of Hull.

VOSSELMAN G. 2001. *Adjustment and filtering of raw laser altimetry data*. OEEPE Workshop on Airborne Laserscanning and Interferometric SAR for Detailed Digital Elevation Models, Stockholm.

WACK R., WIMMER A. 2002. *Digital terrain models from airborne laser scanner data – a grid based approach*. International Archives of Photogrammetry and Remote Sensing, XXXIV/3B, Graz.

ZHANG K. 2003. *A progressive morphological filter for removing nonground measurements from airborne LIDAR data.* IEEE Transactions on Geoscience and Remote Sensing, 41(4): 872–882.

TECHNICAL SCIENCES
Abbrev.: Techn. Sc., No 15(2), Y 2012

HOW TO EVALUATE OPTIMUM USAGE OF A LAND WITH LINDENMAYER'S GRAMMAR

Urszula Żukowska

Department of Mathematical Methods in Computer Science
University of Warmia and Mazury in Olsztyn

K e y w o r d s: Lindenmayer's grammar, L-system, land management, land valuation, assessment of land's usage, cartographic method.

A b s t r a c t

This work presents the approach which combines Lindenmayer's grammar and Bajerowski's method for finding the optimum usage of a land. Purpose of this approach was to build quick method, which can simplify using of cartographic method and includes algorithm based on natural growth. Result of proposed method is a computer program, which supports decision-making process of analyzing usage of a land. The approach gives possibility of starting from any point from a map and finishing in any derivation step. Therefore user can generate many findings quickly, especially in the form of a map, and compare them. It is also possible to find expansion of specified function of a land. Content of the paper is presented below. First, we discuss context-free parametric L-system. Subsequently we outline the Bajerowski's method. Next we present our approach with adaptation of Bajerowski's proposal and with our description of proposed L-system. We give also example of using our approach with some explanation. Eventually, we presented advantages of our system and possible future developments.

Introduction

Initially, an L-system was designed to simulate growth of plants. Then, because of its usefulness, it was applied to many other problems such as growth of other biological organisms, creating the landscape, drawing fractals and even for composing the music. We adapted L-system's evolution mechanism to finding an optimum usage of a land, which is very vital in evaluation of land's value. The result is a computer program, in which user can choose purpose of a land and initial parameters. Subsequently, after a chosen number of iterations user receives an output as a map with charted fields and sequence of productions. It allows interpreting output in two ways and using the map in further analysis.

In our system was have used Bajerowski's (BAJEROWSKI 1996, 2003, *Podstawy teoretyczne gospodarki*... 2003) proposal for estimating the optimum

usage of a land. His idea is about reading features from a cartographic map and then calculating the value for each basic field. Next step is interpretation of the value for every single field as an optimal or not optimal for specified purpose. This allows urban and spatial experts to make decision whether the land should have another purpose. Another purpose can change the value of a land; therefore it is very important to estimate its profitability.

Lindenmayer's grammar and Bajerowski's method

An L-system is a parallel rewriting system. We present basic definition. The definition with some developments can be found in works (PEITGEN et al. 1992, PRUSINKIEWICZ et al. 1995, PRUSINKIEWICZ, LINDENMAYER 1996,). The rewriting process starts from an axiom – initial module. Then it is replaced by configurations of modules taken from set of rewriting rules. Every individual module, which is replaced in an interaction, is called parent or mother or predecessor. A module, which replaces ancestor's module, is called child or daughter or successor. In the rewriting process mother module is replaced with the daughter module.

Let us denote:
– a module with letter $A \in V$ and parameters $a_1, a_2, ..., a_n$ as by $A(a_1, a_2, ..., a_n)$,
– $M = V \times \Re^*$ as a set of modules, where $\Re^*$ is the set of all finite sequences of parameters,
– $M^* = (V \times \Re^*)^*$ as a set of all strings of modules,
– $M^+ = (V \times \Re^*)^+$ as a set of all nonempty strings,
– $C(\Sigma)$ as a logical expression with parameters from Σ,
– $E(\Sigma)$ as an arithmetic expression with parameters from Σ.

Therefore, a parametric context-free L-system can be defined as an ordered quadruple.

$$G = \langle V, \Sigma\ \omega, P \rangle \tag{1}$$

where:
V – the alphabet of the system,
Σ – the set of formal parameters,
$\omega \in (V \times \Re^*)^+$ – a nonempty parametric word called the axiom,
$P \subset (V \times \Sigma^*) \times C(\Sigma) \times (V \times E(\Sigma))^*$ – a finite set of production.

Productions in this system have format:

Predecessor: condition → successor.

Every land has the one optimum usage, which can be achieved by redevelopment. The redevelopment must be done with minimal costs of it. Therefore Bajerowski (BAJEROWSKI 1996, 2003, *Podstawy teoretyczne gospodarki*... 2003) proposed a cartographic method as tool for redevelopment. We have adapted it to L-grammar; therefore we outline the method of finding the optimum usage of a land. The method assumes that we can read features from a map. We can use topographical map and map of land's sorts.

This method can be described in 4 steps:

1. We must put a square grid on a map with a mesh of a chosen size.

2. We must read features from an every single field and put them into the inventory matrix. We use "0" to denote that specified feature does not exist in basic field and "1" otherwise.

3. We must derive optimal function of a land by multiplying transposed matrix of features which can optimize usage of a land by the inventory matrix. Therefore we arrive at the matrix of optimal function of a land.

4. Interpretation of data from step 3 for optimum usage of a land.

Matrices in cartographic method are described as follows:

– The inventory matrix consists of "0" and "1" and their length and width corresponds to length and width of square grid, put on a map.

– The matrix of features for optimum functions of a land, further called the matrix of features consists of names of features, functions of terrain and parameters, which indicates usefulness of a feature for specified function. Values of parameters used in this matrix were specified by land value experts.

– The matrix of optimal function of a land consists of values which are group as less than or equal to zero or greater than zero. First group indicates squares not accepted for specified function and second group indicates squares which are optimal for specified function.

In original method all processes was done manually. Square grid was put on the whole analyzed area and therefore there were two approaches to using Bajerowski's method. First approaches used all squares in specified grid and second one used fields chosen by Monte Carlo method. Values, read from the map, were put to the inventory matrix and after that was calculated multiplication of matrices. The last step demanded user's interpretation of values, and eventually putting the outputs on a new map.

Optimum usage of a land with Lindemayer's grammar and Bajerowski's method

We use all steps from Bajerowski's method but with some changes (ŻUKOWSKA 2008). In our methods this steps can be described as follows:

1. We must put a square grid on a map with a mesh of a chosen size. Done manually or automatically if we have digital map.

2. We must read features from an every single field and put them into the inventory matrix. We arrange these features into groups therefore we use specified values for the specified feature. We accept "0" as a value, which indicates that the feature does not exist in analyzed square. Our inventory matrices are placed in proposed computer program, therefore this step is done half automatically.

3. We must derive optimal function of a land. We still use multiplication of transposed matrix of features which can optimize usage of a land by the inventory matrix, but we use it only for squares chosen by Lindenmayer's grammar.

4. Interpretation of data from step 3 for optimum usage of a land is done automatically in every rewriting of L-system and outputs are presented in a table and a map.

In our system we arrange features from the matrix of features into the followings groups:

1. Water – w,
2. Greenery – z,
3. Structure of terrain – s,
4. Another terrains – i,
5. Roads and infrastructure – dr,
6. Exposure – k,
7. Slopes – p,
8. Kind of a land – u.

Every group has feature with their values. These are:

1. Water: shorelines of a lake – 1, rivers and brooks – 2, canals and ditches – 3, bog and marshland – 4, little standing water – 5, sources – 6, marshy lands – 13.
2. Greenery: border of forests – 7, row of trees – 8, group of trees, groves – 9, single trees – 10, bushes, shrubs, hedges – 11, thickets, bush clump – 12.
3. Structure of terrain: gorges, ravines – 14, bluffs, embankments, excavations – 15, sand – 16, Rocks and boulders – 16.
4. Another terrains: devastated land -18, industrial land – 19, buildings – 20, ruins – 21, cemetery and burial ground – 29, protected area – 30, natural monuments – 31, historical monuments – 32.
5. Roads and infrastructure: power lines – 22, railway – 23, tarmac road – 24, track – 25, lane – 26, footpath – 27, fence – 28.
6. Exposure: north – 33, north-east – 34, east – 35, south-east – 36, south – 37, south-west – 38, west 39, north-west – 40.

7. Slopes: 0–3% slope – 41, 3–6% slope – 42, 6–10% slope – 43, 10–15% slope – 44, 15–25% slope – 45, 25–35% slope – 46, above 35% slope – 47.
8. Kind of a land: meadow I–III class – 48, meadow IV – V class – 49, meadow VI class – 50, pasture I–III class – 51, pasture IV–V class – 52, pasture VI–VIz class – 53, arable Land I–IIIb class – 54, arable land Iva–V class – 55, arable land VI–Viz class – 56.

In our computer system, we used context-free parametric L-system. Our system is defined as follows:

$$G = \langle V, \Sigma\ \omega, P \rangle \tag{2}$$

where:

V – as the alphabet of the system, consists of numbers 0...9, letters – A...Z, a...z,

Σ – the set of formal parameters, consist of parameters: v, w, z, s, dr, i, k, p, u, nr.x, nr.y, f, d, licz,

$\omega \in (V \times \Re^*)^+$ – is a nonempty parametric word called the axiom chosen by a user,,

$P \subset (V \times \Sigma^*) \times C(\Sigma) \times (V \times E(\Sigma))^*$ – is a finite set of production.

Below are described all used parameters,

v – variable where the total sum of values is stored;
w – variable where the value from water group is stored;
z – variable where the value from greenery group is stored;
s – variable where the value from structure of a terrain group is stored;
dr – variable where the value from roads and technical infrastructure group is stored;
i – variable where the value from another terrains group is stored;
k – variable where the value from exposure group is stored;
p – variable where the value from slopes group is stored;
u – variable where the value from kind of land group is stored;

Parameters which assume an integer value dependent on a size of a map and mesh: nr.x nr.y – variable where the coordinates of a specified basic field are stored, respectively x and y.

f – variable where the purpose of a land is stored. Possible values are: 1-agricultural – arable land, 2 – agricultural – pasture, 3 – agricultural – meadow, 4 – forestry – productive, 5 – forestry – ecological, 6 – recreational – individual recreation, 7 – recreational – collective recreation, 8 – recreational without legal possibility of building development, 9 – B – housing estate areas, 10 – P – industrial infrastructure.

d – variable where randomly chosen direction to the next square is stored,
Here possible variables are: dn = 0 (north), ds = 1 (south), dw = 2 (west), de = 3 (east), dne = 4 (north-east), dnw = 5 (north-west), dse = 6; (south-east), dsw = 7 (south-west).
licz – boolean variable where information is stored whether the total sum was calculated for the square (true = 1) or not (false = 0).
ω as an axiom, is a single basic square chosen by a user.

In the proposed system, every single square is stored as an object with all operations done on it.

There is one important function, which prints squares with its parameters as follows:

$$\text{SQ}([\text{nr.x},\text{nr.y}],\ \text{d,f,v,w,z,s,dr,i,k,p,u}) \tag{3}$$

where:
SQ means square and other symbols are described above.

There are a few groups of productions in our system. The First group consist of productions which determine direction of a new square. The second group consists of productions which calculate optimal usage of a land. The third group consist of productions calculates value v for a specified function of terrain.

Productions from the first group are as follows:

1. SQ([nr.x,nr.y], d, f, v,w, z, s, dr, i, k, p, u) : d=0
   →SQ([nr.x -1,nr.y], d, f, v,w, z, s, dr, i, k, p, u),
2. SQ([nr.x,nr.y], d, f, v,w, z, s, dr, i, k, p, u) : d=1
   →SQ([nr.x +1,nr.y], d, f, v,w, z, s, dr, i, k, p, u),
3. SQ([nr.x,nr.y], d, f, v,w, z, s, dr, i, k, p, u) : d=2
   → SQ([nr.x,nr.y-1], d, f, v,w, z, s, dr, i, k, p, u),
4. SQ([nr.x,nr.y], d, f, v,w, z, s, dr, i, k, p, u) : d=3
   → SQ([nr.x,nr.y+1], d, f, v,w, z, s, dr, i, k, p, u),
5. SQ([nr.x,nr.y], d, f, v,w, z, s, dr, i, k, p, u) : d=4
   →SQ([nr.x-1,nr.y+1], d, f, v,w, z, s, dr, i, k, p, u),
6. SQ([nr.x,nr.y], d, f, v,w, z, s, dr, i, k, p, u) : d=5
   →SQ([nr.x-1,nr.y-1], d, f, v,w, z, s, dr, i, k, p, u),
7. SQ([nr.x,nr.y], d, f, v,w, z, s, dr, i, k, p, u) : d=6
   →SQ([nr.x-1,nr.y+1], d, f, v,w, z, s, dr, i, k, p, u).

Productions from the second group are as follows (vv is a parameter, which is used to denote usefulness of o square):

8. SQ([nr.x,nr.y], d, f, v,w, z, s, dr, i, k, p, u) :v>0 $\wedge$ licz=1 →
   SQ([nr.x,nr.y], d, f, v,w, z, s, dr, i, k, p, u) :vv='X'
   This means "denote square as optimal for function f".

9. SQ([nr.x,nr.y], d, f, v,w, z, s, dr, i, k, p, u) : v<=0 ∧ licz=1 →
   SQ([nr.x,nr.y], d, f, v,w, z, s, dr, i, k, p, u) :vv='0'
   This means "denote square as not optimal for function f".
10. SQ([nr.x,nr.y], d, f, v,w, z, s, dr, i, k, p, u) :v=0 ∧ licz=0 →
    SQ([nr.x,nr.y], d, f, v,w, z, s, dr, i, k, p, u) :vv='+'
    This means "count the value v using the productions from third group".

Third group of productions are too long for this paper therefore we present only first ten of productions for agricultural function – arable land. These are:

11. SQ([nr.x,nr.y], d, f, v,w, z, s, dr, i, k, R, u) :f=1 ∧ w=1 ∧ licz=0 →
    SQ([nr.x,nr.y], d, f, v-5,w, z, s, dr, i, k, p, u)
12. SQ([nr.x,nr.y], d, f, v,w, z, s, dr, i, k, R, u) :f=1 ∧ w=2 ∧ licz=0 →
    SQ([nr.x,nr.y], d, f, v-5,w, z, s, dr, i, k, p, u)
13. SQ(nr, d, f, v,w, z, s, i, dr, k, R, u) :f=1 ∧ w=3 ∧ licz=0 →
    SQ([nr.x,nr.y], d, f, v-1,w, z, s, dr, i, k, p, u)
14. SQ(nr, d, f, v,w, z, s, i, dr, k, R, u) :f=1 ∧ w=4 ∧ licz=0 →
    SQ([nr.x,nr.y], d, f, v-1,w, z, s, dr, i, k, p, u)
15. SQ(nr, d, f, v,w, z, s, i, dr, k, R, u) :f=1 ∧ w=5 ∧ licz=0 →
    SQ([nr.x,nr.y], d, f, v-3,w, z, s, dr, i, k, p, u)
16. SQ(nr, d, f, v,w, z, s, i, dr, k, R, u) :f=1 ∧ w=6 ∧ licz=0 →
    SQ([nr.x,nr.y], d, f, v-5,w, z, s, dr, i, k, p, u)
17. SQ(nr, d, f, v,w, z, s, i, dr, k, R, u) :f=1 ∧ w=13 ∧ licz=0 →
    SQ([nr.x,nr.y], d, f, v-1,w, z, s, dr, i, k, p, u)
18. SQ(nr, d, f, v,w, z, s, i, dr, k, R, u) :f=1 ∧ z=7 ∧ licz=0 →
    SQ([nr.x,nr.y], d, f, v-5,w, z, s, dr, i, k, p, u)
19. SQ(nr, d, f, v,w, z, s, i, dr, k, R, u) :f=1 ∧ z=8 ∧ licz=0 →
    SQ([nr.x,nr.y], d, f, v-3,w, z, s, dr, i, k,p, u)
20. SQ(nr, d, f, v,w, z, s, i, dr, k, R, u) :f=1 ∧ z=9 ∧ licz=0 →
    SQ([nr.x,nr.y], d, f, v-3,w, z, s, dr, i, k, p, u)

In our computer program, every single square is represented as an object, which is stored in a dynamic array of objects. Initially, program initiates the specified axiom in the dynamic array. Constructor creates this object using coordinates, randomizing direction for the next square, using chosen function, reading values for certain variables from inventory matrix and marking the counting flag on "0" value (because the firs iteration does not count the total value). Next few steps are repeated in every iteration:

– one function searches every object in the dynamic array and calculates value v if licz=0, and after calculating it sets licz for 1,

– another functions searches dynamic array and make new objects using the direction written in the parameter d (it is counted accordingly to coordinates of checked square) it also checks whether the new square exists in the dynamic array, if it exists there is no initiations of this square again,

– function for printing the output; put the new production on the screen.

To make a new iteration user must push the button; therefore user decides how much iteration will be made.

The method for calculating the value v uses the matrix of features, which is constant in the program. It initiates indices for the matrix of features using the function (indicates a column in the matrix) and value from every parameter (indicates a row in the matrix). Using the indices, method reads values from the matrix of features and sums the values and store the result in the parameter v.

Example of using our system

Using the computer program we must follow the 4 steps:

1. Preparing data such as maps (scanning) and then inventorying features from a map and write them to the computer program. In our example it is fragment of the topographical map of Olsztyn and its outskirts. Single square has side of 500 meters, therefore its area is 250000 square meters=25 hectares which is between 4 and 30 hectares for village or district as suggested in literature (SENETRA, CIEŚLAK 2004).

2. Choosing coordinates of an initial square (axiom) and the number of appropriate functions of the terrain. In our example these are: coordinates – [4,4] and function – 1, that is agricultural – arable land.

3. Making certain iterations. In our example it is five.

4. Visualize the output. We have three forms of output: sequences of squares, tables and map, which visualize the same results in a different way.

After putting the grid on a map we make the inventory of all features, which can be read from a map, and write them into inventory matrices . Then we chose axiom.

The chosen axiom is : SQ([4,4],5,1,0,2,10,0,24,20,36,42,0)

Values from inventory matrices are represented in table 1.

Table 1

Inventory Matrices

w – water								
	1	2	3	4	5	6	7	8
1	0	0	2	2	0	0	5	0
2	5	2	2	5	0	0	1	1
3	2	0	2	2	5	4	1	1
4	0	5	5	2	2	2	5	1
5	5	0	2	5	0	0	0	1
6	5	4	4	2	2	2	1	1
7	5	4	4	5	2	2	1	0
8	0	4	2	2	2	4	1	1

z – greenery								
	1	2	3	4	5	6	7	8
1	7	7	7	7	7	7	7	7
2	7	7	7	7	7	7	7	7
3	0	7	7	7	10	10	7	7
4	0	7	7	10	10	12	7	7
5	7	7	10	10	10	10	10	10
6	7	10	10	10	10	10	0	10
7	7	7	9	10	7	8	12	0
8	7	12	7	7	7	7	12	12

cont. table 1

s – structure of a terrain								
	1	2	3	4	5	6	7	8
1	0	0	15	15	14	14	0	0
2	0	14	14	0	15	0	15	0
3	14	15	15	0	0	0	15	0
4	0	0	15	0	15	0	15	15
5	0	0	0	0	0	0	15	15
6	0	0	0	0	15	14	15	15
7	0	0	0	0	15	14	15	0
8	0	0	15	15	0	15	15	15

dr – roads and technical infrastructure								
	1	2	3	4	5	6	7	8
1	26	23	26	26	26	26	26	26
2	23	26	26	24	24	26	26	24
3	24	24	24	28	24	26	26	26
4	24	27	26	24	24	23	23	25
5	26	26	0	25	24	24	24	23
6	25	25	25	25	24	26	24	24
7	26	26	26	25	25	26	26	0
8	26	26	25	25	26	26	26	0

i – another terrains								
	1	2	3	4	5	6	7	8
1	0	0	0	20	20	0	0	0
2	20	20	0	0	20	20	20	0
3	0	20	20	20	20	20	20	0
4	0	0	20	20	20	20	20	0
5	20	20	0	20	0	20	20	20
6	20	20	20	20	20	20	20	20
7	20	20	0	20	20	20	0	0
8	20	0	0	20	0	0	0	20

k – exposure								
	1	2	3	4	5	6	7	8
1	35	35	36	35	33	33	34	36
2	34	37	40	36	40	34	35	37
3	34	33	34	35	38	36	34	33
4	40	39	40	36	38	38	35	35
5	35	33	40	40	34	37	37	35
6	40	34	40	40	35	36	36	35
7	38	37	36	36	37	37	39	0
8	38	37	36	36	35	34	35	34

p – slopes								
	1	2	3	4	5	6	7	8
1	0	0	42	42	0	0	45	0
2	45	42	42	45	0	0	41	41
3	42	0	42	42	45	44	41	41
4	0	45	45	42	42	42	45	41
5	45	0	42	45	0	0	0	41
6	45	44	44	42	42	42	41	41
7	45	44	44	45	42	42	44	0
8	0	44	42	42	42	44	41	41

u – kind of land								
	1	2	3	4	5	6	7	8
1	0	0	0	0	0	0	0	0
2	0	0	0	0	0	0	0	0
3	0	0	0	0	0	0	0	0
4	0	0	0	0	0	0	0	0
5	0	0	0	0	0	0	0	0
6	0	0	0	0	0	0	0	0
7	0	0	0	0	0	0	0	0
8	0	0	0	0	0	0	0	0

We chose function agricultural – arable land and we arrive at sequences, which are presented below.

After first rewriting:

SQ([4,4],4,1,8,2,10,0,24,20,36,42,0) SQ([3,4],4,1,0,2,7,0,28,20,35,42,0)

After second rewriting:

SQ([4,4],4,1,8,2,10,0,24,20,36,42,0) SQ([3,4],2,1,4,2,7,0,28,20,35,42,0)

SQ([3,5],6,1,0,5,10,0,24,20,38,45,0) SQ([2,5],5,1,0,0,7,15,24,20,40,0,0)

After third rewriting:
SQ([4,4],5,1,8,2,10,0,24,20,36,42,0) SQ([3,4],2,1,4,2,7,0,28,20,35,42,0)
SQ([3,5],0,1,-9,5,10,0,24,20,38,45,0) SQ([2,5],0,1,-13,0,7,15,24,20,40,0,0)
SQ([3,3],6,1,0,2,7,15,24,20,34,42,0) SQ([4,6],1,1,0,2,12,0,23,20,38,42,0)
SQ([1,4],2,1,0,2,7,15,26,20,35,42,0)
After fourth rewriting:
SQ([4,4],2,1,8,2,10,0,24,20,36,42,0) SQ([3,4],7,1,4,2,7,0,28,20,35,42,0)
SQ([3,5],1,1,-9,5,10,0,24,20,38,45,0) SQ([2,5],6,1,-13,0,7,15,24,20,40,0,0)
SQ([3,3],3,1,-3,2,7,15,24,20,34,42,0) SQ([4,6],2,1,6,2,12,0,23,20,38,42,0)
SQ([1,4],7,1,20,2,7,15,26,20,35,42,0) SQ([1,5],0,1,0,0,7,14,26,20,33,0,0)
SQ([5,6],1,1,0,0,10,0,24,20,37,0,0) SQ([1,3],3,1,0,2,7,15,26,0,36,42,0)
After fifth rewriting:
SQ([4,4],1,1,8,2,10,0,24,20,36,42,0) SQ([3,4],0,1,4,2,7,0,28,20,35,42,0)
SQ([3,5],2,1,-9,5,10,0,24,20,38,45,0) SQ([2,5],4,1,-13,0,7,15,24,20,40,0,0)
SQ([3,3],6,1,-3,2,7,15,24,20,34,42,0) SQ([4,6],6,1,6,2,12,0,23,20,38,42,0)
SQ([1,4],5,1,20,2,7,15,26,20,35,42,0) SQ([1,5],6,1,5,0,7,14,26,20,33,0,0)
SQ([5,6],1,1,-4,0,10,0,24,20,37,0,0) SQ([1,3],2,1,22,2,7,15,26,0,36,42,0)
SQ([4,3],2,1,0,5,7,15,26,20,40,45,0) SQ([4,5],4,1,0,2,10,15,24,20,38,42,0)
SQ([3,6],2,1,0,4,10,0,26,20,36,44,0) SQ([2,3],1,1,0,2,7,14,26,0,40,42,0)
SQ([6,6],4,1,0,2,10,14,26,20,36,42,0)

In Figure 1, are presented output in table, where: + – denotes square as optimal for specified function, 0 – denotes square as non optimal for specified function and X – denotes square, for which value v will be calculated in next iteration.

Figure 2 presents the map with results after 5 iterations. Chequered squares indicate fields, which are optimal for agricultural function – arable land. Those squares are located near the road and buildings, which is convenient for this function of land. It is because all special machines used in agriculture can be easily moved from garages to arable lands and crops can be quickly transported to silos or to other parts of the region.

In the Figure 2 squares with big cross indicate area which is not optimal for arable land. In this example most of these squares are located in the forest. The forest is not convenient to arable land, because it demands a lot of additional work of preparing soil. This work increases costs of redevelopment, which should be as little as possible. Therefore that land is not optimal for arable land.

a

	1	2	3	4	5	6	7	8
1								
2								
3				X				
4				+				
5								
6								
7								

b

	1	2	3	4	5	6	7	8
1								
2					X			
3				+	X			
4				+				
5								
6								
7								

c

	1	2	3	4	5	6	7	8
1				X				
2					0			
3			X	+	0			
4				+		X		
5								
6								
7								

d

	1	2	3	4	5	6	7	8
1			X	+	X			
2					0			
3			0	+	0			
4				+		+		
5						X		
6								
7								

e

	1	2	3	4	5	6	7	8
1			+	+	+			
2			X		0			
3			0	+	0	X		
4			X	+	X	+		
5						0		
6						X		
7								

Fig. 1. Output of (*a*) first, (*b*) second, (*c*) third, (*d*) fourth and (*e*) fifth rewriting

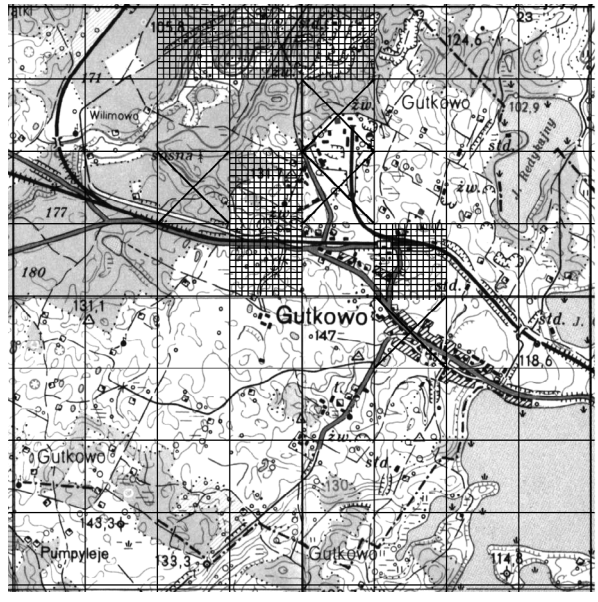

Fig. 2. Output of fifth rewriting in the map of Olsztyn, side of a single square corresponds to 500 meters

Conclusions

The presented approach uses Bajerowski's method of finding the optimum usage of a land and Lindenmayer's grammar. The approach was programmed in Delphi 6.0 as a computer program. This facilitates and quickens the whole process of finding the optimum usage of a land instead of doing the whole process manually.

Moreover, computer program generates the output very quickly whereas with classic approach we have drawn the output results on a map. With our solution we can generate the results even after every rewriting.

In classic method we should calculates all values and we should also decide which value indicates squares which are optimal or not optimal for specified function. In our proposition it is done automatically.

Being done manually, cartographic method can only use a small number of squares. This means using this method for a small area or chose some squares from the whole area. Our approach solves the problem of squares in a different way. User must choose first square, which is an axiom, and the other squares are chosen by the algorithm. In every rewriting process there are some new squares added. We can continue the process till we have the whole area covered but we can stop in every moment. This means that we decide how long the algorithm will work. This solution shows also the possible expansion of specified function of terrain. This point was not considered in discussed method.

Our computer program can be included in GIS as an innovative tool, which uses simulation of natural growth in the contrast of deterministic tools.

Our approach has many advantages but it can be also developed. Today we use digital maps therefore it is possible to add a new feature to our program. The feature could allow automatisation of reading map and generating the inventory matrix. The program was intended for people responsible for land planning or land management therefore it is possible to add features of decision making.

Further developments can also consist of elements from genetic programming, which describe the simulation process more precisely.

Translated by Author

Accepted for print 18.10.2012

References

Bajerowski T. 1996. *Metodyka optymalnego użytkowania ziemi na obszarach wiejskich*. Acta Acad. Agricult. Tech. Olst., Geod. Ruris Regulat., 26, suppl B. Olsztyn.

Bajerowski T. 2003. *Niepewność w dynamicznych układach przestrzennych*. Wydawnictwo Uniwersytetu Warminsko-Mazurskiego, Olsztyn.

MARTYN T. 1996. *Fraktale i obiektowe algorytmy ich wizualizacji.* Nakom, Poznań.

PEITGEN H.-O., JÜRGENS H., SAUPE D. 1992. *Granice chaosu fraktale,* cz. 2. Wydawnictwa Naukowe PWN, Warszawa.

Podstawy teoretyczne gospodarki przestrzennej zarządzania przestrzenią. 2003. Ed. T. BAJEROWSKI, Wydawnictwo UniwersytetuWarminsko-Mazurskiego, Olsztyn.

PRUSINKIEWICZ P. 2004. *Art and science for life: Designing and growing virtual plants with L-systems.* In: *Nursery Crops: Development, Evaluation.* Eds. C. Davidson, T. Fernandez. Production and Use proc XXVI International Horticultural Congress., Acta Horticulturae 630: 15–28.

PRUSINKIEWICZ P., HAMMEL M., HANAN J., MECH R. 1995. *The artificial life of plants. In: Artificial life for graphics, animation, and virtual reality.* Volume 7 of SIGGRAPH '95 Course Notes, ACM Press, pp. 1–38.

PRUSINKIEWICZ P., HAMMEL M., HANAN J., MECH R. 1996. *L-systems: from the theory to visual models of plants*. In: *Proc the 2nd CSIRO Symposium on Computational Challanges in Life Sciences*, Ed. M.T. Michalewicz. CSIRO Publishing,

PRUSINKIEWICZ P., HAMMEL M., MJOLSNESS E. 1993. *Animation of plant development*. Proc SIGGRAPH 93, in Computer Graphics Proceedings, Annual Conference Series, Anaheim – California, pp. 351–360.

PRUSINKIEWICZ P. KARWOSKI R., LANE B. 2007. *The L+C plant-modelling language*. In: *Functional-Structural Plant Modelling in Crop Production*. Springer.

PRUSINKIEWICZ P., LINDENMAYER A. 1996. *The algorithmic beauty of plants.* Springer-Verlag, New York.

PRUSINKIEWICZ P., PALUBICKI W., HOREL K., LONGAY S., RUNIONS A., LANE B., MECH R. 2009. *Self-organizing tree models for image synthesis*. ACM Transactions on Graphics 28(3): 58: 1–10.

SENETRA A., CIEŚLAK I. 2004. *Kartograficzne aspekty oceny i waloryzacji przestrzeni.* Wydawnictwo Uniwersytetu Warminsko-Mazurskiego, Olsztyn

STREIT L., FEDERL P., SOUSA M.C. 2005. *Modelling Plant Variation Through Growth*. Computer Graphics Forum, 24(3): 497–506.

TRACZ W., KLAPEC M. 2007. *Using an expert system for housing utility assessment of terrain*. Proceedings of Artificial Intelligence Studies, vol 4(27): pp. 157–163.

ŻUKOWSKA U. 2008. *Planning of Optimum Usage of a Land with Lindenmayer's Grammar*. Proc IEEE Conference on Human System Interaction, Cracow, Poland, pp. 409–414.

TECHNICAL SCIENCES
Abbrev.: Techn. Sc., No 15(2), Y 2012

CATEGORIZATION OF SIMILAR OBJECTS USING BAG OF VISUAL WORDS AND *k* – NEAREST NEIGHBOUR CLASSIFIER

Piotr Artiemjew, Przemysław Górecki, Krzysztof Sopyła

Chair of Mathematical Methods in Computer Science
University of Warmia and Mazury Olsztyn

K e y w o r d s: Image categorization, *k* – Nearest Neighbor Classifier, Bag of Visual Words.

A b s t r a c t

Image categorization is one of the fundamental tasks in computer vision, it has wide application in methods of artificial intelligence, robotic vision and many others. There are a lot of difficulties in computer vision to overcome, one of them appears during image recognition and classification. The difficulty arises from an image variance, which may be caused by scaling, rotation, changes in a perspective, illumination levels, or partial occlusions. Due to these reasons, the main task is to represent represent images in such way that would allow recognizing them even if they have been modified.

Bag of Visual Words (BoVW) approach, which allows for describing local characteristic features of images, has recently gained much attention in the computer vision community. In this article we have presented the results of image classification with the use of BoVW and *k* – Nearest Neighbor classifier with different kinds of metrics and similarity measures. Additionally, the results of *k* – NN classification are compared with the ones obtained from a Support Vector Machine classifier.

Introduction

One of the most popular supervised classification methods is based on the searching *k* – Nearest Neighbors (*k* – *NN*) objects using a fixed similarity measure or metric. In the classification by means of *k* – *NN* method, the main problem is to identify the best method for computing a similarity between objects, and to find an optimal value of neighbors *k*. It is necessary to identify a measure which works best, but it is obvious that for different data the best method could differ.

In this article we have investigated the problem of selecting a proper measure and *k* parameter, in the domain of images represented by means of Bag of Visual Words (BoVW).

Our methodology involves using SIFT (Scale-Invariant Feature Transform) (LOWE 2004) feature extractor to obtain the collection of keypoints from the considered images. Successively, k-means clustering method is used for quantizing the keypoints into visual words (dictionary construction), which allows us to represent the images by means of the frequencies of visual words which are present in the image.

In the classification process we use different kinds of metrics and similarity measures. We use the Chisquare metric, Euclidean, Canberra, Manhattan, Normalized, Chebyshev distance and modifications of similarity measures like Cosine measure or the Pearson product-moment correlation coefficient (see DEZA E., DEZA M. 2009). Our results are evaluated by Leave One Out (LOO) method and compared with the results of our recent experiments obtained by applying different kernel functions in Support Vector Machine classifier (GÓRECKI et al. 2012c).

As concerning image representation, BoVW is employed, which is well known in generic visual categorization (CSURKA et al. 2004, DESELAERS et al. 2008, HERBRICH et al. 2000) and subcategorization (GÓRECKI et al. 2012b). In particular, an image is represented using frequencies of distinctive image patches (visual words), obtained in a two-step process. In the first step, a keypoint detector is employed to identify local interest points in a dataset of different images. Successively, the keypoints are quantized into visual words, so that one visual word corresponds to a number of visually similar keypoints. In most cases, K-means clustering is used to carry out the quantization, so that each centroid represents a visual word, and a set of visual words is called a "visual dictionary". By counting visual words in the particular image, a feature vector encoding frequencies of visual words is obtained. Given the feature vector, an image can be further classified into a predefined set of categories using supervised machine learning algorithm, such as k-NN or SVM.

Methodology

There are two issues of BoVW image categorization. The first one is the choice of keypoint detector/descriptor. There were many descriptors proposed in the literature, such as SIFT (LEWIS 1998), SURF (BAY et al. 2006), and more recently BRISK (LEUTENEGGER et al. 2011) and FREAK (ALAHI et al. 2012). Their common feature is robustness to changes in image rotation, scale, perspective and illumination. A comprehensive survey of keypoint detectors can be found in (MAK et al. 2008, THORSTEN et al. 1998). Another important

aspect is the choice of the classifier. In this paper SIFT detector and k – NN classifier were chosen.

Our process of image categorization consists of typical steps (CSURKA et al. 2004):

1. Identification of image keypoints – SIFT keypoints were detected for all images in the dataset.

2. Building the visual dictionary – all keypoints identified in the previous step were clustered into K visual words using – K means algorithm. During the experimental session we use different dictionaries.

3. Building the image representation – for each image, the keypoints are mapped to the most similar visual words and then the image feature vector $v = (v_1,...,v_K)$ is obtained, where v_i encodes the frequency of the i-th visual word.

4. Classification – we use the k – NN classifier, and LOO method to evaluate the effectiveness of the classification, the details are in the classification section.

Data

In our experiments we have clustered the keypoints into different numbers of visual words. In any case, the empty clusters are discarded, therefore the number of obtained visual words (attributes) could be smaller than number of clusters considered originally. Our datasets contain the following number of conditional attributes (visual words): 50, 100, 250, 499, 983, 2442, 4736, where the original number of considered visual words are 50, 100, 250, 500, 1000, 2500, 5000.

Fig. 1. An exemplary shoes from five distinctive classes of examined dataset

Fig. 2. An exemplary set of key points

Classification

In this article we use a classic way of classification based on k – NN methodology. We search for neighbors of the test objects in the whole dataset, and the major class is assigned to the test object, where ties are resolved hierarchically. Having obtained all training objects $\{y_i\}$, we classified the test object x in the following way:

(i) We have computed the distance between objects based on the chosen similarity measure or metric, that is $g(x, y_i)$, where g is metric (d) or similarity measure (p).

(ii) For the fixed test object, we have chosen k nearest training objects.

(iii) The most numerous class assigns the decision to the test object. In the case of draws, we have chosen last conflicted class.

Similarity measures and metrics

It is really important to identify the metric or similarity measure which works best for the considered data. For our k – NN classifier we get distance between objects according to the following functions:

The first one $d : X\, x\, X \rightarrow [0, \infty)$ fulfills conditions,

$$(i)\ d\ (x, y) = 0 \Leftrightarrow x = y$$

$$(ii)\ d\ (x, y) = d\ (y, x)$$

$$(iii)\ d\ (x, y) \leq d\ (x, z) + d\ (z, y)$$

which define a metric, and the second one $p : X \, x \, X \rightarrow [0, 1]$

$$(i) \; p(x, y) = 1 \Leftrightarrow x = y$$

$$(ii) \; p(x, y) = p(y, x)$$

$$(iii) \; p(x, y) \in [0, 1]$$

is a similarity measure. The Cosine measure applied in this article gives the values of similarity from the range [-1,1], which is an exception of the above definition.

One of the most popular is Euclidean metric (DEZA E., DEZA M. 2009), defined in the following way,

$$d \; (x, y) = \sqrt{(\Sigma(x_i - y_i)^2)}$$

The Cosine measure (DEZA E., DEZA M. 2009) works as follows,

$$p \; (x, y) = \Sigma_{i=1}^{n} \left(\frac{x \circ y}{||x|| * ||y||} \right)$$

Where the scalar product is defined as,

$$x \circ y = \Sigma \, x_i * y_i$$

Length of vectors is the following

$$||x|| = \sqrt{\Sigma x_i^2}; \;\; ||y|| = \sqrt{\Sigma y_i^2}$$

One of the simplest is Manhattan metric (DEZA E., DEZA M. 2009) defined below,

$$d \; (x, y) = \Sigma \, |x_i - y_i|$$

The normalized distance between objects based on division by the sum of attribute values is called Canberra metric (DEZA E., DEZA M. 2009),

$$d \; (x, y) = \Sigma \, \frac{|x_i - y_i|}{x_i + y_i}$$

And modification of Canberra metric is the Normalized metric normalized by the maximal and minimal values of attributes in their domains,

$$d\ (x,\ y)\ =\ \Sigma\ \frac{|x_i\ -\ y_i\ |}{\max_i\ +\ \min_i}$$

An interesting metric commonly used as a kernel of Support Vector Machine is Chisquare metric [6] defined in the following way,

$$d\ (x,\ y)\ =\ \Sigma\ \left(\frac{(x_i\ -\ y_i)^2}{x_i\ +\ y_i}\right)$$

Another metric, which determines the distance between objects as the maximal distance between attributes of objects, is the Chebyshev distance (DEZA E., DEZA M. 2009),

$$d\ (x,\ y)\ =\ \max\ (|x_i\ -\ y_i|),\ i\ =\ 1,2,...,n$$

The Pearson product-moment correlation coefficient, which measures the linear correlation of objects, is defined as follows,

$$p\ (x,\ y)\ =\ \ |r_{x,\ y}|$$

$$r_{x,\ y}\ =\ \frac{\Sigma\ (x_i\ -\ \bar{x})(y_i\ -\ \bar{y})}{\sqrt{\Sigma(x_i\ -\ \bar{x})^2}\ \sqrt{\Sigma(y_i\ -\ \bar{y})^2}}$$

$$\bar{x}\ =\ \frac{1}{n}\ \Sigma\ x_i,\ \bar{y}\ =\ \frac{1}{n}\ \Sigma\ y_i$$

Data preprocessing

The scalar length of feature vectors extracted from the dataset could disturb classification in case of data with a large number of visual words. For this reason we have normalized feature vectors by scaling their length to unit one, which is done by dividing all object's attributes by the scalar length of objects. It means that for all $x \in U$, and for all $a \in A$, we perform the following operation:

$$a\ (x)\ =\ \frac{a\ (x)}{||x\ ||},\ \text{where}\ \ ||x\ ||\ =\ \sqrt{\Sigma\ x_1^2}$$

Error evaluation

In this article we have evaluated the classification quality by using the standard Leave One Out method, where for n-objects of decision system we create n tests, where each time a different object is treated as test set and the rest of objects are the training set. The effectiveness of Leave One Out method was investigated among others in (MOLINARO et al. 2005). The LOO method is almost unbiased classification error estimator, hence the evaluation of classification quality is close to the real result.

Results of Experiments

The main goal of our experimental session was to identify the best similarity measure or metric and classification parameters for the prepared dataset with use of global k – NN method. Our dataset consists of 200 objects (images), which represent five categories of shoes, the cardinalities of decision classes are the following, 59, 20, 34, 29, and 58 images respectively. The exemplary images of each class and exemplary key points of selected image are in the Figure 1. and Figure 2.

After data normalization, the classification results for Cosine measure and Euclidean metric are the same, because distance between objects in Cosine metric is reduced to the computation of a scalar product of objects, that is equal to Euclidean distance between objects. The Cosine measure gives the same result before and after normalization, because the applied normalization is an internal part of this measure.

In the Table 1 we can see that the best results of classification for normalized and non-normalized data and considered dictionary sizes. For a smaller number of visual words in the range of 50–100 the classification

Table 1

Leave One Out; The result of classification for the best parameter k and a measure of distance between objects, before and after normalization; chi = Chisquare metric, euk = Euclidean metric, cos = Cosine measure, pea = Pearson product-moment correlation coefficient

	50		100		250		500	1000	2500		5000
Before norm	0.920		0.925		0.895		0.910	0.930	0.955		0.965
Measure	chi		euk		pea	euk	pea	pea	pea		pea
k	1		1		1	1	1	1	3		3
After norm	0.890		0.915		0.895		0.910	0.930	0.955		0.965
Measure	chi	man	pea	cos euk	pea	man	pea	pea	pea	cos euk	pea
k	2	4	3	2	1	1	1	1	3	1	3

is better without normalization. The reason is that the number of visual words, not their types, plays a dominant role in distinguishing decision classes. The optimal value of the k parameter is in the set {1, 2, 3}, the most effective measure turns out to be the Pearson product-moment correlation coefficient. The normalization does not have any influence on the Pearson product-moment correlation coefficient, since linear correlation between the objects is maintained, so the best result for a higher number of visual words is the same regardless of a normalization method. What is interesting, the best metric for 50 visual words, before and after normalization, is the Chisquare metric and additionally the Manhattan metric after normalization. For 100 words, the Euclidean metric is the best, (both before and after normalization), and Pearson's measure performs equally well if normalization is applied. For a higher number of words Pearson's measure is the best, but in a few cases the Euclidean and Manhattan metric have equal accuracy to Pearson's measure.

In the Table 2 we have shown the best results and parameters for all metrics chosen for the data with a different number of visual words. It turns out that we achieve the best results before normalization for the Chisquare,

Table 2
Leave One Out; The best result for all metrics and the parameter k before and after normalization

Metric	Before norm	No.of.visual.words		After norm	No.of.visual.words	k
Pearson	**0.965**	5000	3	**0.965**	5000	3
Chisquare	**0.920**	50	1	0.895	100	2
Manhattan	0.900	50	2	**0.910**	100	1
Cosine	**0.960**	5000	3	**0.960**	5000	3
Euclidean	0.925	100	1	**0.960**	5000	3
Normalized	**0.890**	50	1,2,4	0.875	50	1,3
					100	1
Canberra	**0.895**	50	4	0.865	50	3
Chebyshev	**0.875**	100	2	0.830	100	2

Normalized, Canberra, and Chebyszev metric, and after normalization tthe Manhattan and Euclidean metrics work better. As we mentioned before, Pearson's and Cosine measures work equally well before and after normalization.

Considering the best result of classification, we made an assumption that best parameter k has values 1, 2 or 3, and for this reason, in the Figures 3, 4, 5 and 6, we present the average of the classification results for these three parameters. Particularly, in the Figure 3 and 4 we have separate results for all dictionaries, and metrics before and after normalization. These generalized

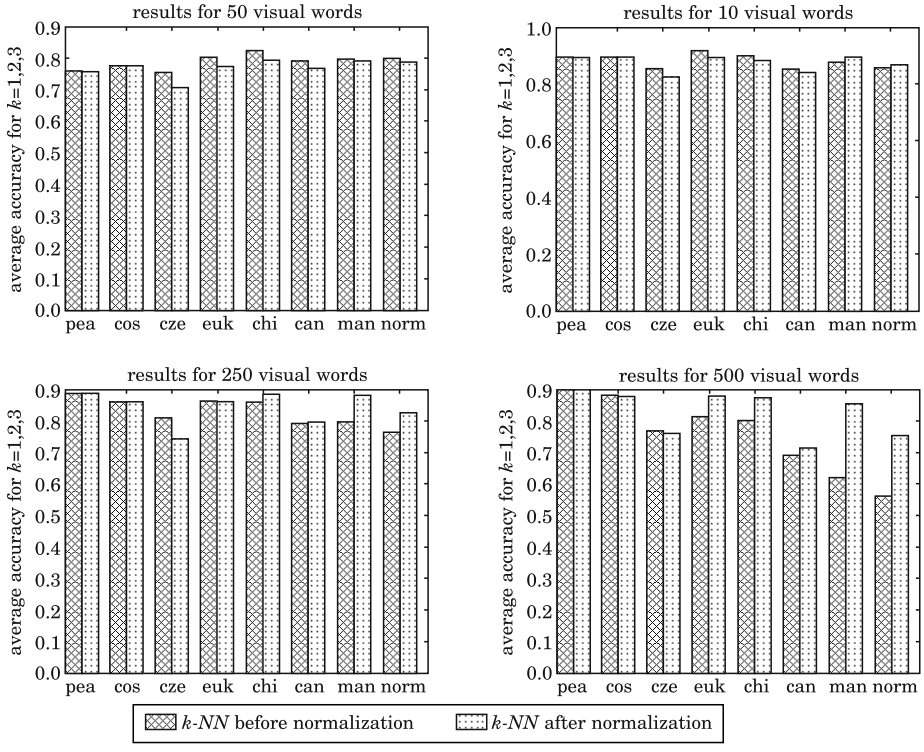

Fig. 3 Leave One Out; k – *NN*; Average result of accuracy for k=1,2,3 and 50–500 visual words

results lead us to the conclusion, that for 50 and 100 words, all metrics work better before normalization, except of Manhattan and Normalized metric in case of 100 words. For 250–5000 words, we obtain the best results for all metrics and measures after normalization, except for Chebyszev metric for 250 words.

In the Figure 5 and 6, we have results for non-normalized data and normalized data respectively. In the plots, we have the results for all metrics vs all dictionaries (the data from the Figure 3 and 4 shown in the different way). In the Figure 7, we have exemplary detail wesult for Pearson's measure with data after normalization. The conclusion is that for 50, 100 and 250 words all the metrics work really steadily before and after normalization. Pearson's and Cosine measure work optimally for all the dictionaries. In case of the Czebyszev metric after normalization, the result of classification is more consistent for all the dictionaries. The Euclidean metric works better after normalization. The result before and after normalization for the rest of the metrics is comparable.

In addition to our results we have compared results of a SVM classifier (CHAPELLE et al. 1997, FAN et al. 2005) with different kernel functions

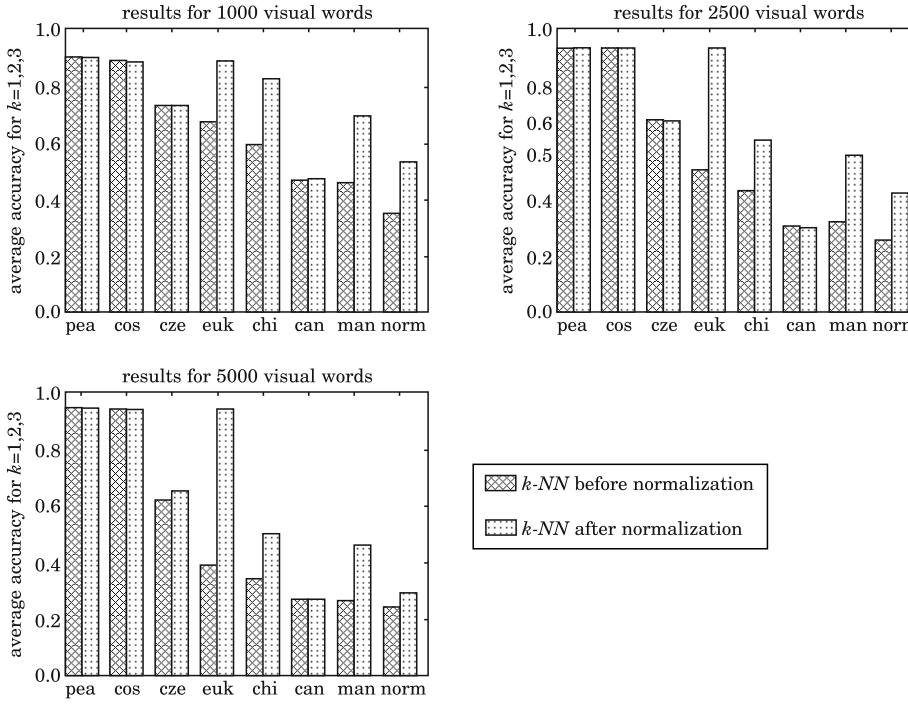

Fig. 4. Leave One Out; k – NN; Average result of accuracy for $k=1,2,3$ and 1000–5000 visual words

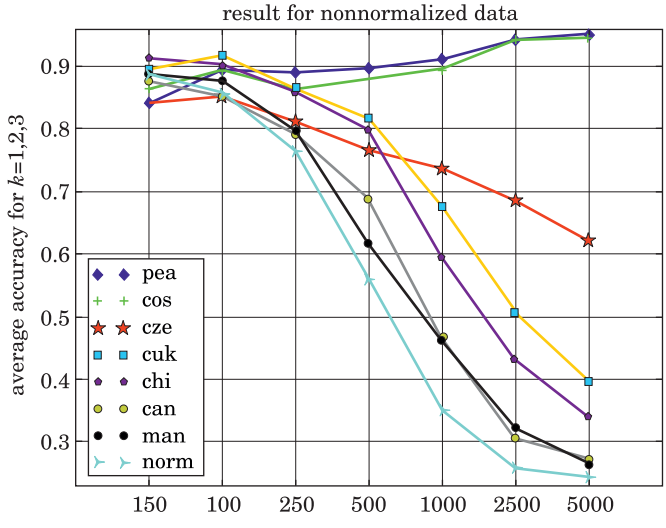

Fig. 5. Leave One Out; k – NN; For data before normalization; Average result of accuracy for $k=1,2,3$ and 50–5000 visual words

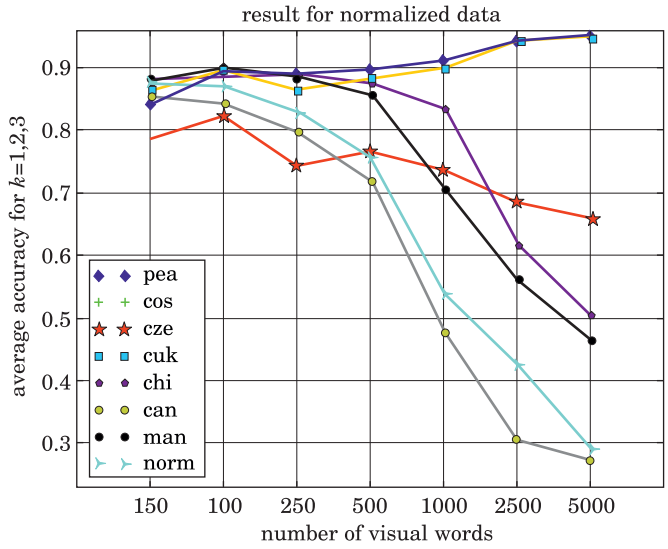

Fig. 6. Leave One Out; k – *NN*; For data after normalization; Average result of accuracy for k=1,2,3 and 50–5000 visual words

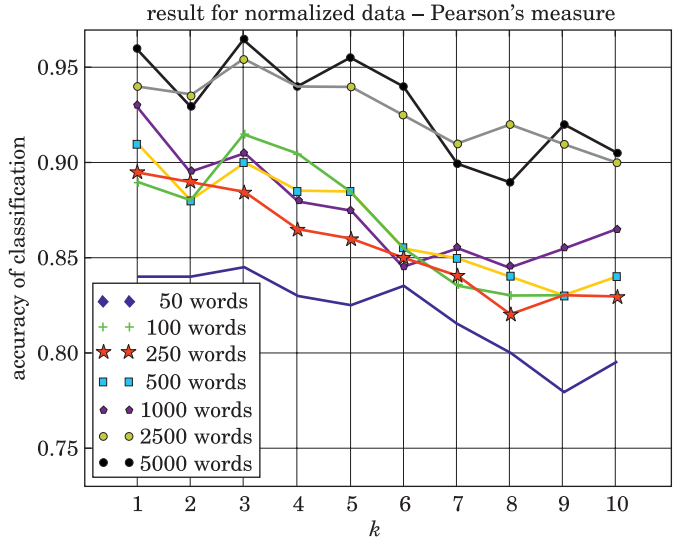

Fig. 7. Leave One Out; k – *NN*; For Pearson's measure with data after normalization; The result of accuracy for k=1,2,...,10 and 50–5000 visual words

(see Tab. 3) (GÓRECKI et al. 2012c), and global $k - NN$ classifier with use of different similarity measures and metrics. We can summarize that for a number of visual words in the range of 50, 100, 2500, 5000, the results are comparable with the $k - NN$ method and even better for a smaller number of words in the range of 50 and 100, but in range of 250, 500, 1000 visual words, the SVM classifier wins by about four percent of classification accuracy.

Table 3
Cross Validation 5; Overall accuracy of Support Vector Machine kernels in relation to visual dictionary size

Kernel	Number of visual words						
	50	100	250	500	1000	2500	5000
Linear	0.870	0.870	0.925	0.940	0.945	0.940	0.940
Chi^2	0.880	0.885	**0.930**	0.940	**0.960**	0.955	0.955
Histogram	0.855	**0.895**	**0.930**	0.935	0.940	**0.960**	**0.965**
RBF	**0.905**	0.890	**0.930**	**0.945**	0.945	0.940	0.940
Cauchy	0.900	0.890	0.900	0.930	0.915	**0.960**	0.905

Conclusions

The results of these experiments show an interesting dependence between the quality of classification by means of a global k– NN method, the number of visual words, and the normalization method. It has turned out that for smaller number of visual words in the range of 50, 100, we get better result for non-normalized data. In case of 50 visual words the best is the Chisquare metric, for 100 visual words the best is the Euclidean metric, and starting from 250 words the best similarity measure for the considered data turn out to be the Pearson product-moment correlation coefficient and Cosine measure. For a higher number of visual words in the range of 250-5000, we achieve better result after normalization. The optimal parameter k for global $k - NN$ classifier and considered dataset is in the set $\{1, 2, 3\}$.

In the future we are planning to check the effectiveness of other methods of classification based on other publicly available datasets. Another goal is to apply other keypoint detectors in our research, so that their effectiveness can be compared with our current results.

Acknowledgements

The research has been supported by grant N N516 480940 from the National Science Center of Republic of Poland and grant 1309-802 from Ministry of Science and Higher Education of the Republic of Poland.

Translated by MATT PURLAND

Accepted for print 12.11.2012

References

ALAHI A., ORTIZ R. VANDERGHEYNST P. 2012. *FREAK: Fast Retina Keypoint*. IEEE Conference on Computer Vision and Pattern Recognition, Rhode Island, Providence, USA,

BAY H., TUYTELAARS T., VAN GOOL L. 2006. *Surf: Speeded up robust features*. ECCV, p. 404–417.

CHAPELLE O., HAFFNER P., VAPNIK V.N. 1999. *Support vector machines for histogram-based image classification*. Neural Networks, IEEE Transactions on, 10(5): 1055–1064.

CSURKA G., DANCE CH.R., FAN L., WILLAMOWSKI J., BRAY C. 2004. *Visual categorization with bags of keypoints*. Workshop on Statistical Learning in Computer Vision, ECCV, p. 1–22.

DESELAERS T., PIMENIDIS L., NEY H. 2008. *Bag-of-visual-words models for adult image classification and filtering*. ICPR, p. 1–4,

DEZA E., DEZA M. 2009. *Encyclopedia of Distances*, Springer.

FAN R., CHEN P., LIN Ch. 2005. *Working set selection using the second order information for training svm*. Journal of machine learning research, 6: 1889–1918.

GÓRECKI P., ARTIEMJEW P., DROZDA P., SOPYŁA K. 2012a. *Categorization of Similar Objects using Bag of Visual Words and Support Vector Machines*. Fourth International Conference on Agents and Artificial Intelligence. IEEE.

GÓRECKI P., SOPYŁA K., DROZDA P. 2012b. *Ranking by k-means voting algorithm for similar image retrieval*. In: ICAISC 1(7267): 509–517, of Lecture Notes in Computer Science, eds. L. Rutkowski, M. Korytkowski, R. Scherer, R. Tadeusiewicz, L.A. Zadeh, J.M. Zurada, Springer.

GÓRECKI P., SOPYŁA K., DROZDA P. 2012c. *Different SVM Kernels for Bag of Visual Words*. In: International Congress of Young Scientist, SMI'2012, Springer.

HERBRICH R., GRAEPEL T., OBERMAYER K. 2000. *Large margin rank boundaries for ordinal regression*. MIT Press, Cambridge, MA.

LEUTENEGGER S., CHLI M., SIEGWART R. 2011. *BRISK: Binary Robust Invariant Scalable Keypoints*. Proceedings of the IEEE International Conference on Computer Vision (ICCV), pp. 2548–2555.

LEWIS D.D. 1998. *Naive (bayes) at forty: The independence assumption in information retrieval*. Springer Verlag, p. 4–15.

LOWE D.G. 2004. *Distinctive image features from scale-invariant keypoints*. Int. J. Comput. Vision, 60: 91–110.

MAK M.W., GUO J., KUNG S.-Y. 2008. *Pairprosvm: Protein subcellular localization based on local pairwise profile alignment and svm*. IEEE/ACM Trans. Comput. Biol. Bioinformatics, 5(3): 416–422.

MIKOLAJCZYK K., LEIBE B., SCHIELE B. 2005. *Local Features for Object Class Recognition*. Tenth IEEE International Conference on Computer Vision (ICCV'05), 1: 1792–1799.

MOLINARO A.M., SIMON R., PFEIFFER R.M. 2005. *Prediction error estimation. a comparison of resampling methods*, Bioinformatics, 21(15): 3301–3307.

NISTR D., STEWNIUS H. 2006. *Scalable recognition with a vocabulary tree*. In IN CVPR, p. 2161–2168.

THORSTEN J. 1998. *Text categorization with support vector machines: learning with many relevant features*. Proceedings of ECML-98, 10th European Conference on Machine Learning, 1398: 137–142. Eds. C. N'edellec, C. Rouveirol. Springer Verlag, Heidelberg, DE.

TUYTELAARS T., MIKOLAJCZYK K. 2008. *Local invariant feature detectors: a survey*. Found. Trends. Comput. Graph. Vis., 3: 177–280.

TECHNICAL SCIENCES
Abbrev.: Techn. Sc., No 15(2), Y 2012

A COMPARISON BETWEEN CONTACT AND TAPPING AFM MODE IN SURFACE MORPHOLOGY STUDIES

***Mirosław Bramowicz*[1], *Sławomir Kulesza*[2], *Kazimierz Rychlik*[3]**

[1] Chair of Materials and Machinery Technology
[2] Chair of Relativistic Physics
[1, 2] University of Warmia and Mazury in Olsztyn
[3] Institute of Mechanised Construction and Rock Mining, Warszawa

K e y w o r d s: atomic force microscopy, AFM, surface topography.

A b s t r a c t

The paper presents recent results from studies of a surface topography of a platinum calibration grid on silicon substrate obtained in both contact and tapping modes of the AFM microscope. The results are analyzed in order to determine the influence of the scan set-up and the SPM probe onto estimated fractal parameters and surface anisotropy ratio.

Introduction

Atomic Force Microscopy (AFM) makes use of the forces between two bodies placed very close to each other (from few nanometers up to tens of nanometers). Such forces result from either atomic or particle interaction at a very small distance. Typically, one of the interacting bodies is a sharp tip mounted on an elastic cantilever, whereas the other is the surface under study (see Fig. 1).

When the tip is approaching the surface, the force appears at a certain point. However, both the magnitude of the force, as well as its character (attractive, repulsive) changes with the tip-surface distance, as it is shown in Figure 2.

In the beginning, the tip-surface interaction is dominated by long-range, attractive forces, for example, magnetic ones. When the tip comes closer to the surface, it is attracted much larger due to electrostatic van der Waals forces of the order of 10^{-12} N. Below 1 nm, however, the tip becomes repelled by the

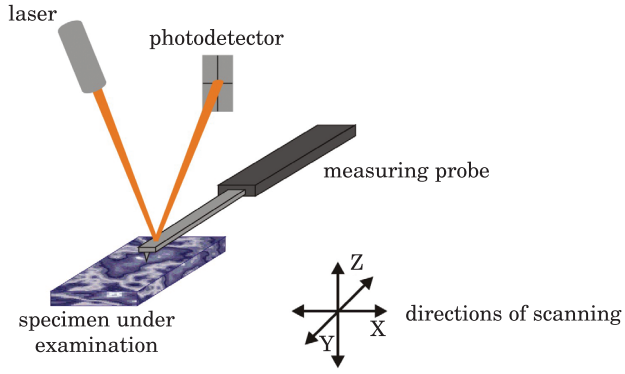

Fig. 1. Schematic description of the AFM principle
Source: MIRONOV 2004.

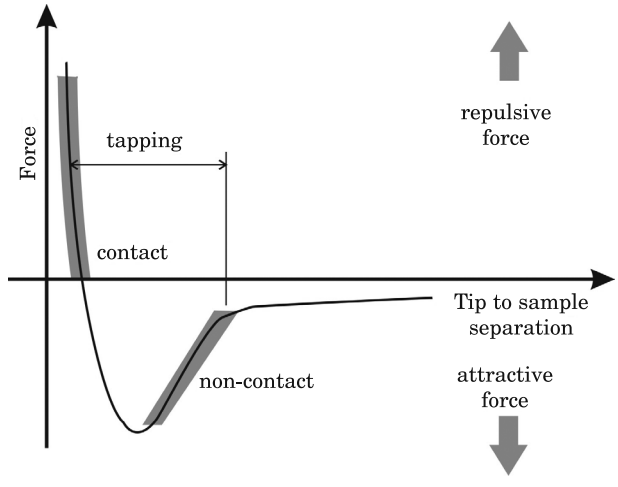

Fig. 2. Forces between the AFM tip and a scanned surface
Source: MIRONOV 2004.

surface as a result of overlapping electron clouds (Pauli exclusion principle). Repulsive forces are of the order of 10^{-9} N, which can be used to adjust the optimal tip-surface distance in the contact and tapping modes (SAINT JEAN et al. 1999). Mutual tip-surface interaction is usually described by the Lennard-Jones potential $U_{L\text{-}J}$:

$$U_{L\text{-}J}(r) = U_0 \left\{ -2\left(\frac{r_0}{r}\right)^6 + \left(\frac{r_0}{r}\right)^{12} \right\} \tag{1}$$

where:
r is the tip-surface distance, r_0 – the tip-surface distance at which the potential reaches its minimum, whereas U_0 – the minimal value of the potential. The first term in Equation (1) corresponds to long-range attractive forces due to dipole interaction, while the second one – corresponds to short-range repulsive forces due to overlapping electron clouds (MIRONOV 2004).

When working in the contact mode, the tip (or the surface, depending on the construction details) is moved along *XY* plane, and the cantilever deflection detected by the 4-section photodiode reflects the surface topography (HOWLAND, BENATAR 2002, BRAMOWICZ, KLYSZ 2007). On the other hand, in the tapping mode the cantilever is additionally forced to oscillate in a vertical direction, at a frequency close to its resonant frequency, and the photodiode measures the amplitude of the oscillation. Despite being used for similar purposes, each scanning mode gives insight into different aspects of the tip-surface interactions (Fig. 2). Contact mode actually relies on the repulsive force solely, while the tapping mode exhibits a large variety of forces, not only repulsive, but also attractive ones.

Experimental procedure

AFM measurements described below concern the effect of the scanning mode on the quality of obtained 3-dimensional surface images and the statistical parameters of the surface topography. Several measurements were carried out using platinum calibration grid (PG) as the reference (grating made from platinum sputtered onto silicon substrate with 1 μm period and 100 nm step height from Bruker). Multimode 8 system (Bruker) allowed for AFM imaging in both contact as well as tapping modes making use of the ScanAsyst-Air SPM probes (the tip radius 2 nm and the cantilever spring constant 0.4 N/m). Each surface profile was sampled at 512 equidistant points, each image was composed of 512 lines. The scan size varied between 0.5 and 50 μm, while the aspect ratio uqual to 1 (square scan area). AFM measurements resulted in 2-dimensional square matrices storing data on local surface heights above a reference level.

In order to characterize the surface topography and to compare the results obtained in the contact and tapping modes, the following statistical parameters were used:
– Root-mean-square deviation of the surface S_q (according to PN-EN ISO 25178-6):

$$S_q = \sqrt{\frac{1}{MN}\sum_{k=0}^{M-1}\sum_{l=0}^{N-1}[z(x_k, y_l)]^2} \tag{2}$$

– Anisotropy coefficient S_{tr} defined as the ratio between the correlation lengths τ of the normalized autocorrelation function $R(\tau,\theta)$ measured along its fastest and slowest decay from the maximum value (1.0) down to 0,2 (MAINSAH et al. 2001):

$$0 < S_{tr} = \frac{\text{Min}\{\tau : R(\tau,\theta) \to 0{,}2\}}{\text{Max}\{\tau : R(\tau,\theta) \to 0{,}2\}} \leq 1 \tag{3}$$

– Fractal dimension D and topothesis K determined using the structure function $S(\tau)$ (MAINSAH et al. 2001):

$$S(\tau) = \langle[z(x) - z(x + \tau)]^2\rangle \tag{4}$$

where:
$\langle\ \rangle$ stands for the average.

On a log-log scale, the structure function $S(\tau)$ draws a characteristic curve that can be approximated by two straight lines: the one inclined at an certain angle for small τ values, and the other which is almost flat for large τ values. The structure function $S(\tau)$ obeys the power law within the small τ range according to (MAINSAH et al. 2001):

$$S(\tau) = K\tau^{2H} \tag{5}$$

where:

$$K = \frac{\pi G^{2(D-1)}}{2\Gamma(5 - 2D)\sin[(2 - D)\pi]} \tag{6}$$

where:
G is the scale factor, Γ is the Euler function, whereas $H = 2 - D$ is the Hurst parameter (HARTMANN 1997, MAINSAH et al. 2001).

Results

Topography maps recorded in contact mode accompanied by the spectra of the area autocorrelation function are shown in Figure 3, and similar data measured in the tapping mode are shown in Figure 4. At first glance, contact mode provides better image contrast, whereas tapping mode exhibits on the scanned surface tiny particles with the mean height not exceeding 10 nm. Such a result is probably due to surface inhomogeneities detected by vibrating probe, because any disturbance to the tip-surface interaction (localized adhesion force, for example) gives rise to huge oscillation frequency shift when working close to the resonant frequency. On that account the tapping mode is far more sensitive to any surface inhomogeneity than the contact mode being, however, less destructive to a sample surface.

By analyzing the spectra of the autocorrelation function for the scan size 0.5 and 1.0 μm shown in Figure 3 and Figure 4, the surface anisotropy can be seen. Indeed, the images exhibit spectra with only one central peak, elongated along the axis of surface anisotropy. On the contrary, when the scan size increases above 5 μm, the spectra of the autocorrelation function become isotropic, although highly periodic.

Figure 5 exhibits significant similarity between both imaging modes in terms of the surface roughness S_q as long as the scan size exceeds 5 μm. For smaller scan areas, however, S_q is noticeably higher in contact mode with respect to tapping mode even though the latter is more sensitive to surface inhomogeneities that should result in larger roughness, as it was mentioned previously. Unfortunately, no reason has been given so far to explain observed discrepancy.

Analysis of 2-dimensional spectra of the autocorrelation functions along the main axes of anisotropy (a1 and a2) for the scan size 0,5 and 1 mm, and along the x and y directions for the scan size 5, 10, 20 and 50 mm, allowed for determination of the anisotropy coefficient S_{tr} according to Eq. (3). The plot of S_{tr} vs. scan size is shown in Figure 6.

Figure 6 shows that independent of the scanning mode, S_{tr} values rise asymptotically to a value close to 1 when the scan size is larger than 5 μm. Small deviation from the unity is probably due to the tip asymmetry as the tip shape convolves with the topography, but this effect is not concerned here. What is important, S_q approaches asymptotical value when the scan size exceeds the grid period. On the other hand, for the scan size equal to 0,5 and 1 μm, S_{tr} values significantly decrease, because the scan size does not cover a single pattern cell. In such a case, anisotropy ratio strongly depends on the scan size. Similar observations were reported previously (BRAMOWICZ 2009) from studies of the anisotropy coefficient of the microstructure of martensitic steel in Ni-Mn-Ga alloys.

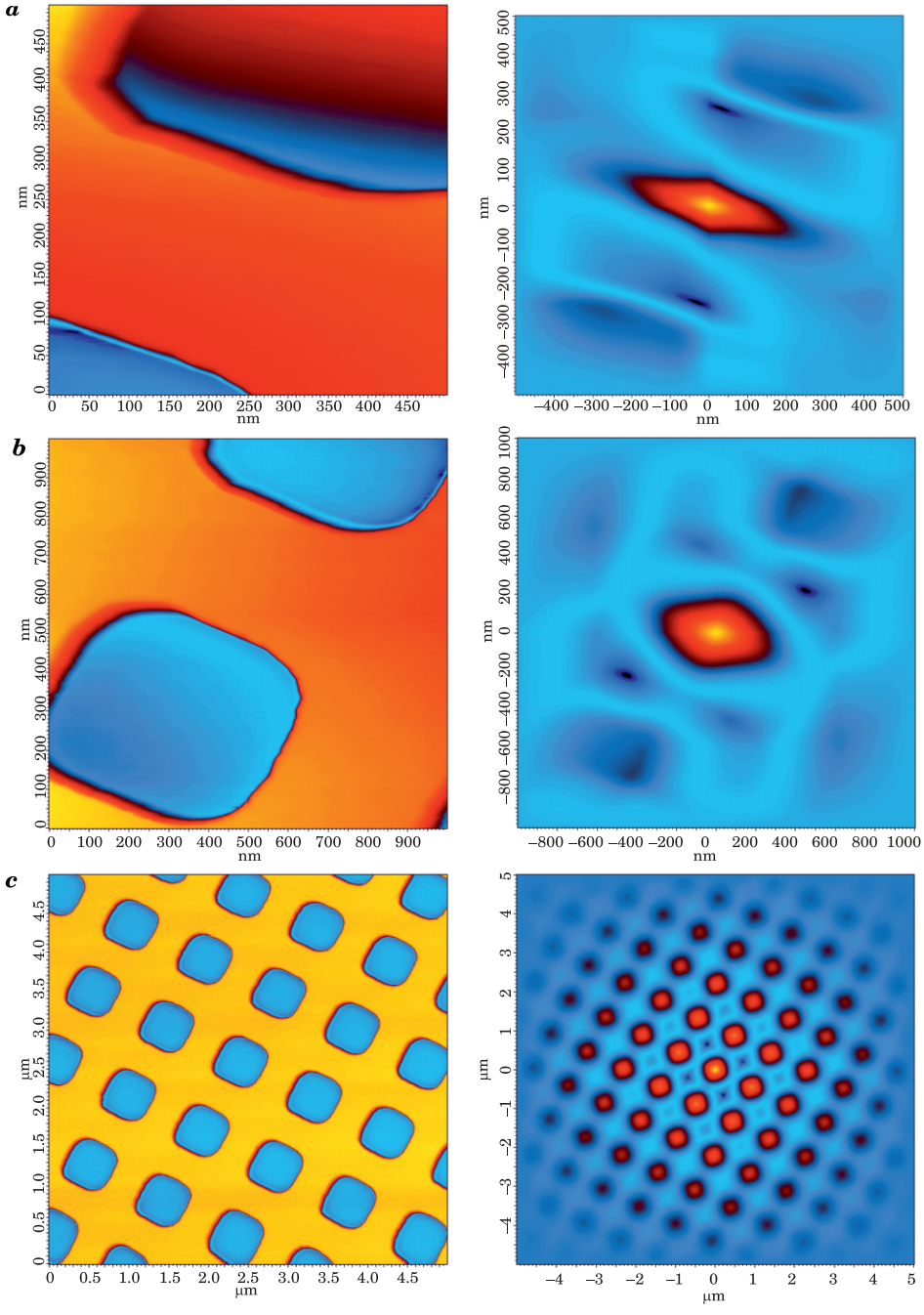

Fig. 3. Surface topography (left) and the spectra of the surface autocorrelation function (right) of the reference PG sample in the contact mode. Scan size, respectively: *a* – 0,5×0,5 μm, *b* – 1×1 μm, *c* – 5×5 μm

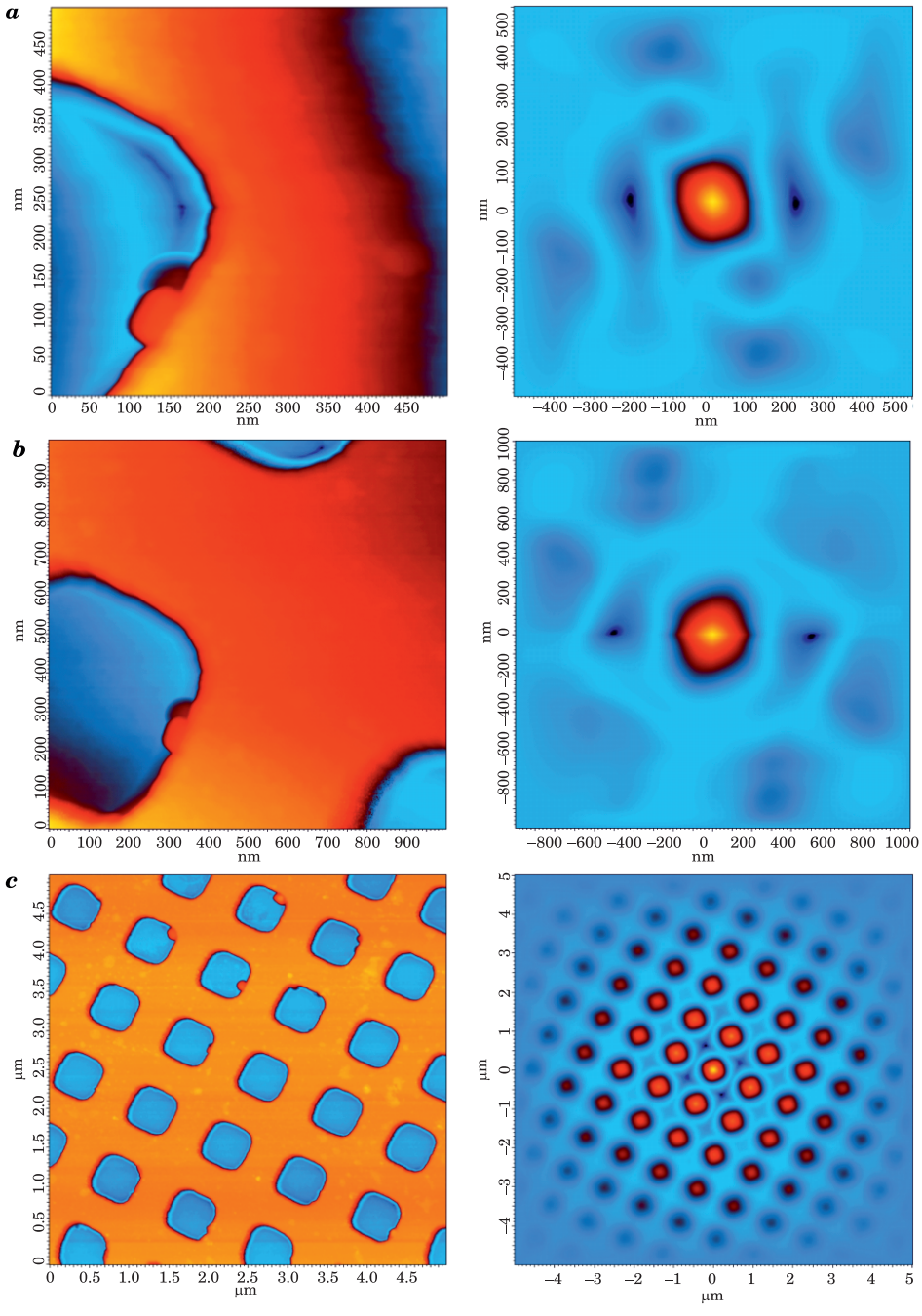

Fig. 4. Surface topography (left) and the spectra of the surface autocorrelation function (right) of the reference PG sample in the tapping mode. Scan size, respectively: *a* – 0,5×0,5 μm, *b* – 1×1 μm, *c* – 5×5 μm. Note the surface inhomogeneities seen in the topography images

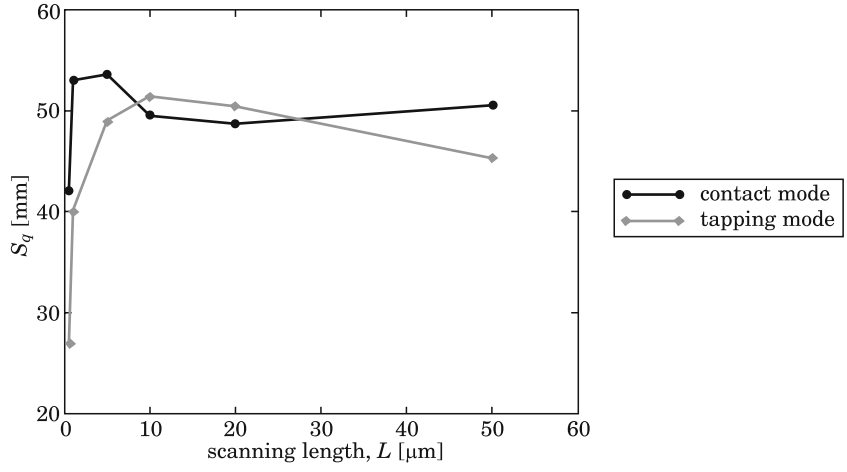

Fig. 5. Changes in root-mean-square roughness S_q as a function of the scan size in contact mode (circles) and tapping mode (squares)

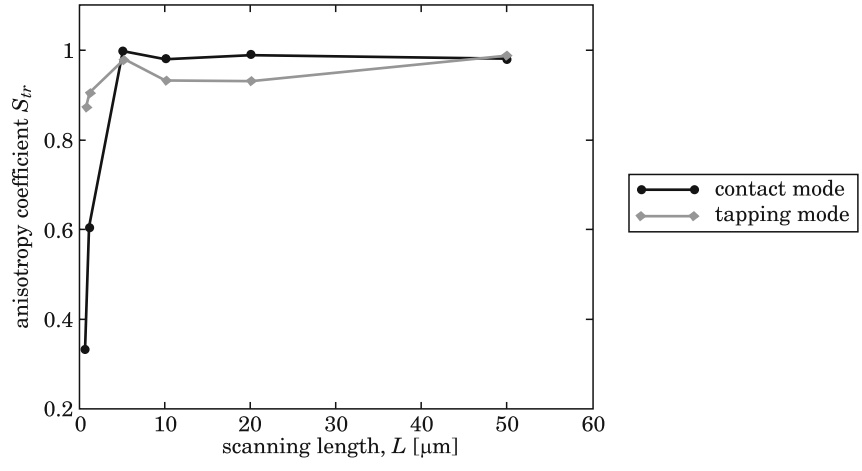

Fig. 6. Plot of the anisotropy coefficient S_{tr} as a function of the scan size in contact mode (circles) and tapping mode (squares)

Plots of the structure function $S(\tau)$ defined according to Eq. (4) for the scan size larger than 5 μm are shown in Fig. 7 and Fig. 8. Each plot is drawn for the scan directions parallel to the coordinate axes (x and y, respectively).

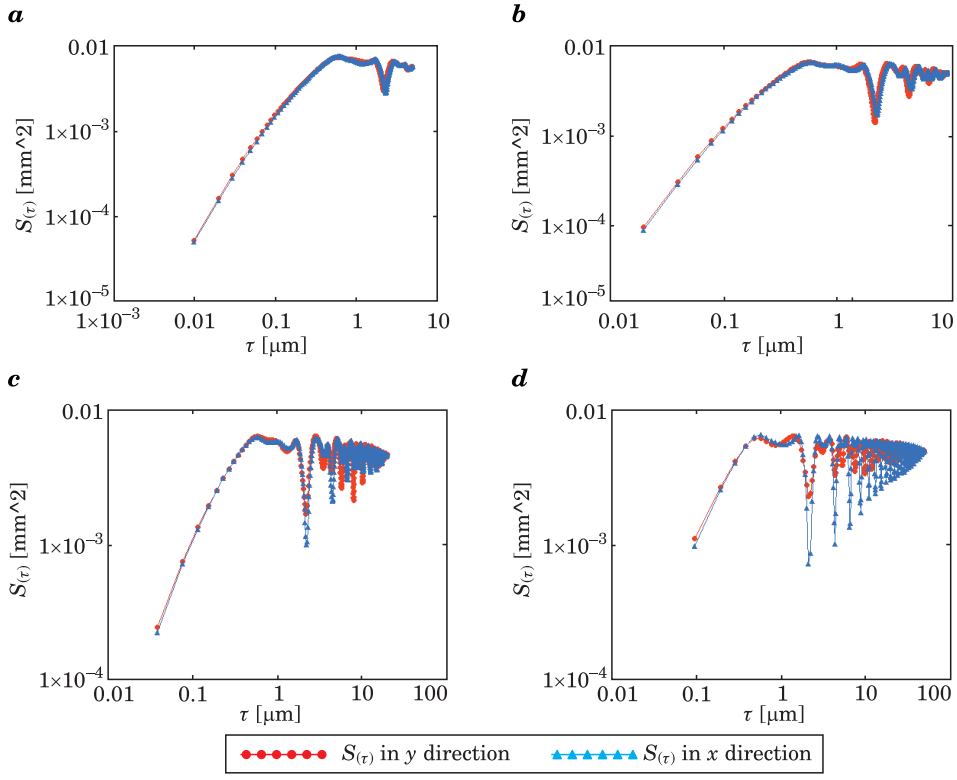

Fig. 7. Structure function $S(\tau)$ in contact mode for the scan size: *a* – 5×5 μm, *b* – 10×10 μm, *c* – 20×20 μm, *d* – 50×50 μm

Plots of the structure function shown in Figure 7 and Figure 8 are very similar independent of the scan direction, including the slope (corresponding to fractal dimension D), and the vertical intercept (corresponding to the topothesis K). As a rule, the fractal parameters of the isotropic surfaces become constant in any direction. For smaller scans, however, plots of the structure function $S(\tau)$ have different slopes depending on the scan direction.

In order to determine the fractal parameters of the sample surface assuming its self-affinity, log-log plots of the structure function $S(\tau)$ were drawn in Figure 9 for the scan size of 5, 10, 20 and 50 μm. Pronounced and reproducible linear range of each curve was approximated by the straight line, slope of which was twice as large as the Hurst parameter H ($a = 2H$), which subsequently allowed for determination of the fractal dimension D ($D = 2 - H$). As seen in Figure 9, estimated fractal parameters have similar values, especially the topothesis K. Additionally, the linear parts of the $S(\tau)$ curves in the tapping mode almost perfectly overlap, while in the contact mode a small

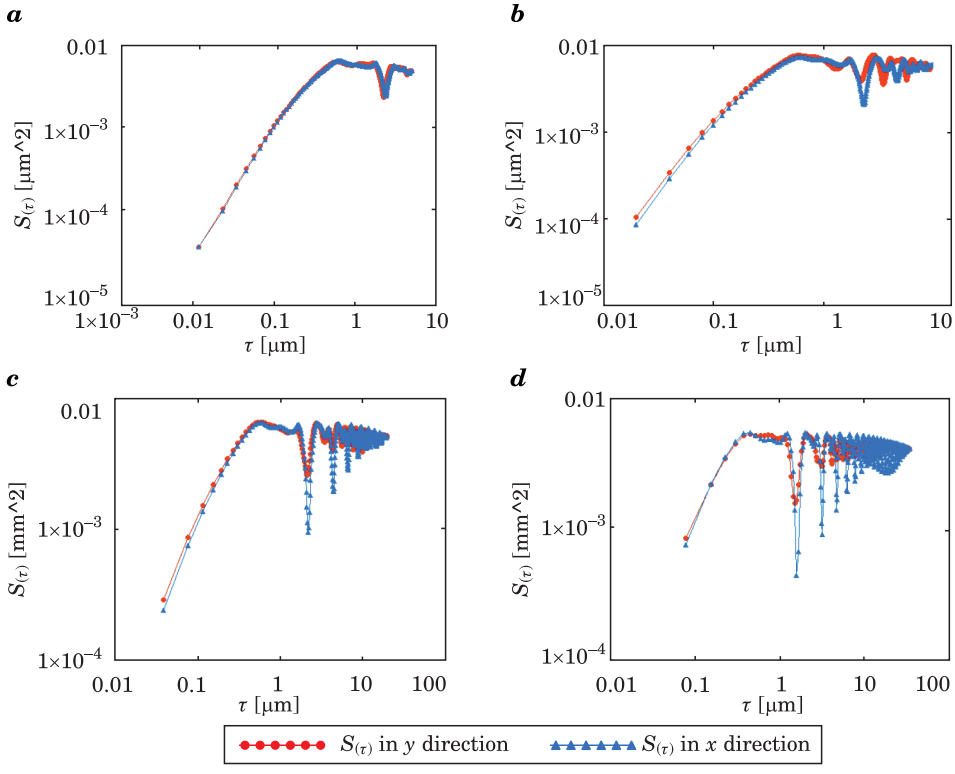

Fig. 8. Structure function $S(\tau)$ in tapping mode for the scan size: *a* – 5×5 μm, *b* – 10×10 μm, *c* – 20×20 μm, *d* – 50×50 μm

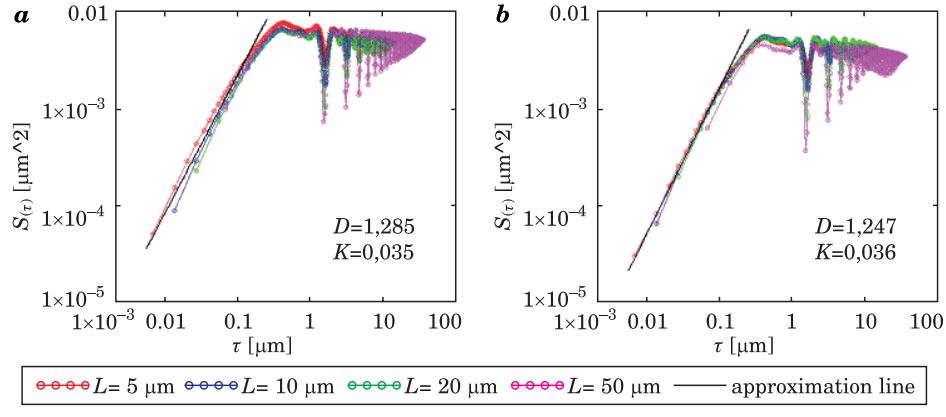

Fig. 9. Results of the straight line fit to the linear range of the structure functions and estimated fractal parameters obtained for isotropic images in: *a* – contact, *b* – tapping modes

deviation from the main direction can be observed that gives rise to a small deviation in the fractal dimension D.

AFM measurements do not exhibit the real surface topography. In fact, the AFM images are distorted by the tip shape and hence they provide the convolution of two curves, namely the surface and the tip curvature. However, all the measurements described in the paper were carried out using identical AFM probes, so that a comparison between contact and tapping modes is still possible. Figure 10 shows examples of scanning profiles (surface sections) recorded in both modes, which look very similar. This leads to conclusion that

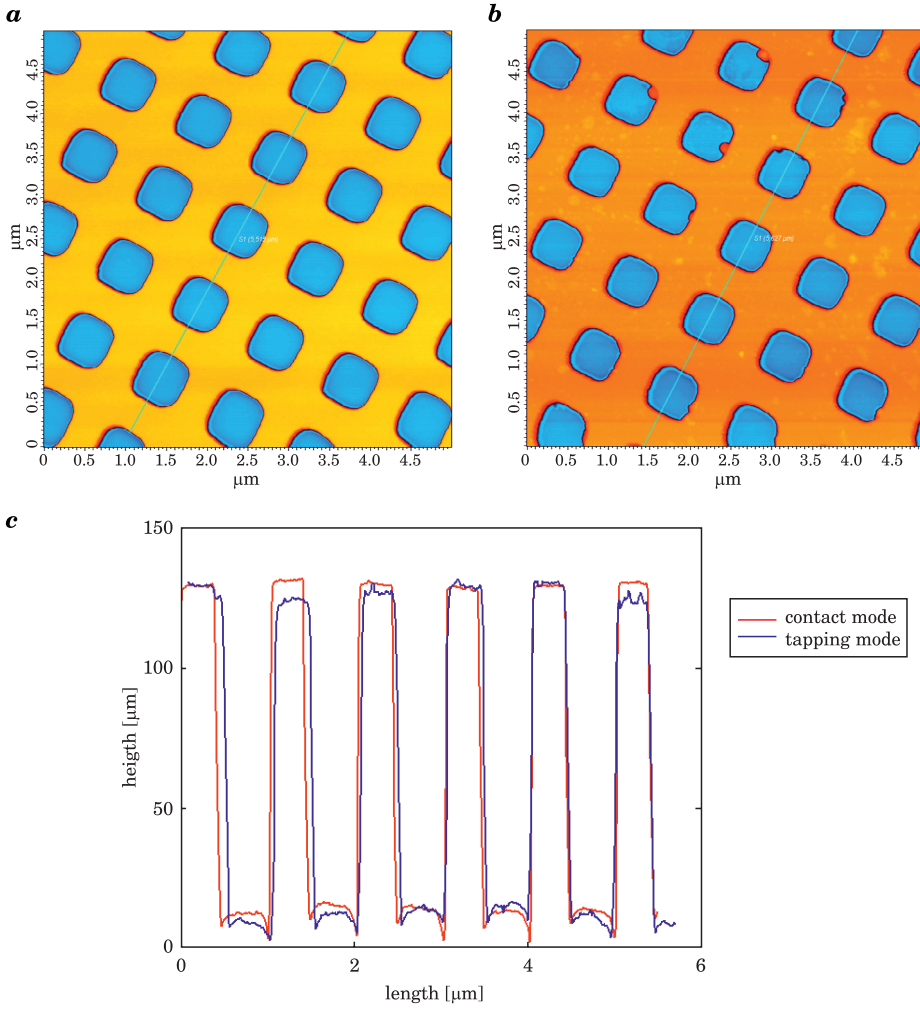

Fig. 10. Section profiles of the surface in: contact (red) and tapping (blue) modes

the differences in surface topography observed in contact and tapping modes are mainly due to the scanning method, and more specifically – the smallest distance between the tip and the surface.

Conclusions

A comparison between AFM measurements of the surface topography in contact and tapping modes reveals that in the multifractal domain, that is when at least one periodic element of the topography appears in the image, anisotropy coefficient S_{tr} can be assessed on AFM results obtained using either contact or tapping mode. The same applies to fractal parameters, although with small differences in the fractal dimension D. Note, however, that recorded images are results of many various tip-surface interactions, and hence getting the real surface topography in meso- as well as microscale requires deconvolution to be made prior fractal analysis.

Translated by Sławomir Kulesza

Accepted for print 16.11.2012

References

Bramowicz M., Klysz S. 2007. *Application of Atomic Force Microscopy (AFM) in the diagnosing of a surface layer*. Research Works of AFIT, 22: 167–174.

Bramowicz M. 2009. *Zastosowanie mikroskopii sił atomowych (AFM) w ocenie stopnia anizotropii mikrostruktury*. Inżynieria Materiałowa, 4: 235–238.

Hartmann U. 1997. *An Elementary Introduction to Atomic Force Microscopy and Related Methods*. Institute of Experimental Physics, University of Saarbrucken, D-66041 Saarbrucken, Germany.

Howland R., Benatar L. 2002. *STM/AFM Mikroskopy ze skanującą sondą elementy teorii i praktyki*. Tłum. M. Woźniak, J.A. Kozubowski (WIM PW), Warszawa.

Mainsah E., Greenwood J.A., Chetwynd D.G. 2001. *Metrology and Properties of Engineering Surfaces*. Kluwer Academic Publishers.

Mironov V.L. 2004. *Fundamentals of Scanning Probe Microscopy*, The Russian Academy of Sciences. Institute of Physics of Microstructures, Nizhniy Novgorod.

Saint Jean M., Hudlet S., Guthmann C., Berger J. 1999. *Van der Waals and capacitive forces in atomic force microscopies*. J. Appl. Phys., 86(9): 5245–5248.

PN-EN ISO 25178-6:2011 – Specyfikacje geometrii wyrobów (GPS). Struktura geometryczna powierzchni: Przestrzenna.

TECHNICAL SCIENCES
Abbrev.: Techn. Sc., No 15(2), Y 2012

A STRATEGY FOR AUTOMATIC ELIMINATION OF MECHANICAL INSTABILITY IN STRUCTURAL ANALYSIS OF SPATIAL TRUSS TOWER MODEL

Józef Pelc

Department of Mechanics and Machine Design
University of Warmia and Mazury in Olsztyn

K e y w o r d s: lattice, transmission tower, spatial model, finite element method.

A b s t r a c t

A method for structural analysis of lattice transmission towers considered to be spatial trusses is proposed. It consists in automatic elimination of mechanical instability from the structure. The instability result from the existence of the so-called out-of-plane nodes in a structure model. The method is based on blocking the possible displacements of out-of-plane nodes and the information concerning the need for blocking the specific displacement is obtained from analysis of the system stiffness matrix. Through application of the spatial rod finite elements lattice transmission towers may be analysed with the use of spatial truss models. The short characteristic of the in-house computer program applied for identification of truss members not satisfying the load capacity criterion, comparison of the results obtained by use of the method and ones obtained by applying the plane truss model and the frame model with the reduced member flexural stiffnesses are also presented.

Introduction

In engineering practice there exist structures, which have computational models in form of spatial trusses. Due to numerical difficulties associated with these models, they are commonly replaced with frame models. It can be shown that the member forces in frame model differ from those that occur in the spatial truss model under the same loading conditions. So the question is: do computational difficulties have to dictate the need to seek a substitute for the spatial truss model?

In the case of applying additional loading to existing lattice transmission towers (e.g. with optical fibre cables) and assessment of their condition or determination of safe work time period for them, it is necessary to check the load capacity criteria for all members of the structure. In many countries the

standard regulations recommend assuming the truss model of the tower. Then it becomes an important task to determine efficiently the values of member forces in the truss subjected to load combination specified in the regulations. During the times preceding the computer era the task was simplified, i.e. plane trusses corresponding to the individual faces of a tower were analysed. The plane truss member forces were being determined generally by the use of graphical or analytical methods. Currently computer programs, mainly based on the finite elements method (FEM), are used for that purpose (RAKOWSKI, KACPRZYK 2005). Breaking the spatial truss down into plane substructures is not only an arduous method of low effectiveness but also it may be a source of errors due to both the simplifications related to that method and the process of specifying loads applied to plane trusses. Lattice transmission towers in their nature are spatial structures and treating them as three-dimensional systems should be the natural consequence of that fact.

Recently a large number of papers have been published on many important aspects of the analysis of towers for overhead transmission lines such as: non-linear analysis (ALBERMANI, KITIPORNCHAI 2003), prediction of structure limit load (KEMPNER et al. 2002) or dynamic analysis (GANI, LÉGERON 2010). We should, nevertheless, differentiate between the research papers from specific requirements formulated in the standard regulations in force in a given country. The former ones allow better understanding of the structure behaviour and more precise assessment of the safety reserve as well as improving the applicable standards while the latter ones must be met absolutely in relation to both the designed structures and the existing ones but additionally loaded or undergoing a change caused by the influence of various factors (e.g. corrosion, ageing).

Truss is one of the simplest load bearing structure but structural analysis of a three-dimensional truss tower model by FEM encounters serious difficulties related to the mechanical instability of the system resulting from the occurrence of the so-called out-of-plane nodes. Attempts at overcoming that difficulty were undertaken in various ways, e.g. by using beam elements for analysis of the spatial truss or by inserting internal dummy rods with lower longitudinal stiffnesses than the truss members (DA SILVA et al. 2005). Manual addition of the dummy rods to the computational model is a time consuming and arduous work. Additionally, a priori prediction of the rods stiffnesses is not an easy task and it may yield erroneous results. A similar situation appears in the analysis of truss by the use of beam elements but reduction of members bending stiffnesses is required. Excessively small reduction results in a stiffer frame structure and the axial force values obtained may be different than for the truss. Excessively large reduction on the other hand may cause numerical difficulties resulting from poor conditioning of the system stiffness matrix. The

use of beam elements requires additional input data for each element. It is related to the necessity of entering the points coordinates to define the orientation of the principal inertia axes of the beam cross section in space.

This paper presents the effective method for overcoming the inherent difficulties encountered in spatial truss analysis by FEM. It consists in automatic blocking of the additional degrees of freedom of the structure related to the out-of-plane nodes by means of the additional external dummy rod elements. Their locations are determined on the analysis of the stiffness matrix of the structure.

Automatic elimination of the mechanical instability of the truss tower model

The process of standard structural analysis of a lattice tower consists of some stages: assuming the computational model of the structure as the truss, determining the loading, applying forces to nodes, computing truss member forces and verifying the load capacity criterion for all the members.

Figure 1 presents a fragment of the truss tower model with two adjacent faces. The nodes marked with black circles referred to as the spatial nodes are characterised by the rule that displacement of such a node in any direction requires elongation/shortening of the members connected to the node. The other nodes marked by circles (out-of-plane nodes) have constrained mobility in the plane of one face but in the direction perpendicular to that face they can displace. The occurrence of the out-of-plane nodes in the truss structure results in its mechanical instability, i.e. system stiffness matrix becomes singular.

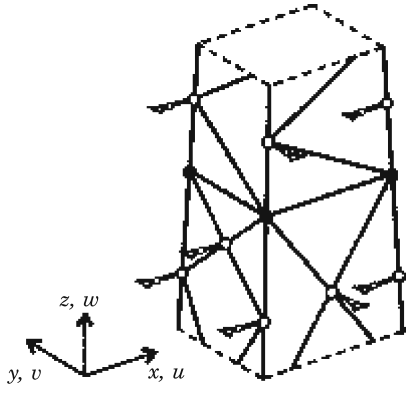

Fig. 1. Out-of-plane nodes and dummy rods

On the whole three-dimensional truss model cannot be analysed in a simple way by FEM using the truss elements, i.e. 2-noded truss elements with six degrees of freedom. To overcome the numerical difficulties it is possible to apply additional constraints on the degrees of freedom of out-of-plane nodes. For example, it is possible to impose the condition that the out-of-plane nodes are subject to displacements assuring that they remain within the plane of the face in which the members connected to the nodes are located. Commercial general-purpose FEM programs allow applying constraints of that type, although manual identification of out-of-plane nodes within the tower computational model and defining for each of them additional constraints may be a highly work-intensive task. That is why a method was proposed for automatic blocking of out-of-plane node displacements by attaching dummy rods to the nodes to eliminate their undesirable mobility (Fig. 1). Each such a rod blocks one degree of freedom of a node. The method, however, should be found for identification of the degrees of freedom that require blocking. It can be noticed that in the truss with out-of-plane nodes, considered within the global system of coordinates x, y, z, on the main diagonal of the structure stiffness matrix, in cells corresponding to degrees of freedom related to the possible displacements of those nodes, terms of low values, differing clearly from the other terms, occur. In case of the out-of-plane nodes located on the non-tapered tower segments the values of those terms can be zero. For the purpose of determining the condition of blocking the excess degrees of freedom the value of the so-called blocking threshold must be determined. It can be set quite precisely on the examination of the main diagonal terms of the stiffness matrix of structure with out-of-plane nodes not blocked.

In-house computer program for structural analysis of lattice towers

The presented method for dealing with out-of-plane nodes may be applied if access to the system stiffness matrix is possible. Most FEM programs give such a possibility. In the in-house computer program targeted to the effective structural analysis of lattice transmission towers the presented method for automatic elimination of the mechanical instability from the spatial truss model was applied. The program was developed considering the necessity for efficient analysis of a large number of truss towers. The computations were performed mainly because of the additional loading of existing structures with optical fibre cables and in the process of determination of safe work time period for old towers.

The analysis of a truss tower model is performed in two stages. During the first stage, after assembling the structure stiffness matrix and application of the boundary conditions, the program subroutine examines the terms on the main diagonal of the matrix and if the term value is lower than the blocking threshold the given degree of freedom is being blocked. This involves generating the additional massless rod and setting it perpendicularly to the appropriate tower face. One end of the rod is located in the node to be blocked and the other is pinned supported. When the automatic addition of all the necessary dummy rods is completed the second stage of the analysis follows which is typical for the finite element analysis of a structure. The in-house program is provided with the procedure analysing the values of forces in dummy rods. In case of blocking an inappropriate degree of freedom a noticeable force value occurs and the user is alerted. The practice shows that only in a few cases minor modifications (addition or removal) of dummy rods in the tower model were necessary.

A CAD type program (in this case IntelliCAD) equipped with a set of functions written in the AutoLISP language performs the pre-processor and post-processor tasks in the tower analysis. On completing the tower finite element model its database is exported in DXF format, which is then read and processed by external program (data generator) to write the model data text file readable for the in-house program. The program is based on the FEM using three-dimensional truss-type elements (axial tension or compression), however, the method of blocking out-of-plane nodes and analysis of load capacity criterion, according to the standard regulations in force, were implemented. The program determines safety factor for each tower member in case of the given load combination. The factor depicts the degree of satisfying the member load capacity criterion. Program also generates the drawings of all the tower faces and the cross-arms and linking elements in which the hazardous members are marked in the appropriate colour. The drawings allow rapid location of unsafe members in the structure analysed.

Results generated by 3d truss tower model vs. the results obtained using the plane model and frame model

For the verification of the presented method of handling with out-of plane nodes in the three-dimensional truss tower model the results of computations obtained using the method were compared with those obtained with the use of the plane truss model and the spatial frame model. The spatial truss model was computed using the in-house program while the plane and frame models were solved using MSC.Marc Mentat system.

The actual transmission tower of 38.83 m high loaded with wind acting in the direction perpendicular to the transmission line (direction of the x axis depicted in Fig. 2a) was chosen for the comparative study. Under conditions of normal rime that load case represents in general the most rigorous test of load

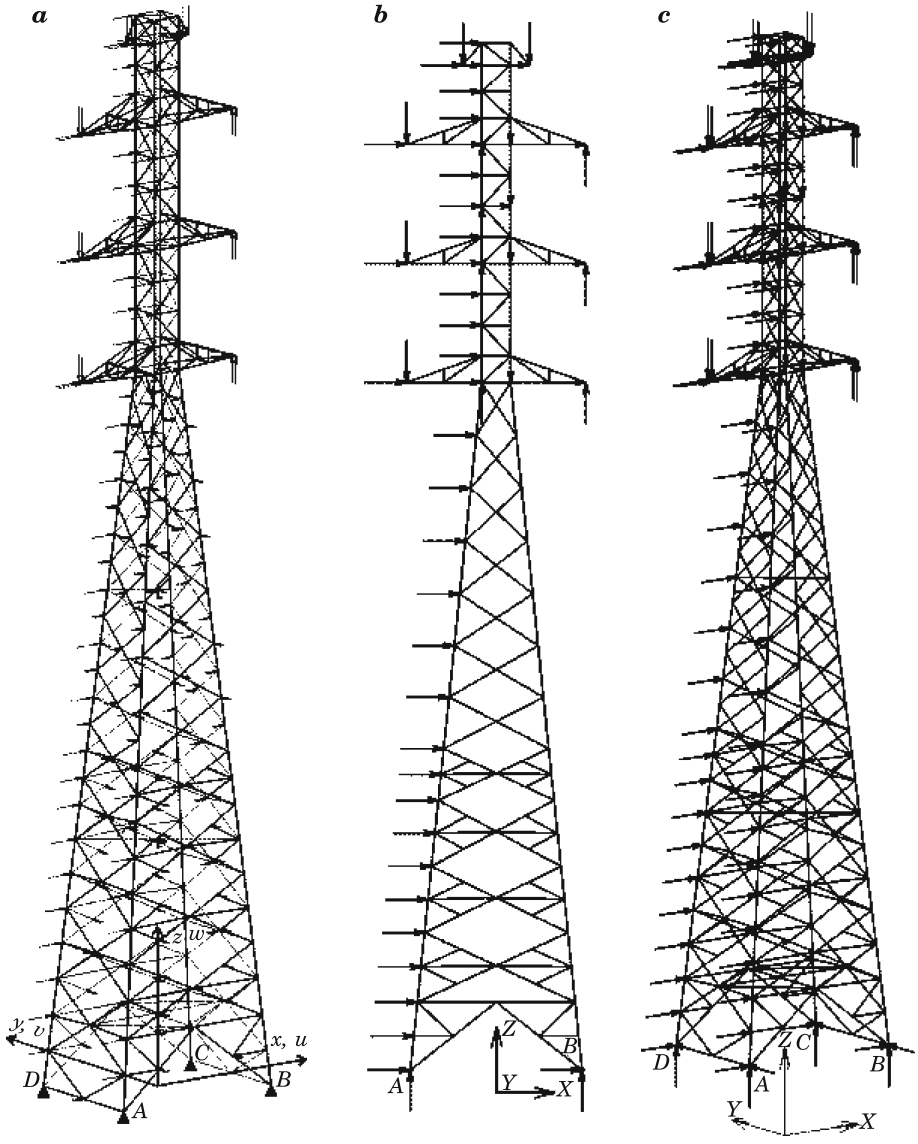

Fig. 2. Transmission tower models: a – 3D truss with out-of-plane nodes degrees of freedom blocked, b – plane truss, c – 3D frame

bearing capacity of tower. The plane model of the tower was defined by the *AB* tower face with out-of-plane nodes removed.

Three-dimensional truss tower model

To determine the value of the blocking threshold for the structure analysed in the global coordinate system (x, y, z) shown in Figure 2a, the values of k_{ii} terms located on the main diagonal of the structure stiffness matrix are being watched. After arranging those terms in ascending order the graph of their variability can be drawn. It can be seen from Figure 3 that some terms have low values (the initial part of the graph) and they correspond to the undesirable degrees of freedom of the model. For the tower under consideration the blocking threshold has the value $7.2 \cdot 10^6$ N/m and on its base the program has generated dummy rods that allow blocking the excess degrees of freedom of the truss model. Given small taper of the tower body (1:10 in *xz* plane and 1:14 in *yz* plane) the rods are rotated by small angles about the x or y axis to set them perpendicular to the appropriate tower face. The taper of the tower body is defined as the value of the tangent of the tower face slope to the vertical plane. In the case considered 148 dummy rods were generated: 54 in the direction close to the x axis and 92 to y axis and 2 in the direction of z axis.

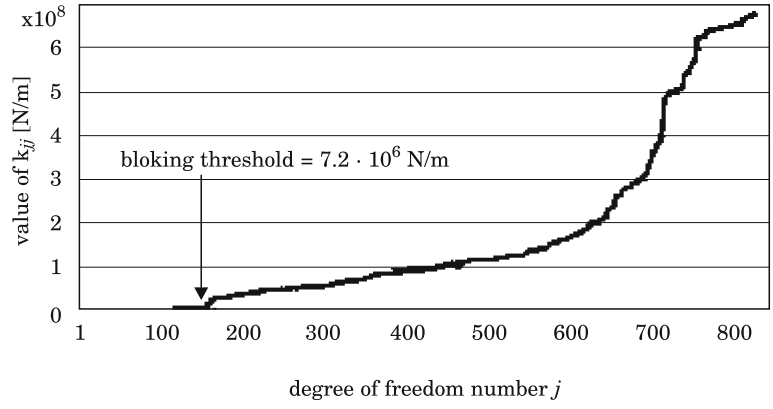

Fig. 3. Stiffness matrix diagonal terms values for the 3D truss tower model

External loads are applied to the nodes in the directions that do not correspond with the blocked degrees of freedom of the model. Nevertheless, as a result of self weight loading vertical forces are applied to all nodes, including the out-of-plane nodes. As the dummy rods are not positioned horizontally, negligible forces due to the structure self weight occur in them. Maximum

values of the reaction forces components at the supports of dummy rods (0.099, 0.025, 0.343 kN) divided by the minimum values of reaction forces in nodes at the tower base (19.03, 8.98, 129.67 kN) are: $R_{fx}/R_{x\min}$ = 0.52%, $R_{fy}/R_{y\min}$ = 0.28% and $R_{fz}/R_{z\min}$ = 0.26% respectively. The possibility of shifting the gravity forces from the out-of-plane nodes to the adjacent "normal" nodes could be considered, however, as a consequence of minor values of the forces in dummy rods induced by the gravity forces that action is not necessary. Very low values of reaction forces by the dummy rods indicate also blocking the appropriate, i.e. excess, degrees of freedom of the structure.

Plane tower model

The plane model was obtained by projecting the AB tower face, shown in Fig. 2a, on the vertical plane containing points A and B. The arrangement of members in this model is presented in Fig. 2b.

Three-dimensional frame tower model

The frame model shown in Fig. 2c can well predict the values of member axial forces in the lattice tower treated as the truss if the flexural stiffnesses of the members is very low. It cannot, however, be excessively small because then the mechanical instability may occur as in the case of the truss model with out-of-plane nodes. The issue of reducing the tower beams flexural stiffnesses must be solved then.

The members of the analysed tower have angle sections but for the purpose of reduction of data input their cross sections were substituted with circles. The cross section area of a circle was equal to the actual one whereas moment of inertia was assumed to be equal to the minor principal moment of inertia for the member angle section.

For the purpose of selecting the appropriate degree of reduction for members flexural stiffnesses the frame model was computed several times changing the values of the moment of inertia. The values of actual minor moments of inertia were assumed to be the reference values. Changed values of moments of inertia were obtained by multiplying the reference values with a factor (tab. 1).

The consecutive rows of the table present the values of the: extreme axial force, extreme bending moment, square root of the sum of squares of displacements for all the nodes of the structure and displacements of nodes that revealed large variations. Analysis of Table 1 indicates that the frame with the

Table 1
Influence of the frame members flexural stiffness on section forces and displacements of selected nodes

	I/I_{min}	0.01	0.02	0.1	0.2	0.5	1	2	5	10
N_{max}	kN	-164.7	-164.7	-164.7	-164.7	-164.7	-164.6	-164.5	-164.2	-163.7
M_{max}	kNcm	7.2	7.2	7.2	7.7	13.9	25.7	49.1	111.5	198.6
Δ	cm	148.49	143.95	142.43	142.36	142.28	142.17	141.97	141.42	140.65
u_2	cm	8.17	4.09	0.82	0.41	0.16	0.08	0.04	0.02	0.01
v_{169}	cm	0.58	0.29	0.05	0.02	0.00	0.00	0.00	-0.01	-0.01
w_2	cm	-0.78	-0.38	-0.07	-0.03	-0.01	0.00	0.00	0.01	0.01

lowest member flexural stiffnesses but still assuring the stable solution should have the elements with the values of the moments of inertia reduced 5-fold in relation to the values of the minor moments of inertia of the angle cross sections. In particular the monotonically decreasing function Δ has the inflection point for $I/I_{min} = 0.2$ as shown in Figure 4. Additionally, the bending moment starts changing its value significantly at that point. The results obtained for that frame model were further compared with those for the truss models of the tower.

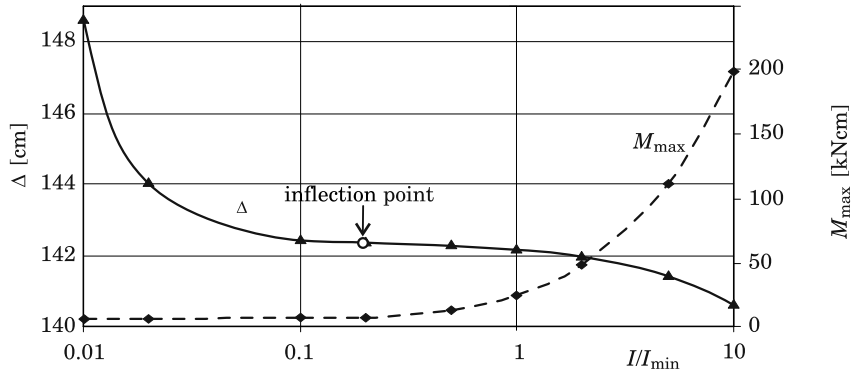

Fig. 4. Variations in the root from the sum of squares of displacements for all nodes and the extreme bending moment in the function of the members flexural stiffness parameter

Computational results

Table 2 presents the parameters of the tower models and the extreme values of the tower crown displacement and member axial forces obtained. Deformation of the tower model with the dummy rods attached to it and a real tower deformation do not coincide; nevertheless, the value of crown displacement is almost the same as for the plane model and for the frame model.

Table 2

Specification of the differences in the tower models analysed

Tower Model	3D truss	Plane truss	3D frame
Number of elements	829	217	681
Number of nodes	424	110	276
Number of degrees of freedom	1272	220	1656
Crown displacement [cm]	21.26	20.53 (-3.4%)	21.26 (0.00%)
Max axial force [kN]	127.00	125.57 (-1.13%)	126.90 (-0.08%)
Min axial force [kN]	-164.58	-164.15 (-0.26%)	-164.69 (0.07%)

The values of extreme axial forces determined using the analysed models are very close. The percentage differences do not exceed 1.2%. That observation, however, do not apply to all the members. In Figure 5 and 6 the percent differences in force values are presented. The differences are small in significantly loaded members. Larger differences occur in slightly loaded members, which, however, are not critical elements in the assessment of the entire structure load capacity. It should be noticed, nevertheless, that in the plane model of the structure the distribution of axial forces is different than in the spatial model as a consequence of neglecting the slope of the tower face and disregarding the influence of the internal members. It was established that the points farthest away from the horizontal axis in the Figure 5 correspond to the members possessing common nodes with the members connecting opposite faces of the tower that are not considered in the plane model.

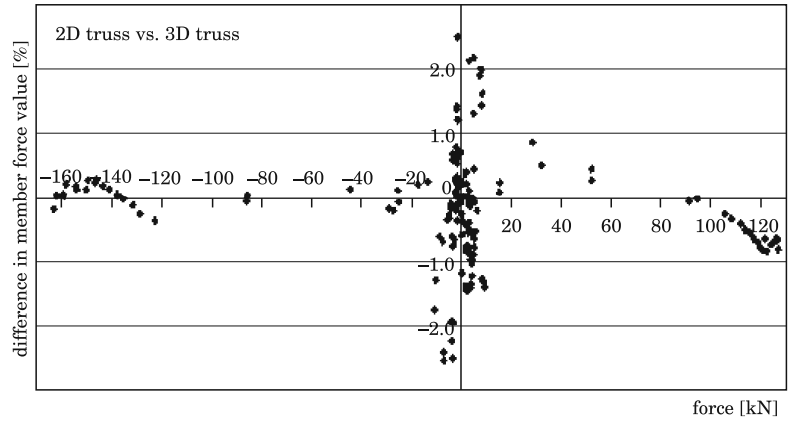

Fig. 5. Differences in the values of forces in the tower members obtained using the plane and the spatial truss models

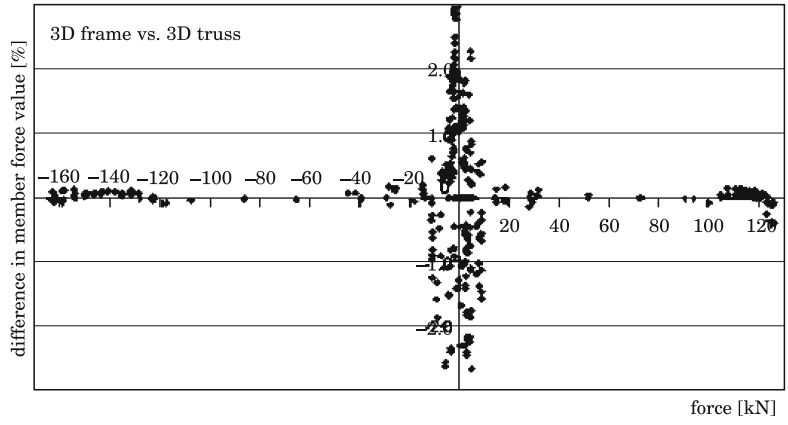

Fig. 6. Differences in the values of forces in the tower members obtained using the frame and the spatial truss models

Despite reduction of the members flexural stiffnesses, in the frame model the distribution of forces is different than in the truss model due to the influence of bending effects. The frame model gives low values of axial forces in the members that in the truss model are zero force members. In that type of members the percentage differences in force values are generally large. Opposite signs of forces in some insignificantly loaded members were also observed. For example, the member compressed by small force in the truss model is elongated by a small force in the frame model (e.g. member No. 21: N^{TRUSS} = -0.04 kN, N^{FRAME} = 0.03 kN). Then the corresponding points of the graph are outward the range presented and have not been shown in the figures.

Reasonably good correspondence between the values of the extreme displacements and forces (see Table 2) obtained using the analysed models confirms effectiveness of the presented method for automatic blocking of the mechanical instability in the three-dimensional truss tower model. It should be emphasised that the 3D truss tower model represents better the work of a spatial truss than a plane or frame model. This results from the fact that dummy rods are positioned perpendicularly to the members connected to the out-of-plane nodes and do not take any components of axial forces carried by the members.

Conclusions

Due to existence of the out-of-plane nodes in truss transmission tower model its numerical analysis, as three-dimensional structure, requires special

approach. The proposed method of automatic removal of the mechanical instability from the finite element model with rod elements (tension/compression) has proved effective. The results obtained confirm the possibility of applying the described method of blocking out-of-plane nodes in models of typical lattice transmission towers.

Analysis of spatial lattice structures, especially with bolted or riveted joints, by the use of spatial truss model seems to be more natural approach then the use of substitute model i.e. frame model. Preparation of the truss tower model requires less time and is less arduous than determining of frame model because every frame element requires the coordinates of the additional node (point) defining the orientation of the neutral axes of the beam cross section in space and problems with reduction of beams flexural stiffnesses also appear. Models composed of truss elements allow shortening the work time necessary for preparing them.

Translated by JERZY GOZDEK & AUTHOR

Accepted for print 12.11.2012

References

RAKOWSKI G., KACPRZYK Z. 2005. *Finite element method in structural mechanics*. Oficyna Wydawnicza Politechniki Warszawskiej, Warszawa.

ALBERMANI F.G.A., KITIPORNCHAI S. 2003. *Numerical simulation of structural behaviour of transmission towers*. Thin Wall Struct, 41: 167–77.

KEMPNER Jr L., DO T.T., MUELLER III W. 2002. *Lattice transmission tower analysis moves beyond the simple truss model*. Electric Light & Power, 80(12): 22, 2p.

GANI F., LÉGERON F. 2010. *Dynamic response of transmission lines guyed towers under wind loading*. Can. J. Civ. Eng., 37: 450–64.

DA SILVA J.G.S., VELLASCO P.C.G.D.S., DE ANDRADE S.A.L., DE OLIVEIRA M.I.R. 2005. *Structural assessment of current steel design models for transmission and telecommunication towers*. J. Constr. Steel. Res., 61: 1108–34.

TECHNICAL SCIENCES
Abbrev.: Techn. Sc., No 15(2), Y 2012

EVALUATION OF OXYGEN PERMEABILITY OF POLYETHYLENE FILMS

***Stanislav Zeman*[1], *Lubomír Kubík*[2]**

[1] Department of Production Engineering
[2] Department of Physics
Slovak University of Agriculture in Nitra, Slovak Republic

K e y w o r d s: oxygen permeability, polyethylene film, packaging, mulching.

A b s t r a c t

The paper dealt with the evaluation of the oxygen permeability of the polyethylene films applied in the mulching and food packaging. The construction of the equipment is discussed. The design and the construction of the equipment was realized with applying of the standard EN STN 77 0333.The measurement of the permeability of the oxygen trough the polyethylene Bralen 2–63 with 9% colored concentrate Maxithen HP 533041 – violet film was realized by means of modified method. The values of the permeability P_x, 1794.25 $cm^3 \cdot m^{-2} \cdot d^{-1}$. $(0.1\ MPa)^{-1}$ of the oxygen trough the film of the thickness of 50 μm was evaluated. The coefficient of permeability P, $4.2560 \cdot 10^{-16}$ $mol \cdot m^{-1} \cdot s^{-1} \cdot Pa^{-1}$, coefficient of diffusion D, $4.3999 \cdot 10^{-10}$ $m^2 \cdot s^{-1}$ and solubility coefficient of the gas in the film S_p, $9.6735 \cdot 10^{-7}$ $mol \cdot m^{-3} \cdot Pa^{-1}$ were determined.

Introduction

Materials suitable of packaging of foods and mulching are applied on the base of polymers in the present time. The protection of original quality of food against external undesirable effects is the function of the packaging materials. Required protection of foods can be achieved with one layer of polymer, or in the case of need, with multilayer film, includes different polymers, surface films and metallic films. Barrier properties, i.e. protection of the package, are related mainly with the ability to transmit the gases and vapors, which are damaging of the quality of the product. Degradation processes of foods are dependent on the time and temperature (JASSE et al. 1994, ASHLEY 1985, PYE et al. 1976). The oxygen is harmful for foods of vegetal or animal origin. It causes the oxidation of the higher fatty acids. Internal atmosphere of gases, as are CO_2 a N_2, is modified of the preservation of the quality of the foods (JASSE et al., 1994). Polyethylene plastic films have great importance in the horticul-

ture. The plastic films applied as mulch, affect the radiation balance of the environment by means of absorption and reflection of the light by their surface and they change of the microclimate of the cultivated plants (TABER 2010).

WANG et al. (1998) studied oxygen and ethylene permeabilities which have been determined at 19°C for three kinds of polyethylene films (LDPE, LLDPE and HDPE) and in the temperature range 4–30°C for LDPE. At constant temperature, ethylene and oxygen permeabilities decrease with increasing density. The temperature dependence of oxygen and ethylene permeabilities was found to be Arrhenius in the temperature range tested, with activation energies of 47.7 and 44.1 kJ/mol for ethylene and oxygen respectively.

PAPIERNIK et al. (2002) describe an apparatus useful for obtaining permeability data. The model may be fitted to the data to determine mass transfer coefficients. The assembled equipment provides a sealed permeability cell, where a sample of the film to be tested is sandwiched between two static half-cells. Vapor is spiked to one side of the film and the concentrations in the spiked and receiving chamber are monitored until equilibrium. The permeability cells described here were gas-tight for >40 d. This approach produces reproducible measures of mass transfer coefficients that are not dependent on the size of the experimental apparatus.

KAMAL et al. (1984) studied oxygen and water vapor permeability on binary polyethylene/polyamide immiscible blends incorporating three polyethylene resins (LDPE, LLDPE, and HDsPE), and three polyamide resins (PA-6, PA-6,6, and modified PA-6,6 m). It was found that the incorporation of PA into PE reduces the oxygen permeability while water vapor permeability is increased. In the range of 0 to 30 weight percent of PA, the oxygen permeability of PE was reduced by a factor of 2.8 to 3.6. Maximum water vapor permeabilities increased: for HDPE by a factor of about 2.6 to 3.1 and for LDPE and LLDPE blends by about 1.6.

Material and Methods

Fundamental principles of the permeability

Sorption of gases and their transmission trough the polymer depends on the permeability and the diffusion. Amount of gas Q (mol), which is transfer through the membrane, is defined by the equation (JASSE et al. 1994):

$$Q = \frac{D \cdot \sigma \, (p_1 - p_2) \, S \cdot t}{h} \tag{1}$$

where:
D – coefficient of diffusion, m^2/s,
p_1 – external pressure, Pa,
p_2 – internal pressure, Pa,
h – thickness of membrane, m,
σ – Henry's constant, $mol \cdot Pa/m^3$,

On the assumption of thermodynamic equilibrium, the coefficient of permeability P is given by the equation:

$$P = D \cdot \sigma \tag{2}$$

Permeability is depended on solubility and diffusivity. These quantities are functions of optional volume, cohesive energy and polymer morphology. Than coefficient of permeability is defined:

$$P = \frac{Qh}{S(p_1 - p_2)\, t} = \frac{Qh}{S\Delta pt} \tag{3}$$

After applying equation of state for ideal gas $pV = nRT$ we can obtain equation of coefficient of permeability P $[mol \cdot m^{-1} \cdot s^{-1} \cdot Pa^{-1}]$ suitable of experimental measurement:

$$P = \frac{Qh}{S\Delta\, pt} \cdot \frac{pV}{nRT} = \frac{pVh}{tS\Delta pRT} \tag{4}$$

where:
P – coefficient of permeability P, $mol \cdot m^{-1} \cdot s^{-1} \cdot Pa^{-1}$,
p – pressure, Pa,
V – volume of gas, m^3,
R – universal gas constant, $R = 8314\ J \cdot kmol^{-1} \cdot K^{-1}$,
T – temperature, K.

We can also obtain permeability of the membrane P_x $[m^3 \cdot m^{-2} \cdot s^{-1} \cdot Pa^{-1}]$ from the equation:

$$P_x = P\,\frac{V}{Qh} \tag{5}$$

Fick's second law of diffusion can be obtained by first calculating a conservation equation with respect to volume,

$$\frac{\partial C_h}{\partial t} = D\left(\frac{\partial^2 C_h}{\partial z^2} + \frac{1}{S}\frac{\partial S}{\partial z}\frac{C_h}{\partial z}\right) \tag{6}$$

where:
C_h – molar concentration, mol · m^{-3},
z – coordinate, m.

By setting S to be constant, equation (6) describes unsteady state diffusion, which is Fick's second law of diffusion. Together, Fick' first and second laws describe how much solute moves across the film (diffusion flux) and reveal how the solute concentration changes within the film (concentration profile). To apply Fick's laws, certain assumptions must be made (Fig. 1). Let C_{1h} be the concentration of downstream solution and let C_{10} be the concentration of upstream solution. If H is the partition coefficient which relates pressure in gas to concentration in the film, then $c_{10} = HC_{10}$.

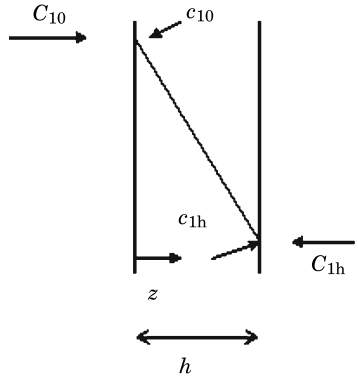

Fig. 1. Steady-state concentration profile in a thin membrane. C_{10} is proportional c_{10} and the partition coefficient H. Infinite reservoirs on both sides are assumed

Initially, the downstream solution is assumed to be free of upstream solution. At time zero, the membrane is also assumed to be free of upstream solution. For $t > 0$ the amount of upstream solution in the membrane is c_{10} at $z = 0$: Furthermore, where $z = l$ the amount of upstream solution is said to be zero.

The boundary conditions restrict the downstream solution to be free of the upstream solution. In experiments it has been found that the concentration is negligible. These boundary conditions allow equation (6) to be transformed into an ordinary differential equation, which will describe a pseudo-steady state in the system.

SIEGEL and CUSSLER (2004) describe the characteristic of lag time in the diffusion model. After using separation of variables on Fick's second law and imposing the aforementioned conditions to obtain:

$$c_h = c_{h0} - \frac{c_{h0} z}{h} - \frac{2c_{h0}}{\pi} \sum_{n=1}^{\infty} \sin\left(\frac{n\ \pi\ z}{h}\right) \exp\left(\frac{-\ Dn^2\ \pi^2\ t}{h^2}\right) \tag{7}$$

And after calculation the limit of the above equation at large times:

$$\frac{c_h}{c_{h0}} = \frac{SD}{Vh}\left(t - \frac{h^2}{6D}\right) \tag{8}$$

where V is the ratio of the volume in the air chamber to the area of the fabric. This limiting equation revealed that there is a lag time for the system to reach the desired pseudo-steady state. Namely, the system can not be described by an ordinary differential equation when

$$t < \frac{h^2}{6D} \tag{9}$$

The limiting equation also reveals that the permeability of the membrane can be found experimentally by calculating the best-fit slope of the equation. Similarly the lag time Θ (s) can be found by experimentally calculating the x-intercept of the best-fit line of the pseudo-steady state data points (Fig. 2).

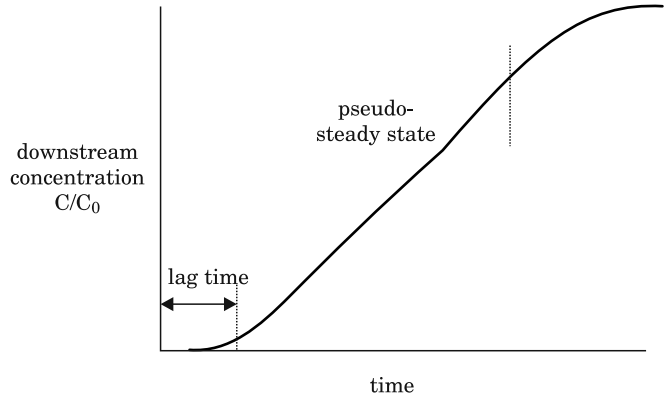

Fig. 2. Typical permeation/lag time curve: normalized downstream concentration versus time in a thin membrane initially free of solute. The code created estimates the pseudo-steady state section (RUTHERFORD, DO 1997)

Then we can obtain the coefficient of diffusion D [$m^2 \cdot s^{-1}$] (PAULY 1999) from the equation (8):

$$D = \frac{h^2}{6\,\Theta} \tag{10}$$

where:

h – thickness of film, m,
Θ – lag time, s.

The solubility coefficient S_p [$mol \cdot m^{-3} \cdot Pa^{-1}$] can calculate from the equation (BROŽOVÁ 2008):

$$S_p = \frac{P}{D} \tag{11}$$

where:
P – coefficient of permeability P, $mol \cdot m^{-1} \cdot s^{-1} \cdot Pa^{-1}$,
D – diffusion coefficient, $m^{-2} \cdot s^{-1}$.

The solubility coefficient S_p express the solubility of the oxygen in the film. Methods of determination of gas permeability are described in JASSE et al. (1994), PYE et al. (1976), KOROS et al. (1992), SOHAIL (1997). Polymer's materials present large scale structures and properties which depend on their chemical structure, methods of preparation and conditions of processing. Significant participation of additives and application of polymer mixtures influence barrier properties of films trough CO_2, O_2, N_2, or water vapors (LEE 1980).

Standard method

The nature of the test of the gas isobaric method is the interferometric determination of the concentration of the tested gas which penetrated trough tested sample from the chamber filled with the pure tested gas to the chamber with the air. Total gas pressures on either side of the sample are equal and the diffusion of the gas trough the tested sample depends on the difference of the partial pressure in the both chambers (EN STN 77 0333).

Instrument as well as standard procedures for measuring the oxygen permeability are available but measurement of the concentration of the oxygen is proposed by means of optical interferometric method with the laboratory

interferometer with two-part gas chambers of the length 100, 50, 25 and 10 cm. This method is difficult and the interferometer is not available in common. The digital oxygen meter Mesura which measured the relative concentration of the oxygen was used instead of interferometer and the absolute values of concentration had to be calculated from the tabulated values of the air and oxygen at the real conditions. All others conditions of the standard were kept to the terms.

Design of measurement equipment

Methods of detection and measurement of parameters of permeability of packaging materials of gases are specified in the standard EN STN 77 0333. The method was modified for the conditions of our test. Permeability of gases is determinated at the barrier tests of the materials as one of the specific parameter of the protective efficiency of the packaging. The design of measurement equipment was projected. The design is considered universal for the basic measurements. It represents sufficiently the principles of measurement and correspondents with the standard EN STN 77 0333.

Diagram of design of equipment of measurement of gas permeability packaging materials by means of isobaric method is presented in the Figure 3 and

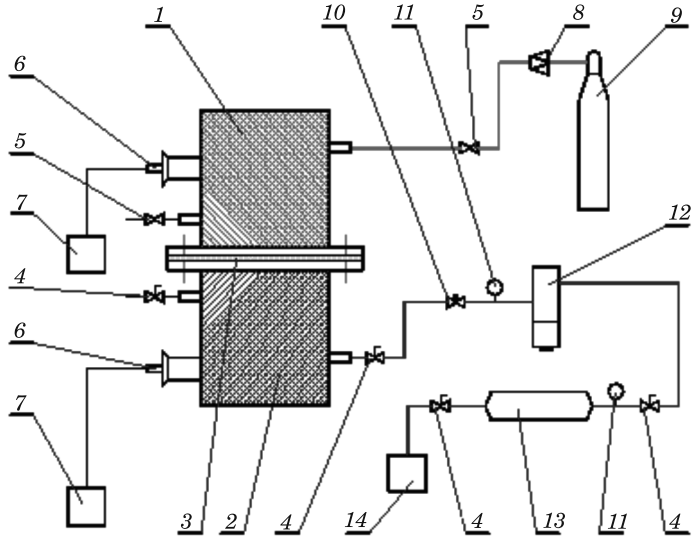

Fig. 3. Design of equipment of measurement of gas permeability: *1* – upper chamber, *2* – bottom chamber, *3* – membrane of measured material, *4* – ball valve, *5* – needle valve, *6* – oxygen probe, *7* – digital oxygen meter, *8* -pressure control valve, *9* – pressure oxygen cylinder, *10* – one way throttle valve, *11* – manometer, *12* – filter regulator, *13* – air tank, *14* – compressor

equipment is presented in the Figure 4. The bottom chamber (2) was firmly attached on the desk and above it upper chamber (1) was attached by means of nuts. Tested material (3) was inserted between two chambers. Two – part test chamber was made of stainless steel and so resistant to corrosion and chemical effects. All parts of the chambers were equipped with the admission valve and the outlet valve (4, 5) and the outlet for the insertion of the oxygen probe (6). Pressure oxygen cylinder (9) was used of supply of pure oxygen (99.5%). The amount of the oxygen was adjusted by means of the pressure control valve in the upper chamber (1). The volume of the each chamber was 1.128 dm^3. Diameter of the effective area between the chambers was 70 mm. Compressor (14) was used to the perfusion of the bottom chamber with the air. Adjusting of the air in this branch was integrated by means of the one way throttle valve and the filter regulator (10, 12). The digital oxygen meters Mesura (7) were applied of measurement of the amount of diffused oxygen.

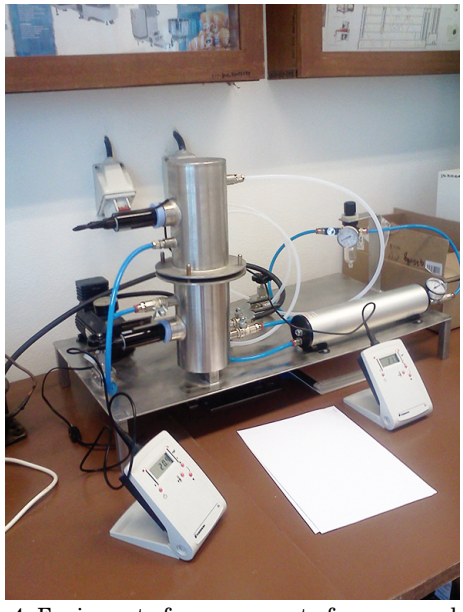

Fig. 4. Equipment of measurement of gas permeability

Basis of the test of the isobaric method is the determination of the concentration of the testing gas, which diffused trough the tested material from the chamber filled with pure testing gas to the chamber with the air. The pressures of the gases on both are equivalent. The samples have to be planar, pure and without mechanical damage. The samples are conditioned during 24 hours in the laboratory conditions. The temperature and the moisture are

continually controlled. The dimensions of volumes V_1, V_2 and S are determined before the test, where V_1 is the volume of the upper chamber of the testing vessel measured in m^3 with the precision of ± 5 %, V_2 is the volume of bottom chamber of the testing vessel measured in m^3 with the precision of ± 5% and S is the testing area of the sample measured in m^2.

Procedure of the test

The upper chamber was perfused with the testing gas and the bottom chamber with the air before the measurement as long as the homogenous environs was reached in the each of the both chambers. The suitable flow of the both gases is about 600 $cm^3 \cdot min^{-1}$. The time of the perfusion has to be at least 30 minutes and it is prolongs if the material is less permeable. The supply of the testing gas is stopped after the perfusion and all valves of the both chambers are closed. The time of the permeation of the testing gas trough the sample is started in the moment. The diffusion of the gas between both chambers is in the progress for a period of 24 hours.

The coefficient of permeability P is determined on the base of the equation (4) from the equation (BROŽOVÁ 2008):

$$P = \frac{\Delta p_p}{\Delta t} \frac{Vh}{Sp_i} \frac{1}{RT} \tag{12}$$

where:

p_i – pressure of the gas in the initial volume V, Pa,
V – calibrated volume, m^3,
h – thickness of the film, m,
Δp_p – increasing of the pressure of the gas transferred into calibrated volume V, Pa,
Δt – time of the duration of the diffusion, d,
S – area of the film, m^2,
R – universal gas constant, $R = 8314\ J \cdot kmol^{-1} \cdot K^{-1}$,
T – temperature, K.

The coefficient of permeability P was obtained from the increasing of the concentration $\Delta\rho_p$ [$kg \cdot m^{-3}$] of the gas permeated trough the film to the calibrated volume V in a time Δt because the oxygen probes measured the relative concentration of the oxygen and the absolute values of concentration had to calculated from the tabulated values of the air and oxygen at the real conditions. After applying equation of state for ideal gas the coefficient of permeability P can obtain from the equation:

$$P = \frac{\Delta\rho_p}{\Delta t}\frac{Vh}{S\rho_i}\frac{1}{RT} \tag{13}$$

where:

ρ_i – density of the gas in the initial volume V, $\mathrm{kg \cdot m^{-3}}$,

$\Delta\rho_p$ – increasing of the density of the gas transferred into calibrated volume V, $\mathrm{kg \cdot m^{-3}}$.

We can also obtain permeability of the membrane P_x $[\mathrm{m^3 \cdot m^{-2} \cdot s^{-1} \cdot Pa^{-1}}]$ after applying the equations (5) and (13) and equation of state for ideal gas $pV = nRT$, from the equation:

$$P_x = \frac{\Delta\rho_p\, VM}{\Delta t\, S\, \rho_i^2 RT} \tag{14}$$

where:

M – molecular mass, $\mathrm{kg \cdot mol^{-1}}$.

Results and discussion

The permeability of pure oxygen (99.5%) trough polyethylene films of the thickness of 50 μm was measured. Samples of film contained 91% of polyethylene Bralen RA 2 – 63 and 9% colored concentrate Maxithen HP 533041 – violet. The films were made in the company Slovnaft, a.s., Bratislava and the colored concentrate were made in the company Gabriel-Chemie, Lázně Bohdaneč.

The conditions of measurement are described in the Table 1. The measurement was realized at the temperature 22°C, 30% of moisture of the air and the barometric pressure 102 600 Pa. Measured quantities needed of calculating of the result quantities are presented in the Table 2.The absolute values of densities were calculated from the relative values measured by the oxygen probes. The oxygen probes were calibrated on the value of 20.9% of oxygen in the air on the beginning of the test. The perfusion of the equipment by the air and oxygen during 30 minutes on the beginning of the test caused the increasing of the initial values of the oxygen probes from the 20.9% to the 23% in the bottom chamber and to the 98% in the upper chamber. Value of 98% of the amount of the oxygen in the upper chamber is real, but the value of 23% in the bottom chamber was occasioned by means of sensibility of the oxygen probe on the speed of the air flow.

Table 1

Conditions of measurement

Symbol	Unit	Quantity	Description
V_1	m^3	0.0011283	volume of upper chamber
V_2	m^3	0.0011283	volume of bottom chamber
d_s	m	0.07	diameter of the film sample
S	m^2	0.0038465	area of the film sample
h	μm	50	thickness of the film
b	Pa	102 600	barometric pressure of the air
T	K	295	temperature of the air
φ	%	30	relative moisture of the air
M	kg/kmol	32	molar mass of the O_2
R	J/kmol · K	8314	universal gas constant

Table 2

Measured quantities

Symbol	Unit	Quantity	Description
Δt	d	1.0382	time of the duration of the permeation
ρ	kg/m^3	1.1965	density of the air at the temperature 295 K
ρ_{O2}	kg/m^3	1.3386	density of the O_2 at the temperature 295 K
ϕ_{1O2i}	% (vol.)	98.0	initial relative concentration of the O_2 at the temperature 295 K measured by the oxygen probe in the upper chamber
ρ_{1O2i}	kg/m^3	1.3118	initial density of the O_2 at the temperature 295 K measured by the oxygen probe in the upper chamber
ϕ_{2O21}	% (vol.)	23.0	initial relative concentration of the O_2 at the temperature 295 K measured by the oxygen probe in the bottom chamber
ρ_{2O21}	kg/m^3	0.2752	initial density of the O_2 at the temperature 295 K measured by the oxygen probe in the bottom chamber
φ_{2O22}	% (vol.)	23.7	final relative concentration of the O_2 at the temperature 295 K measured by the oxygen probe in the bottom chamber
ρ_{2O22}	kg/m^3	0.2836	final density of the O_2 at the temperature 295 K measured by the oxygen probe in the bottom chamber
$\Delta\rho_{O2p}$	kg/m^3	0.0084	increasing of the density of the O_2 at the temperature 295 K in the bottom chamber

Dependence of the volume concentration of the oxygen on the time in the upper chamber during the test is presented in the Figure 5. Dependence of the volume concentration of the oxygen on the time in the bottom chamber during the test is presented in the Figure 6.The coefficient of permeability P was calculated by the equation (13).

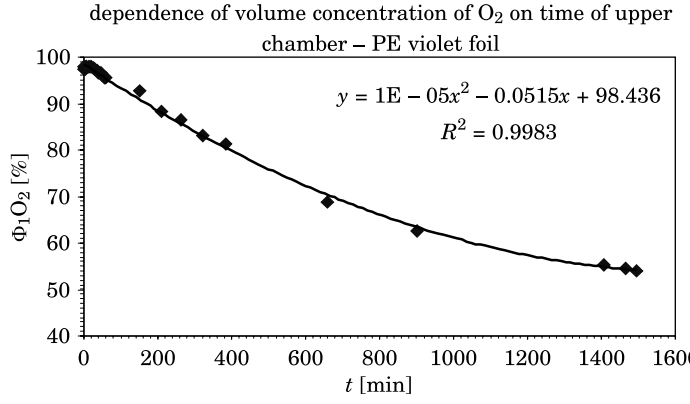

Fig. 5. Dependence of the volume concentration of the oxygen on the time in the upper chamber during the test

The permeability of the film P_x was calculated from the equation (14). The coefficient of diffusion D of the membrane was determined from the equations (8) and (10).The solubility coefficient S_p of the membrane was determined from the equation (11). The measured values from the Table 1 and Table 2 were used for the calculation.

The time lag Θ was calculated by performing linear regression analysis on only the data points that contribute to the pseudo-steady state. The model implied the regression should be linear and the general form used was $y = b + ax$, where a and b were estimated on the base of the equations (8) as it is presented in the Figure 7.

The tangent in the Figure 7 represents pseudo-steady state and its slope represents the slope of the equation (8). Then the diffusion coefficient D is determined:

$$D = \frac{V\,ha}{S} \tag{15}$$

where:
a – slope.

Results of the transport coefficients of the oxygen trough the PE film are presented in the Table 3. Transport properties are also related to the thickness of the film. The polyethylene Bralen 2 – 63 with 9% colored concentrate Maxithen HP 533041 – violet film showed the high values of the coefficients. The film was high permeable for the oxygen. The film is not very suitable for the food packaging but it is suitable for the mulching of the plants.

Table 3
Transport properties of the polyethylene Bralen 2 – 63 with 9% colored concentrate Maxithen HP 533041 – violet film for the oxygen permeability, thickness of the film 50 μm

Transport properties	Experimental values	Experimental values related to the film thickness	
Coefficient of permeability P [mol · m^{-1} · s^{-1} · Pa^{-1}]	$4.2560 \cdot 10^{-16}$	coefficient of permeability P [mol · m^{-1} · s^{-1} · Pa^{-1}]	$1.8387 \cdot 10^{-15}$
Permeability P_x [cm^3 · m^{-2} · s^{-1} · (0.1 MPa)$^{-1}$]	1794.2500	permeability P_x [cm^3 · m^{-1} · s^{-1} · Pa^{-1}]	0.1038
Coefficient of diffusion [m^2 · s^{-1}]	$4.3999 \cdot 10^{-10}$	coefficient of diffusion [m^3 · s^{-1}]	$2.2000 \cdot 10^{-14}$
Solubility coefficient S_p [mol · m^{-3} · Pa^{-1}]	$9.6735 \cdot 10^{-7}$	solubility coefficient S_p [mol · m^{-2} · Pa^{-1}]	$4.8368 \cdot 10^{-11}$

The developed instrument was not compared with the instrument described in the standard (EN STN 77 0333) because the construction of the instrument is not trivial thing. The developed instrument was only constructed and tested and the obtained data were compared with the data in the literature. BHADHA (1999) presented the values of the permeability P_x in the range from 0.4120 to 0.0375 [cm^3 · m/m^2 · s · Pa] and the values obtained by means of the developed instrument were 0.1038 [cm^3 · m/m^2 · s · Pa]. Advantages of the developed method are the simple detection of the relative oxygen concentration. Disadvantage of the developed method is the necessity to calculate the absolute values of the oxygen concetration from the tabulated values of the air and oxygen at the real conditions. The accuracy of the developed method depends on the accuracy of the measurement of relative concentration of the oxygen by means of instrument Mesura, depends on the accuracy of determination of the density of oxygen at the same condition and depends on the applied theoretical methods for determination of the quantities. The electronic accuracy of the instrument Mesura was 0.1% of oxygen on the scale 100% of oxygen. The accuracy of the determination of the density of the oxygen depends on the accuracy of the measurement of the temperature of the gas and the pressure of the gas. The accuracy of the measurement of the temperature was ±0.5°C and the accuracy of the measurement of the pressure of the gas was ±50 Pa. Density of oxygen was calculated from the equation of state for ideal gas. The accuracy of the determination of the density was ±0.0029 kg/m^3, i.e. ±0.22% related to the value of the oxygen density 1.3386 kg/m^3 or ±34.5% related to the value of the oxygen density 0.0084 kg/m^3 (increasing of the density of the O_2 at the temperature 295 K in the bottom chamber).

The accuracy of the determination of the coefficient of permeability P was ±5.1145.10^{-17} [mol/m · s · Pa], i.e. 12.02%. The accuracy of the determination of

the permeability P_x was ±15.684 [cm^3/m^2 · d · (0.1 MPa)], i.e. 0.8%. The accuracy of the determination of the coefficient of diffusion D was ±16.07 · 10^{-11} [m^2/s], i. e. 36.53% and accuracy of the determination of the solubility coefficient S_p was ±1.1624 · 10^{-7} [mol/m^3 · Pa], i.e. 12.01%.

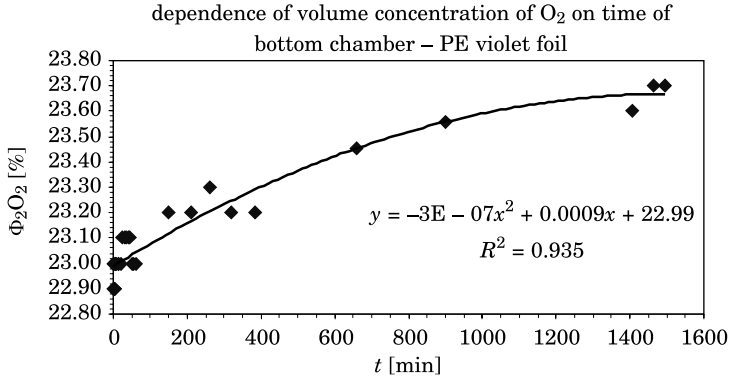

Fig. 6. Dependence of the volume concentration of the oxygen on the time in the upper chamber during the test

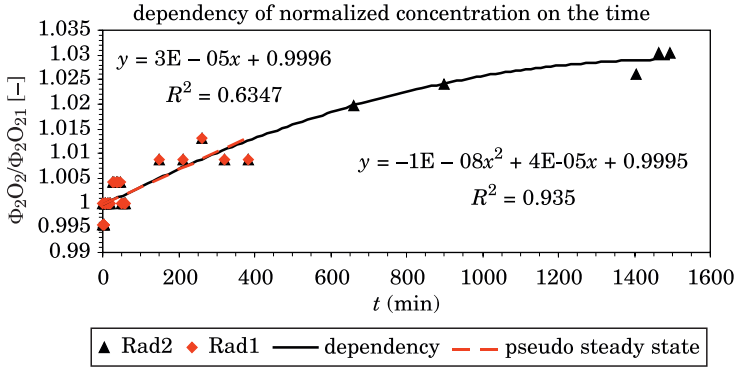

Fig. 7. Dependence of normalized concentration on the time

Conclusion

The design of the equipment of the measurement of the oxygen permeability of the packaging and mulching material was realized and the equipment was constructed. The design and the construction of the equipment was realized with applying of the standard EN STN 77 0333. The measurement of the permeability of the oxygen trough the polyethylene Bralen 2 – 63 with 9% colored concentrate Maxithen HP 533041 – violet film was realized. The

measurements and the calculations of the permeability were modified and personal access was applied. Modified measurement enabled to obtain the experimental values comparable with other authors. The measurements confirmed that the designed equipment is suitable of measurement of the permeability of the oxygen, but the improvement of the measurement of the gas concentration will be needed for the measurement of the absolute concentration of gases. The permeabilities of the oxygen trough the studied films were high. The polyethylene films are suitable for mulching technologies and no suitable for the food packaging.

Translated by LUBOMÍR KUBÍK

Accepted for print 26.09.2012

References

ASHLEY R.J. 1985. *Permeability and plastics packaging*. In: Polymer Permeability. Ed. J. Comyn, Elsevier Applied, London, p. 269–308.

BHADHA M.P. 1999. *How weld hose materials affect shielding gas quality*. Welding Journal, 2: 35–40.

BROŽOVÁ L. 2008. *Měřent permeability kyslíku u fólií pro uchování a ochranu archiválií*. Ústav makromolekulární chemie, AV ČR, [online] Published: April, 11st 2011. [cited 26.3.2012].Accesible:http://www.nkp.cz/restauratori/2008/Vavrova_Ohlidalova_2008.pdf, p. 7–14.

CUSSLER E.L. 2003. *Diffusion: Mass Transfer in Fluid Systems*. 6th Ed. Cambridge, Cambridge University Press, p. 581.

JASSE B., SEUVRE A.M., MATHLOUTHI M. 1994. *Food Packakging and Preservation*. Blakie Academic and Professional an imprint of Champan & Hall, Glasgov, London, 1994, p. 275.

EN STN 77 0333: 1987. *Determination of gas permeability of packaging materials*.

KAMAL M.R., JINNAH I.A., URACKI L.A. 1984. *Permeability of oxygen and water vapor through polyethylene/polyamide films*. Polymer Engineering & Science, 24(17): 1337–1347.

KOROS W.J., COLEMAN M.R., WALKER D.R.B. 1992. *Controlled permeability polymer membranes*. Annu. Rev. Mater. Sci., 22: 47.

LEE W.M. 1980. *Selection of Barrier Materials from Molecular Structure*. Poly. Eng. Sci., 20: 65–69.

PAPIERNIK S.K., ERNST F.F., YATES S.R. 2002. *An apparatus for measuring the gas permeability of films*. J. Environ Qual. 31(1): 358–361.

PAULY S. 1999. *Permeability and diffusion data*. In: Polymer Handbook, 4th Ed. J. Brandrup, E.H. Immergut, E.A. Grulke, John Wiley & Sons Inc. 543–569.

PYE, D.G., HOEN H.H., PANAR M. 1976. *Measurement of gas permeability of polymers*. Journal Appl. Polym. Sci., 20: 287–301.

RUTHERFORD S.W., DO D.D. 1997. *Review of Time Lag Permeation Technique as a Method for Characterisation of Porous Media and Membranes*, Adsorption, 3: 283–312.

SIEGEL R.A., CUSSLER E.L. 2004. *Reactive barrier membranes: some theoretical observations regarding the time lag and breakthrough curves*. Journal of Membrane Science, 229: 33–41.

SOHAIL H., JACK Y. 1997. *ATR-FTIR spectroscopic studies of the structure and permeability of sulfonated poly (ether sulfone) membranes*. Journal Chem. Soc., Faraday Trans., 93: 1613–1620.

TABER H.G. 2010. *Mulches and Drip Irrigation for High Tunnels*. Iowa High TunnelFruit and Vegetable Production Manual. [online] Published: June, 18th 2010. Accesible: http://www.extension.iastate.edu/Publications/PM2098.pdf [Cited: 22.8.2011].

WANG Y., EASTEAL J.A., CHEN D. 1998. *Ethylene and oxygen permeability through polyethylene packaging films*. Packaging Technology and Science, 11(4): 169–178.

Reviewers of Years – book 2012

Ivan Barabash
Zoltan Bologh
Jarosław Bosy
Costin Chiru
Antonio Coelho
Dinara Dallaeva
Guillermo E. Defossé
Sakamon Devahastin
Apostolos P. Fournaris
Jacques Fournier
Jarosław Frączek
Emil Gatial
Gabriela Gheorghe
Józef Hernik
Zbigniew Kacprzyk
Daria Kępińska
Bernard Kontny
Marian Kopczewski
Radoslav Majdan
Marek Molenda
Leszek Mościcki
Krzysztof Pancerz
Jan Pawlak
Foued Peakesson
Jacek Przybył
Paweł Rowiński
Adam Rybka
Khalid Saeed
Czesław Suchocki
Ziemowit Suligowski
Panmanas Sirisomboom
Ahmet Sivacioelu
Jaroslaw Teska
Gyula Tóth
Paweł Tylek
Jan Unucka
Martin Weinmann
Matthew James Witz
Milan Zmindak